UNIVERSITY OF CAPE TOWN
IYUNIVESITHI YASEKAPA • UNIVERSITEIT VAN KAAPSTAD

BLAST IMPACT & SURVIVABILITY RESEARCH UNIT

BISRU

An Experimental Investigation into the Anisotropic Behaviour of Bovine Femoral Cortical Bone

Andrew Roginsky

Supervised By:

Mr Trevor Cloete
Mr Ernesto Ismail

Dissertation presented for the Degree of Master of Science in Mechanical Engineering at the University of Cape Town

The financial assistance of the National Research Foundation (NRF) towards this research is hereby acknowledged. Opinions expressed and conclusions arrived at are those of the author and are not necessarily to be attributed to the NRF

Abstract

To increase our level of knowledge of the human body for various applications, the behaviour of cortical bone needs to be understood. To understand and model the behaviour of cortical bone, knowledge of the strain rate dependent behaviour is required. Many authors have investigated these properties, however, the literature appears to be ambiguous and incomplete, with little focus being placed upon the intermediate strain rate regime ($1s^{-1}$ to $100s^{-1}$). The ambiguity arises as each author presents an averaged data set which does not describe the level of scatter or precise testing methods, nor does it correspond with other authors work [33, 56, 27, 2, 62]. Furthermore, bone should display distinct anisotropic properties due to the microstructural layout. However, no author has published or recorded a complete data set detailing the anisotropy of bone across any species.

The intermediate strain rate regime is of particular interest due to Paul [50], capturing a distinct transitional behaviour of cortical bone between low and high strain rates. The apparent lack in intermediate regime research is due to the difficulty in attaining constant strain rate testing conditions within this region using conventional methods. Consequently, due to the absence of data, no accurate model has been developed to simulate the behaviour observed.

The focus of this dissertation will therefore be to redesign and fabricate the previously used intermediate strain rate testing device, provide an accurate data set across both quasi-static and dynamic regimes, and a phenomenological model which is able to capture this strain rate dependent behaviour. In order to develop an understanding of the scatter presented in each orientation, light microscopy, inverse light microscopy, and SEM of the specimens is performed. What is observed is that each orientation displays a distinct microstructural layout with fractures propagating in a distinctly different manner based on the strain rate regime. Furthermore, counter to previous findings, the strength of bone across a variety of samples does not appear consistent, however, the longitudinal and radial orientations still display strain rate sensitivity (per sample) which was captured using the improved phenomenological viscoelastic model.

Declaration

I, Andrew Roginsky, hereby:

1. Grant the University of Cape Town free license to reproduce this dissertation, entitled: An Experimental Investigation into the Anisotropic Behaviour of Bovine Femoral Cortical Bone, in whole or in part, for the purpose of research.

2. Declare that:

(a) I know the meaning of plagiarism and declare that all the work in the document, save for that which is properly acknowledged, is my own. This thesis/dissertation has been submitted to the Turnitin module (or equivalent similarity and originality checking software) and I confirm that my supervisor has seen my report and any concerns revealed by such have been resolved with my supervisor.

(b) This dissertation or any part of this dissertation has not been submitted in the past, or is being, or is to be submitted in this or any other form for a degree at the University of Cape Town or any other University.

(c) I am now presenting this dissertation for examination for a degree in Masters of Science in Mechanical Engineering.

Signed by candidate

.....

Andrew Roginsky
November 2016

Acknowledgements

I would like to acknowledge the following people and groups for the input they have provided in order to allow for the completion of the following masters dissertation, for without them this project would not have been made possible:

- Mr Trevor Cloete and Mr Ernesto Ismail for the supervision and guidance provided which has allowed me to complete this dissertation.
- Ms Kelsey Hilton, for her assistance in designing the initial load cell, corresponding nuts and tools, and Reflective Objectography Sensor striations on the wedge bars. All further work and modifications are however my own.
- Mr Charles Harris for the countless hours spent machining bovine bone specimens in order for me to be able to complete my MSc and testing.
- Mr Pierre Smith and the UCT Mechanical Engineering workshop staff for their expertise, manufacturing advice and hours placed into the manufacturing of my mechanical designs and subsequent iterations.
- Mr Julian Mayer for the help and expertise in strain gauging the load cells constructed and electrical advice.
- Mrs Penny Louw and staff at the Center for Materials Engineering for the help and guidance when performing quasi static testing and histological analyses.
- Mrs Miranda Waldron, from the Electron Microscope Unit, for the help in performing histological analyses on my samples utilising the Scanning Electron Microscope(SEM).
- The BISRU supervisors, staff, students and team for the help, guidance and ideas during my MSc.
- Professor Gerald Nurick and Ms Amber Convery for the hours spent proof reading and helping correct any grammatical errors I may have had.
- My family for the constant support they have provided me in every way.

Contents

List of Figures

Nomenclature

- Anisotropic - Property variance with change in axes
- Anterior - In biological context, this means the front of the body
- BISRU - Blast, Impact, Survivability and Research Unit
- Cortical bone - Outer hard compact bone
- Collagen - Proteins occuring as a major component of connective tissue
- Compliance - In a machine sense, this is the magnitude of machine deformation during the testing procedure
- Dashpot - Damper used in numerical analysis
- Distal - In biological context, this the area situated furthest away from the point of attachment/origin
- Fading memory - Feature of a viscoelastic material by which a memory exists that will influence the current stress properties
- Fibrolamellar/Plexiform - Formation of collagen fibers in layers
- Haversian - Axial canals within cortical bone
- Heterogenous - Composition of dissimilar elements without uniformity
- Hydroxyapatite - An inorganic constituent of the bone matrix
- Intermediate strain rate regime - 1:50/s strain rate region
- Lamellae - Thin layers of collagen fibers
- Longitudinal - The axis orientation which runs with the length of the bone.
- Macroscopic - Properties visible to an unaided eye
- Maxwell element - The arrangement of a spring and dampener in series
- Microscopic - Properties invisible to an unaided eye
- Osteon - A basic structural unit of bone, consisting of one or more concentric layers of bone around a longitudinal vascular channel
- Osteonal density - Number of osteons per square millimetre
- PMMA - Poly(methyl methacrylate)
- Posterior - In biological context, this means the back of the body
- Proximal - In biological context, this the area situated at the point of attachment/origin

- Quasi-static - Process that resembles an infinitely slow procedure such as very slow strain rates
- Radial - The axis orientation which runs through the thickness of the bone.
- ROS - Reflective objectography sensor
- SEM - Scanning electron microscope
- Trabecular - Soft spongy bone enclosed by the cortical bone
- Transverse - The axis orientation which runs with the circumferential direction of the bone. I.e: Hoop axis
- Viscoelasticity - Ability for a material to display solid and fluid like properties
- Voigt element - The arrangement of a spring and dampener in parallel

Chapter 1

Introduction

The properties of bone have been of interest for a number of years with studies conducted for the purpose of protection and to increase our level of knowledge of the human body [33, 36, 56, 4, 5, 42, 13, 9, 62]. These properties (microstructural layout, age, etc.) are of particular interest when trying to understand the macroscopic fracture of bone which often occurs in incidents such as vehicle collisions, accidental falls, projectile or blunt force trauma, etc. Bone is a complex hierarchical composite material compromising of an organic matrix (collagen), minerals (hydroxyapatite crystals), and a viscous fluid constituent which fills any form of porosity present. Within the body, bone is found in two distinct forms. Cortical bone forms the hard outer layer of a bone and may present in a variety of thicknesses depending on the function of the bone, while trabecular bone forms the internal sponge like complex geometry which contains the bodies bone marrow reserves.

Due to this complexity, the stiffness properties of bovine bone appear to vary significantly with strain rate [33, 36, 62, 13]. Recently, Paul [50], recorded a distinct transition which occurred between the low and high strain rate regime. This transition occurs within the intermediate strain rate (ISR) regime (1/s - 100/s). Previously to Paul [50], there has been a distinct gap in the literature within the ISR regime due to the difficulty in the testing processes. The difficulty arises as the testing procedure must occur at a near constant strain rate due to the dependence of the material properties on the strain rate [33, 36]. Thus, the testing machinery must be able to, at start, attain the required testing strain rate near instantaneously and sustain this to prevent false data. As no internationally acceptable testing methodology exists for testing within the ISR regime, researchers have attempted to test and construct testing apparatuses for this regime with Stander [57] reporting on the apparatus conceptualized and reported by Cloete *et.al.* [12] which is capable of achieving strain rates of the order of 3/s - 10/s.

Furthermore, the results currently available within literature do not quantify the level of scatter nor standard deviation for the respective data sets which introduces a level of uncertainty in the average results reported. In light of the results obtained within this dissertation, a further concern has arisen as to whether researchers account for the machine compliance (deformation of the machinery during testing) within the associated test data as this has been determined to significantly influence the stiffness properties of the specimens.

For the purpose of this dissertation, the stiffness properties of bovine femoral cortical bone from the mid-diaphysis are investigated. Bovine bone is used instead of human bone due to the ease of obtaining samples with no need to obtain ethical clearance. As bone displays anisotropic tendencies [47, 2], this is investigated in the context of the longitudinal(length direction), transverse(hoop direction) and radial(through thickness) orientation and compared with relative literature. Based on the work of Cloete *et.al.* [14, 13], the mechanical properties of bovine bone obtained from slaughter age cattle can be expected to produce consistent results between individuals. However, in light of the data found within this dissertation, this does not appear

to be the case with stiffness properties varying across samples.

This dissertation will also focus on the intermediate strain rate apparatus redesign and fabrication, for the purpose of ISR testing to be conducted, in order to allow for a greater range of strain rates.

1.1 Plan of development

The structure of this dissertation will be as follows:

- Chapter two presents the literature review conducted in order to understand the implications that intrinsic and extrinsic factors may have on the mechanical properties of bovine bone.
- Chapter three presents the design and improvement of the intermediate strain rate testing machine.
- Chapter four details the method used to prepare and manufacture specimens in all three directions. This chapter also details the techniques and methods followed in order to accurately calibrate both the quasi-static and intermediate strain rate testing machines and analyse the data correctly.
- Chapter five presents the results obtained from testing specimens. Any variation or discoveries found within the testing will be discussed within this chapter.
- Chapter six has been added as an introductory chapter in order to gauge an understanding into the microstructure of bovine bone anisotropically through various forms of imaging.
- Chapter seven presents the modifications applied to the existing model and its application.

Chapter 2

Literature Review

2.1 Introduction

Bone is a complex multifunctional geometrical framework which forms the mechanical structure of the human body, protects vital organs such as the heart and lungs, provides a calcium and phosphorus mineral reservoir, and protects the body against dangerous minerals such as lead[34].

For the purpose of this dissertation, the mechanical properties of bovine bone are of interest and hence the purpose of the literature review is to:

- Describe the physiology of femoral cortical bone.
- Describe the differences and similarities between bovine and human femoral cortical bone.
- Describe the anisotropy associated with bone.
- Describe the preparation and storing techniques for bone specimens.
- Investigate the factors influencing the mechanical properties of bone.
- Investigate mechanical testing techniques with respect to strain rate dependence.
- Investigate possible biological reasons for variation within the data.
- Investigate analytical modeling techniques.

2.2 Physiology of femoral cortical bone

A strange feature of this field is that both the structural elements of a skeleton and its constituent material are refered to as "bone". Hence a bone (a structure) is made of bone (a material). All bones are made up of both trabecular (soft spongy bone enclosed within the cortical bone) and cortical (outer hard compact) bone. For the purpose of this dissertation, femoral cortical bone is of particular interest as it not only provides the primary load bearing structure of an animal but also provides relatively large testing samples[4].

2.2.1 Material Properties

Bone is considered to be a heterogeneous composite material primarily consisting of three vital components, hydroxyapatite, proteins (type 1 collagen) and water[10, 60]. The material properties are dependent on the arrangement and quality of these constituents. The properties are measured micro[49, 40, 41, 32] and macro [10, 43] quasi-statically by determining the mineral crystal size, the porosity of the bone, and whether micro cracks[65, 4] exist within the bone specimens and how these influence the recorded data. However, these methods do not take into consideration the age of, or extrinsic (diet, freezing, etc.) factors affecting, the bone.

The purpose of testing bovine bone is to begin to develop material models and property lists so that when testing of human bone is possible, the transition will be simple and testing equipment and procedures will be well established to classify human bone. Institutes have tested on human cadaveric bone [62, 48], however, in order to begin to build a material model with as little variation as possible, bovine bone is easier to use. This is due to bovine bone being readily available with no ethical clearance required. This is beneficial as numerous tests are required to be performed to begin to capture and quantify the behaviour of bone. The complexity of this behaviour is summarised by Johnson *et.al.* [36] where a clear strain rate dependence is shown.

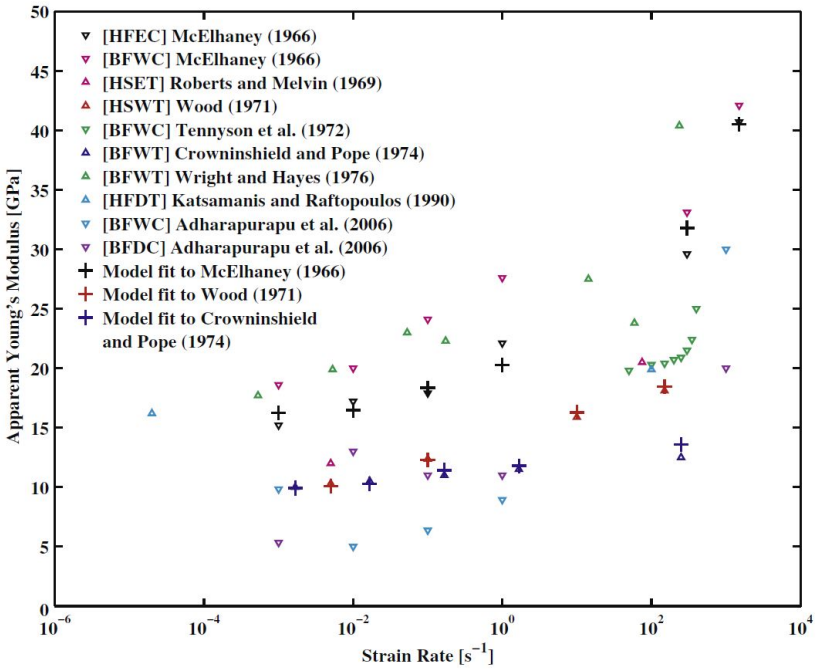

Figure 2.1: Apparent modulus vs strain rate as reported by Johnson *et.al.* [36]

2.3 Factors influencing mechanical properties

The mechanical properties of bone are influenced by factors pertaining to the specific subject (bovine), such as age and health, but also to external factors relating to the testing procedures.

2.3.1 Age

Bones exhibit a change in material properties as the subject increases in age. There is typically an increase in mechanical strength in the early years of life, and a degradation in later years. For example, a bone may have experienced different circumstances forcing remodeling and differential strengthening of bone; this is due to these properties being dependent on the direction of the most strenuous loading[30]. Several studies to investigate how age related accumulation of micro damage, such as micro fractures/cracks, will impact the material properties in the form of decreasing elastic moduli and strength or fracture toughness [4, 29, 17, 66, 25] have been performed. This strengthens an argument made by Hui and Johnston in 1988 that age can be used as a predictor of fracture [29]. Hence this will have to be taken into account when sourcing the specimens.

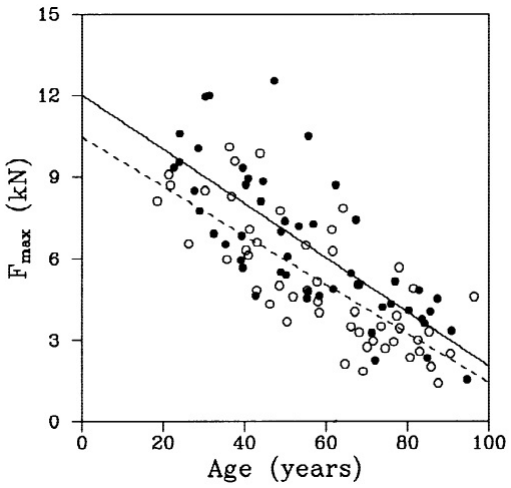

Figure 2.2: Maximum compressive load vs age as reported by Ebbesen *et.al.* [17] where the open circles represent females and the filled circles represent males

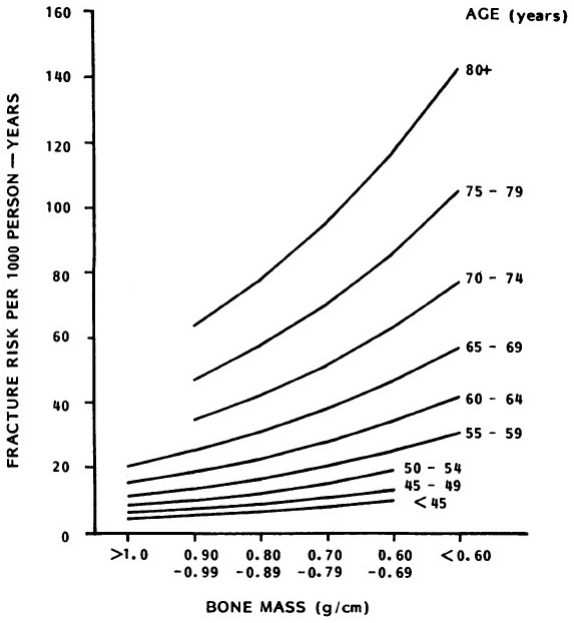

Figure 2.3: Age as an indicator of fracture risk as reported by Hui [29]

2.3.2 Density

Literature indicates that material property variation due to bone mineral density or concentration changes is also closely related to that of the age and gender of the subject. Studies performed by a number of authors[4, 17, 29, 27, 31] demonstrate that the age of subjects influences the bone mineral concentration within cortical and vertebral bone and that the change in density also further influences the apparent modulus of the specimen. However, variation between gender is not significant, thus, an increase in fracture risk may arise due to the bone mineral content decreasing significantly with age.

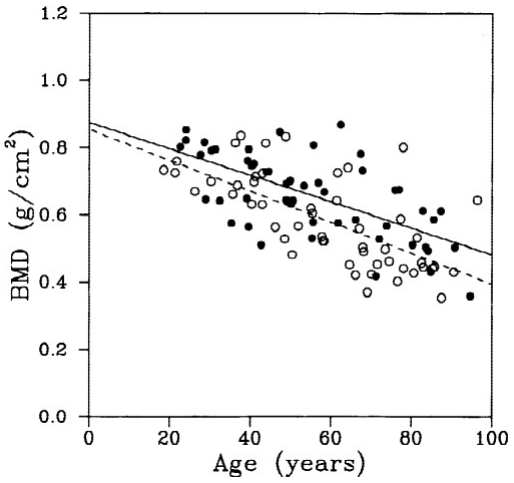

Figure 2.4: Bone mineral density depreciation as a factor of age as reported by Ebbesen *et.al.* [17] where the open circles represent females and the filled circles represent males

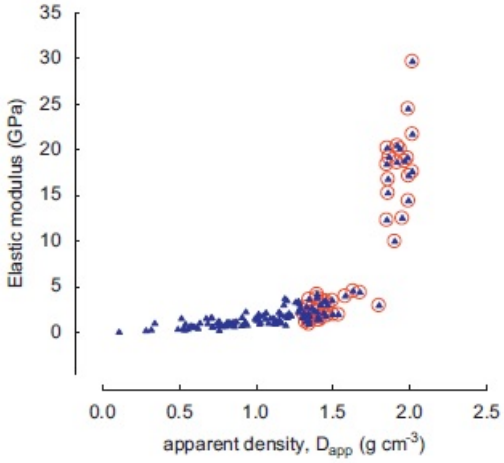

Figure 2.5: Comparison between the elastic modulus and apparent density for both cancellous and cortical specimens together reported by Zioupos *et.al.* [31]

2.3.3 Storing techniques of specimens

The method of storing as well as the fluid solution the specimen is stored in must be considered. In previous work specimens were stored in a frozen condition post-machining[50]. Studies completed by Zwaards *et.al.* [61], and Kaye *et.al.* [5], show no significant changes in elastic moduli or material properties due to freezing or the duration that specimens are frozen for.

Studies conducted on bovine, ovine, and human bone by Unger *et.al.* [58], Wieding *et.al.* [35], and Kuninori *et.al.* [38], shows that freezing does not significantly alter any mechanical properties of the fresh samples. The addition of formalin, however, appears to change the material properties substantially and so cannot be used. Figure 2.6 demonstrates the percentage deviation from the control, due to preservation methods, during testing at approximately 0.001/s and 0.1/s strain rates:

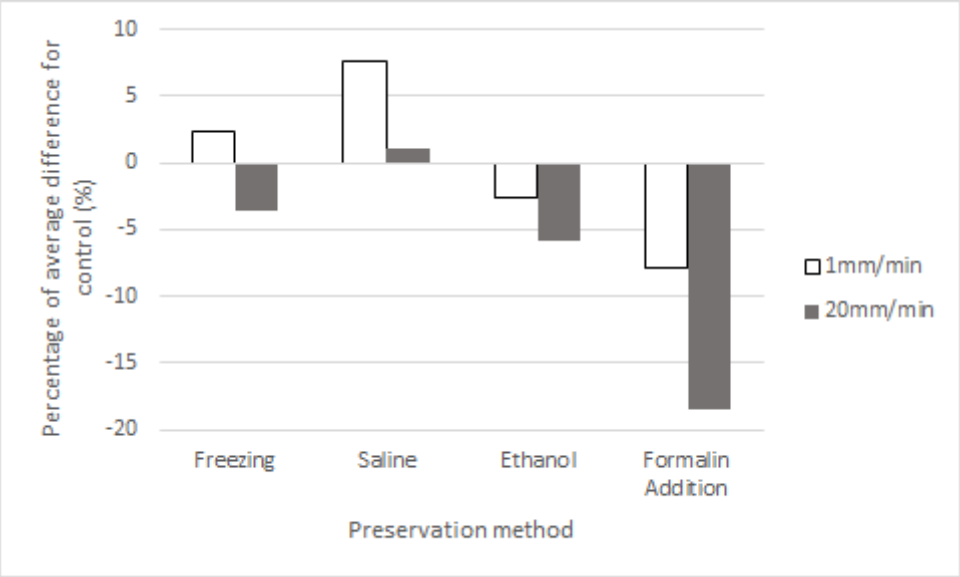

Figure 2.6: Effects of various preservation methods, of bovine bone, as reported by Kuninori *et.al.* [38] at two prescribed loading rates

The literature consensus is that storage of bone specimens for mechanical testing is preferably performed in a saline solution, at temperatures below -18 ° C. However, storage in pure physiological saline solution can lead to Calcium leaching and thus reduces the relaxation modulus properties if not combined with freezing [21, 42, 50, 20].

Higgs [42] conducted a study to compare samples stored in alcohol to those stored in physiological saline solution. It was found that alcohol affected the visco-plastic response by dehydrating the sample's water content thus causing a more brittle response. This, however, could be reversed with insignificant property changes by rehydrating the samples in a physiological saline solution.

In an interview with Dr Guillaume Dubois [16] the storing solution used within the work that he had conducted was a physiological saline solution that consisted of 9g/L of salt. The reasoning behind this is due to the human body consisting of a normal concentration of 6g/L of NaCl with the addition 3g/L in order to substitute for the missing ions usually located within the human

body. This is appropriate during testing due to the short time being allocated for thawing and testing. This argument is further supported by Kuninori *et.al.* [38] where the following is stated:

"*Saline (0.9 mass % aqueous NaCl solution) was used exhaustively during the processing of bone specimens, starting from the short-term preservation period up to the implementation of mechanics testing and others, as it has the same osmotic pressure as that of the living body but without an antiseptic effect.*" [38]

While the argument presented is based on human physiology, no studies pertaining to the salinity of other species are available. As such, the proposed storage solution was used without adjusting for the bovine origin of the samples.

As specimens are not stored for significantly long periods and are frozen prior and post testing with the minimum allowed thawing time, a physiological saline solution is appropriate as the material properties will not change significantly [61]. However, during thawing and testing, a Calcium buffered solution is recommended in order to prevent Calcium leaching and any associated material property variation. The allocated thawing and testing time may be insignificant enough not to require a change in solutions [50].

A further test conducted by Wieding *et.al.* [35], focused on the decomposition of bone. Fresh samples were place in the open at room temperature for fourteen days. Mechanical properties were then observed for these specimens by conducting four point bend tests using a mechanical testing machine. Differences in the elastic moduli and specific elastic/plastic energies were noted. Figure 2.7 demonstrates the differences in these properties. While these results are interesting, the small sample size (12) does not provide good statistical certainty.

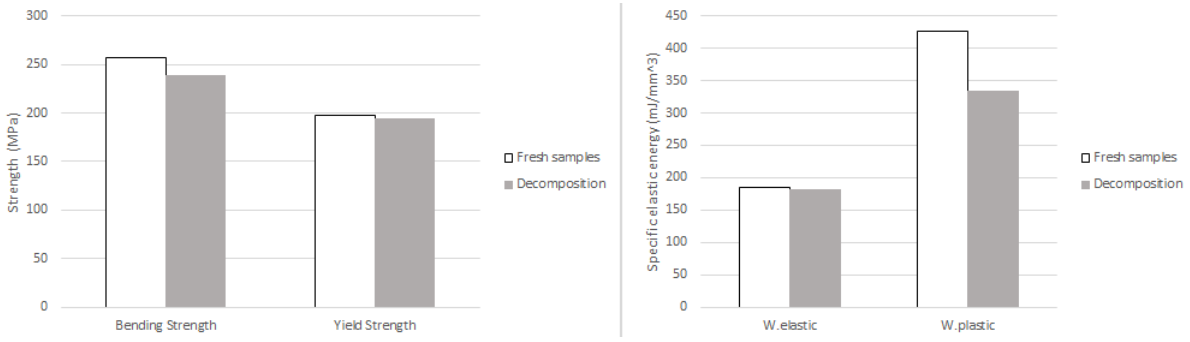

Figure 2.7: Decomposition (14 days) effects on specimens by Wieding *et.al.* [35]

2.3.4 Loading direction

At a mesoscopic scale bone is highly irregular, but for ease of macroscopic analysis, three principal orientations are considered, namely the transverse, longitudinal, and radial directions. Bone material properties, and ultimate stresses, vary with the loading direction, and hence bone is classified as anisotropic[47, 60, 42, 59, 62]. Figure 2.9 shows a review of results from numerous studies, presented by the United States Army Research Laboratory [62], comparing the strength of human cortical bone in the longitudinal and transverse orientation. These results, show that numerous species, including humans and bovines exhibit anisotropic bone strengths.

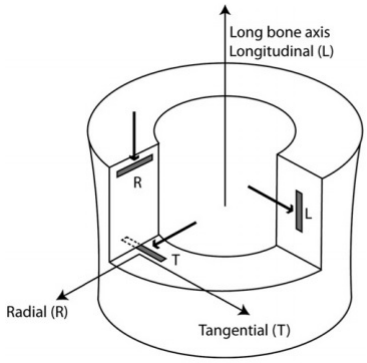

Figure 2.8: Principal loading directions presented [59]

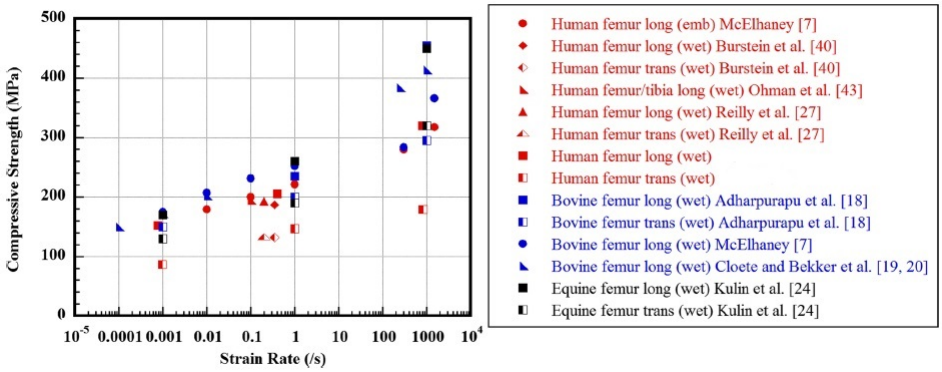

Figure 2.9: Compressive strength of cortical bone as a function of strain rate as reported by Weerasooriya *et.al.* [62]

2.3.5 Strain rate sensitivity

Multiple studies have been conducted upon bone and the strain rate variation within testing methods [3, 8, 9, 11, 27, 33, 47, 42, 50, 60, 62], with Bekker [7] concluding that the elastic modulus will increase with increasing strain rate. Recently, Paul [50] recorded a complex transition occuring within the intermediate strain rate regime (1/s - 100/s). Research performed within the intermediate strain rate regime is insufficient, as demonstrated in Figure 2.9, and difficult to perform using conventional methods. The difficulty arises as quasi-statically, the apparatuses are not capable of accelerating to intermediate strain rates (1/s - 100/s) within the given time. This is contrary to high speed testing which is unable to achieve such low strain rates. To capture this behaviour, a custom intermediate strain rate testing apparatus was prototyped by Stander [57] and will be discussed in further detail in chapters 3 and 4. This captured transition is significant as it demonstrates the degree of the inherent nonlinear behaviour over this region for bovine bone which has previously never been recorded. Figure 2.10 demonstrates the model created by Paul which is able to capture the compressive stress behaviour, at a constant strain rate, for a given strain:

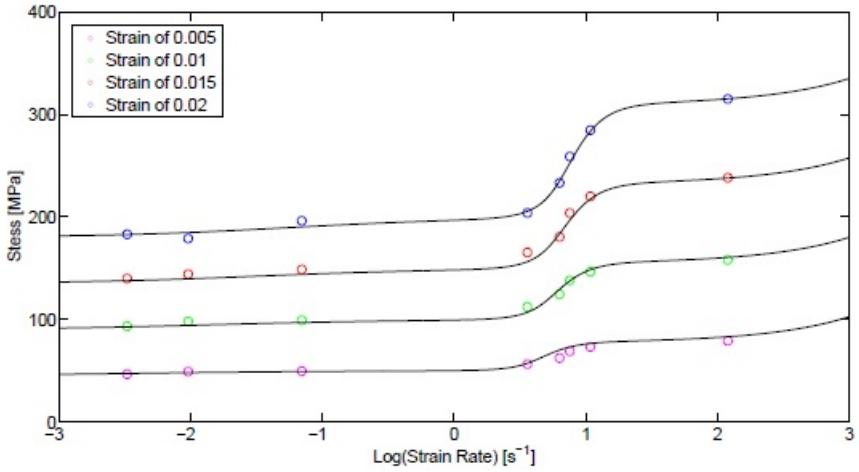

Figure 2.10: Complete response of longitudinal bovine bone as reported by Paul [50]

It can be seen that the intermediate strain rate regime is of importance due to the change in compressive strength with varying strain rate in this regime. However, research regarding the anisotropy and compressive behaviour within this region is insufficient on a macroscopic scale and requires additional focus during testing procedures and data capture.

2.4 Imaging and microstructual fibre direction

The microstructure of bovine bone occurs in two distinct formations, fibrolamellar (formation of collagen fibers in layers) to Haversian (formation of collagen fibers in cylinders) which form when bone remodeling occurs. For remodeling, bone must be subjected to a significant mechanical stress over a period of time. This will initiate the process of resorption (a process where bone absorbs itself) followed by the growth of secondary osteons which are more commonly known as Haversian systems [1, 7, 43]. Due to this remodeling, there is an increased need for nutrients which is accounted for by the Haversian system forming a central canal. This canal consists of a vein, artery and nerve to feed the surrounding tissue.

Mayya *et.al.*, [1] demonstrates this variation by manufacturing 5 mm cubes from both the anterior and posterior aspects of the bovine femoral bone and comparing the microstructure as shown in Figure 2.11.

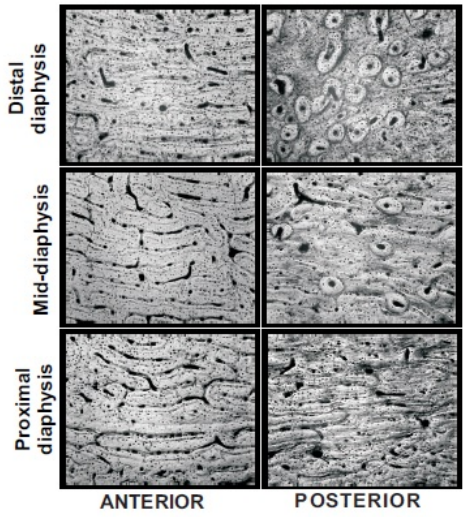

Figure 2.11: Change in microstructure from posterior to anterior aspect for young bovine femoral bone as reported by Mayya *et.al.* [1]

This clearly demonstrates the variation in microstructure from posterior to anterior of the bone. Mayya *et.al.* [1], maps distinct bone microstructure through the length of a bone. This is displayed in Figure 2.12.

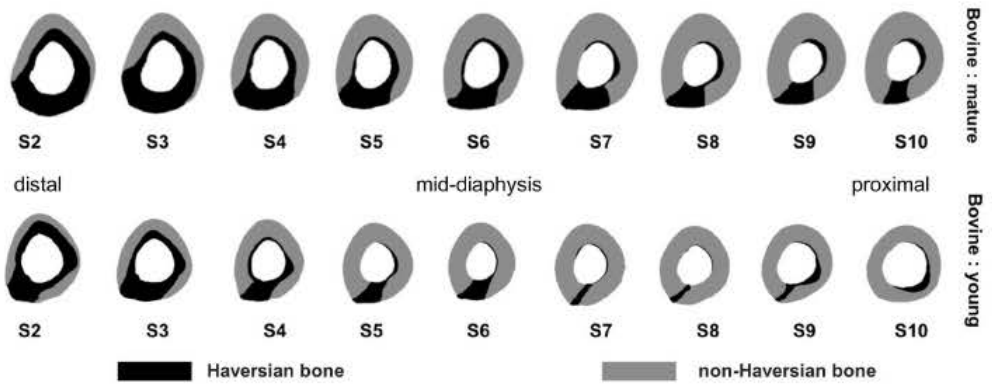

Figure 2.12: Identified areas of distinct microstructure as reported by Mayya *et.al* [1] where the top of each bone is the anterior portion

Mayya *et.al.* performed several compression tests which yielded varying results between posterior and anterior aspects. There is a bias, however, towards the posterior specimens tending to resist compression more greatly than the anterior, although, there is insufficient data for this to be accurately confirmed. The osteonal density(number of osteons per sq. mm) of the specimens is investigated by Mayya *et.al.* and a linear relationship, with a correlation of 0.97, between the peak compressive stress and osteonal density was found. Again the validity of this relationship cannot be statistically validated due to insufficient data existing.

Other conclusions drawn by Mayya *et.al.* [1] are that non-Haversian bone is identified as being weaker than Haversian bone and that the fracture surfaces analysed display distinct differences for the microstructure identified. The results from Mayya *et.al.* provide a useful microstructural analysis. These findings may help to quantify the variation found within the recorded data.

The imaging performed within the literature [1, 7, 43] utilises both scanning electron microscopy (SEM) and optical microscopy. Both are useful and necessary as each displays different characteristics.

SEM utilises a gold palladium coating upon the surface of the specimen in question in order to determine what surface features and anomalies are present. As the SEM requires the emission of x-rays from the interaction of the electrons with the specimen, objects within cavities are difficult to image. This is due to the capture of the x-rays by surrounding structures.

Alternatively, optical microscopes provide some of the information not captured by SEM imaging. Both standard and inverse light microscopy may be used. This is performed in order to create different types of illumination within the specimen which may result in different features presenting themselves. Inverse light microscopy is useful in viewing microstructual detail [9] as higher magnification is able to be attained. Standard light microscopes simply provide low magnification analysis of the surface structure which is typically more useful in a faster analysis to determine the overall condition of the specimen.

2.5 Testing Techniques

To test within strain rates from 0.001/s - 1000/s, different testing techniques are required. These methods are generally classified as quasi-static, intermediate, and high speed. The following section will therefore deal with the techniques that have been used in literature.

2.5.1 Quasi static

Quasi-static testing was conducted via a Zwick quasi-static mechanical testing machine at UCT by both Paul [50] and Bekker *etl.al.* [7, 8, 9]. Other authors who have presented test data for bovine bone include Adharapurapu *et.al.* [2] and McElhaney [33], who used standard servo-hydraulic testing systems. Zioupos [66] and Currey *et.al.* [25], also utilised the Zwick testing machine for testing, however the testing performed was for three and four point bending. The Zwick quasi-static mechanical testing apparatus is an internationally accepted machine in terms of performing quasi-static testing for a wide range of materials, both in tension and compression. Typically, there are two different types of machines available. These are electrical screw driven machines and servo-hydraulic frames. Both types of machines consists of a main frame, a form of displacement measurement, a load cell, and a movable cross head [57]. Servo-hydraulic frames are preferred to screw driven machines due to the versatility that the hydraulic system allows in terms of force and displacement. Screw driven machines are unfortunately limited by the size and power of the motor supplied. Furthermore, screw driven machines often prone to wear and heat damage. Reviewing the work performed by Bekker and Paul, it was found that compliance had not been removed from their test data which can provide an explanation into the reason for their modulus values lying considerably lower than other literature. As the maximum force within the quasi-static regime does not exceed 5kN for bone [50, 7], this may be a reason as to why previously, compliance had been overlooked.

2.5.2 Dynamic

Dynamic testing includes strain rates of 1/s - 1000/s. High strain rates are attainable using a Split Hopkinson Bar (SHB) technique as demonstrated by authors such as Paul [50], Bekker *et.al.* [7, 8, 9], Adharapurapu *et.al.* [2] and Hansen *et.al.* [26]. The SHB technique is a internationally renowned high strain rate apparatus (>100/s) which compresses a specimen between two bars, the incident and transmitted bar. Strain gauges are attached to both bars which are used to identify the incident and reflected stress histories and from this, determine the material properties. However, tests within the intermediate strain rate regime of 1/s - 100/s are difficult to achieve as the SHB technique is unable to attain such low strain rates and standard tensile testing machines are unable to attain such high strain rates. Within tensile testing, this can be achieved comfortably by using fixtures such as "slack adaptors" or "run-up fixtures", however, within compression testing an initial gap is required between the specimen and upper anvil [50, 12]. In the literature there is a lack of intermediate strain rate data with currently only Paul achieving results within this region for bone using the intermediate strain rate testing apparatus prototype. [50, 57]

2.5.2.1 Intermediate

Intermediate testing has been performed with the introduction of the wedge bar by Cloete *et.al.* [12, 50, 57]. The design utilises many of the SHB components and principles, however, fundamentally the design is different. The name of the apparatus is taken from the shape of the loading bar which replaces the incident and transmitted bar. Conventionally the SPHB

compresses a specimen between the incident and transmitted bar. Within the wedge bar, the specimen is compressed vertically between a platform and load cell. This is demonstrated in Figure 2.13 by Stander [57]:

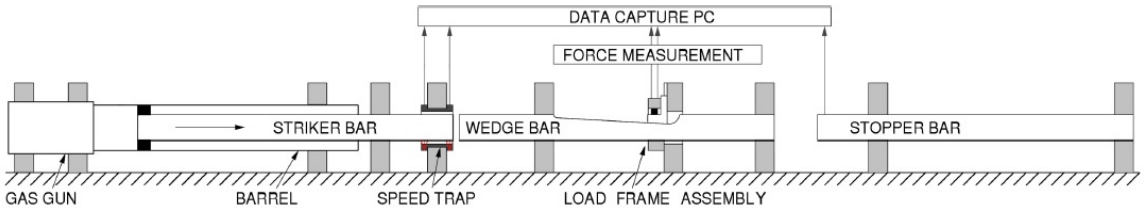

Figure 2.13: Wedge bar schematic as reported by Stander [57]

A loading platform is positioned on the top of the wedge bar, and compresses the specimen against the loading frame and loadcell. The underside of the platform matches the slope on the wedge bar to ensure smooth movement. As the bar is propelled, the specimen platform moves up the slope, compressing the specimen against the load cell.

Other methods of intermediate strain rate testing include the quasi-static mechanical testing apparatus and Serpentine bar mechanical testing apparatuses [63]. As the material properties are dependent on the strain rate [33, 36, 13], the testing procedure must occur at a near constant strain rate. The testing machinery must, at start, be able to attain the required testing strain rate near instantaneously and sustain this to prevent falsified and inconsistent results. Thus, testing using the above stated methods, in this strain rate range, is ill-advised as the specimen is required to be in contact with the load cell and base plate. Due to this requirement, the Zwick quasi-static mechanical testing machine is unable to reach the required loading rates in a short enough time due to the inertia of the machine components. Thus, non-constant strain rate loading of the specimens occurs during the initial travel of the machine. However, the specimens fail at very low strains, and thus testing with the machine in this strain rate regime is not possible. The Serpentine bar, developed by Whittington *et.al.* [63], allows for an increased time duration in order to achieve larger strains. This is achieved by setting up a series of impedance matched tubes in order to decrease the total length of the bar. Previously this has been used to trap momentum and recover dynamically fractured specimens [53]. However, the report only compares data at a strain rate of 300/s and does not detail the intermediate strain rates reached and consistency of these results. This is due to the author believing that the ISR regime lies in the range of 5/s - 500/s which as we have demonstrated already, is not the case.

2.6 Viscoelasticity

2.6.1 Introduction

Viscoelasticity is defined as the ability for a material to portray both the properties of viscous materials (fluids) and elastic materials (solids). Viscoelastic materials are used in the application of everyday features, for example in helmets and shoe insoles (in order to prevent transmission of shock to the person). This can be further subdivided into three sub categories in order to describe various properties that a material may exhibit.

Creep: A progressive deformation that a material may undergo while subjected to constant stress[39].

Relaxation: The decrease in stress within a material if the strain is held at a constant state[39].

Recovery: The ability of a material to undergo a decrease in deformation in the condition that all loading is removed[39].

The following section will therefore detail the following:

- An introduction into viscoelastic components often used as a basis for more complex models.
- A discussion into current viscoelastic models which are able to capture the complexity found within bone.
- A review into possible alternative solving methodologies for nonlinear behaviour.

2.6.2 Basic viscoelastic models

Viscoelastic properties are most simply captured by using a combination of springs and dampers (dashpots) which may be either linear or nonlinear, or a combination of the two in any configuration. The two most basic models are a series (Maxwell) and parallel (Kelvin-Voigt) configuration[15, 22].

Considering a linear case initially, a spring will produce a deformation which will be proportional to the load applied whereas for a dashpot, the rate of change of deformation is proportional to the load applied at a given instant[22]. The following equations can therefore be deduced:

$$\sigma = K\varepsilon \tag{2.1}$$

$$\sigma = \eta\dot{\varepsilon} \tag{2.2}$$

Where K symbolises the spring constant with unit MPa, η symbolises the dashpot constant with unit MPa.s, and σ symbolises the stress in MPa.

Maxwell Model

The series combination of a spring and dashpot is referred to as a Maxwell model as shown in Figure 2.14.

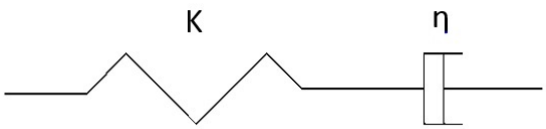

Figure 2.14: Maxwell model

In this configuration the stress is equal in each component, while the total displacement is the sum of each.

$$\varepsilon_{total} = \varepsilon_{spring} + \varepsilon_{dashpot} \tag{2.3}$$

$$\sigma_{total} = \sigma_{spring} = \sigma_{dashpot} \tag{2.4}$$

Differentiating equation (2.1) and substituting both equation (2.1) and (2.2) into equation (2.3), the following relationship can be generated, which is regarded as the constitutive Maxwell equation:

$$\dot{\varepsilon}(t) = \frac{\sigma(t)}{K} + \frac{\dot{\sigma}(t)}{\eta} \tag{2.5}$$

Assuming a linear strain path under a constant strain rate, equation (2.5) may be integrated as a first order linear differential equation, which yields:

$$\sigma(t) = \eta\dot{\varepsilon(t)}\left[1 - exp\left[\frac{-k\varepsilon}{\eta\dot{\varepsilon(t)}}\right]\right] \tag{2.6}$$

Kevin-Voigt

The parallel combination of a spring and dashpot is referred to as a Kelvin-Voigt model as shown in Figure 2.15.

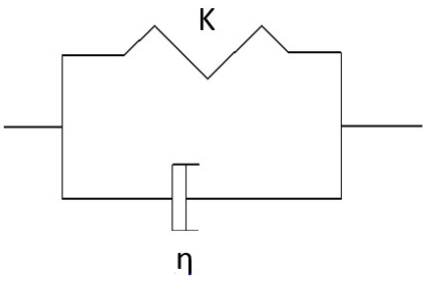

Figure 2.15: Kelvin-Voigt model

Here, the stress per component will be additive, while the deformation(strain) will be equal over all the components as described in equation (2.7) and (2.8)

$$\sigma_{total} = \sigma_{spring} + \sigma_{dashpot} \tag{2.7}$$

$$\varepsilon_{total} = \varepsilon_{spring} = \varepsilon_{dashpot} \tag{2.8}$$

Substituting both equation (2.1) and (2.2) into equation (2.7), the following relationship is generated:

$$\sigma_{total}(t) = K\varepsilon(t) + \eta\dot{\varepsilon}(t) \tag{2.9}$$

Standard Linear Model

The standard linear model is a common starting point upon which models have been created in order to begin to simulate the behaviour of both cortical and cancelous bone, such as work by van der Westhuizen [9], Johnson *et.al.* [36], Roylance [54], and Shim *et.al.* [56]. The standard linear model consists of a Maxwell element in parallel with a spring in order to simulate fading memory, defined as the ability of recent history of a material to govern current stresses, that a material may demonstrate. The fundamental starting model and equation is shown in Figure 2.16 and equation (2.10).

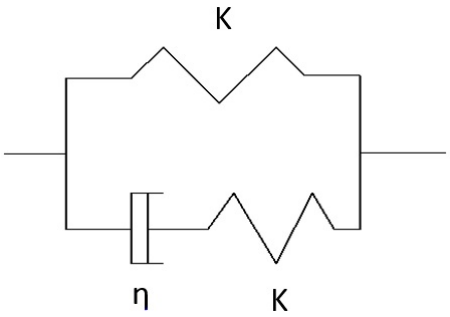

Figure 2.16: Standard Linear Model

$$\sigma_{Total} = \sigma_{Spring} + \sigma_{Maxwell} \tag{2.10}$$

This well known model is particularly useful as it represents a material with an inherent base stiffness resulting from the single spring element in parallel with the linear Maxwell element. However, bone is not considered to behave in a linear manner [7, 50, 26, 62, 3, 9]. In order to begin simulating structures such as bone, non-linearities within the structure have to be taken into account. Bone has been found to be a highly strain rate dependent material by numerous authors [50, 26, 62, 3, 9], and must therefore be included in the numerical model. The nonlinear viscoelastic behaviour is most simply captured by making the system react to changes in strain rate in a nonlinear manner. Using the damper model, one could achieve this by filling the damper with non-Newtonian fluid.

$$\sigma_{dashpot}(t) = C\dot{\varepsilon}(t)^n \tag{2.11}$$

$$\eta = C\dot{\varepsilon}(t)^{n-1} \tag{2.12}$$

Where n is the power law index. For n = 1, the viscosity will represent a Newtonian fluid. If n is between 0 and 1 or greater than 1, the viscosity will represent a shear thinning or shear thickening fluid consequently.

A constitutive equation for a nonlinear Maxwell element is derived using equation (2.12). As the total stress is the sum of each parallel branch stress, the standard model may be represented by the addition of Kε.

$$\dot{\varepsilon(t)} = \frac{\dot{\sigma}}{K} + \left[\frac{\sigma}{\eta}\right]^{1/n} \tag{2.13}$$

Modifying the constant n changes the level of nonlinearity where n = 1 returns the standard linear model. Additionally, including multiple sets of these components allows for more complex behaviour to be explained.

2.6.3 Viscoelasticity of cortical bone

While the nonlinearity of cortical bone has been modelled using viscoelasticity by numerous authors [14, 2, 24, 50, 9, 36, 44, 56], only the work of Paul [50] has shown the sharp transition between behaviour at low and high rates, and has captured this using a nonlinear viscoelastic model.

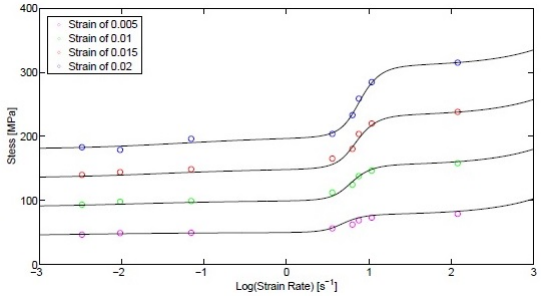

Figure 2.17: Demonstration of the represented model for the strain rate dependance behaviour of bovine cortical bone for a range of strains as reported by Paul [50]

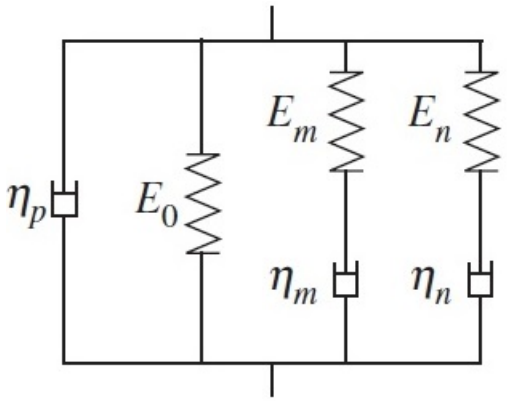

Figure 2.18: Physical model representation as reported by Paul [50]

$$\sigma = E_0\varepsilon + \eta_p\dot{\varepsilon}^p + \eta_m\dot{\varepsilon}^m\left[1 - exp\left[\frac{-E_m\varepsilon}{\eta_m\dot{\varepsilon}^m}\right]\right] + \eta_n\dot{\varepsilon}^n\left[1 - exp\left[\frac{-E_n\varepsilon}{\eta_n\dot{\varepsilon}^n}\right]\right] \tag{2.14}$$

The stress in such a nonlinear viscoelastic model, as demonstrated in equation (2.14), is found by integrating equation (2.15):

$$\sigma(t) = E_0\varepsilon + \eta_p\dot{\varepsilon(t)}^p + \int_0^t E_m\varepsilon(\dot{\tau})^m e^{\frac{-E_m}{\eta_m}(t-\tau)}d\tau + \int_0^t E_n\varepsilon(\dot{\tau})^n e^{\frac{-E_n}{\eta_n}(t-\tau)}d\tau \tag{2.15}$$

Paul then presents the stress for a constant strain rate as described by equation (2.14). However, two issues arise. The first is that the equation is not that which is found through integration of

equation (2.15). Secondly, if the units, per component, of equation (2.14) are investigated, these are unable to provide the unit of stress (Pa), specifically with respect to the strain rate power law term, however, this model still provides a good initial fit to the data, though it cannot be used to represent the behaviour of bone. This is further discussed in Section 7.2 - 7.3.

2.6.4 Alternative possible numerical techniques

Ricatti Equations

Analytical solutions to nonlinear differential equations only exist for a small family of problems. If the nonlinearity is limited to the Maxwell form,

$$\sigma_{spring} = K\varepsilon_1^m \tag{2.16}$$

$$\sigma_{dashpot} = \eta\varepsilon_2^{\frac{1}{n}} \tag{2.17}$$

$$\varepsilon = \varepsilon_1 + \varepsilon_2 \tag{2.18}$$

$$\frac{1}{mK^{\frac{1}{m}}}\sigma^{\frac{1-m}{m}}\dot{\sigma} + \frac{\sigma^n}{\eta^n} = \dot{\varepsilon} \tag{2.19}$$

where ε_1 and ε_2 represent the strain for the nonlinear spring and damper with m and n representing a parameter for the degree of nonlinearity, η and K represent the viscosity and stiffness respectively as previously stated, then a Ricatti equation is formed as shown in equation (2.19). Monsia [45] presents a solution to the homogeneous problem, on the basis of a linear strain path, but does not present the particular solution which is required in order to model a physically meaningful problem.

Fractional Calculus

Fractional calculus has recently become a new method and topic of discussion when researching viscoelasticity [64, 46, 18, 37, 23, 28, 55], even though Koeller [37] began introducing the application of fractional calculus to the theory of viscoelasticity in 1984. Fractional calculus is primarily used as a method to describe hierarchical structures which may be represented by the layout in Figure 2.19.

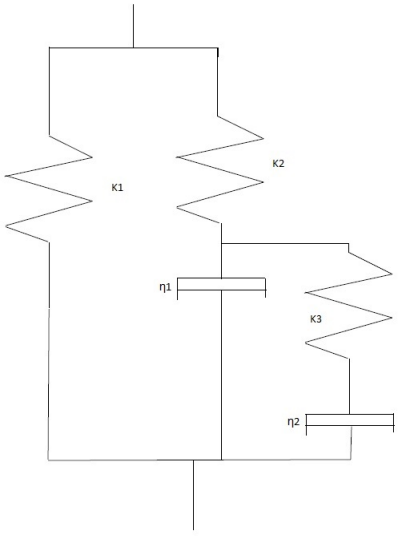

Figure 2.19: Representation of a hierarchical model

Additional branches may be added in order to increase the hierarchical level of the overall system, and thus delay or introduce system complexity, however, these branches will not increase

the overall stiffness. The addition of branches will instead vary the response of the system. This may be seen if the dashpots are to lock (no damping effect), the system will effectively be two branches consisting of a branch with a single spring and a second branch with multiple springs. Due to this behaviour, linearly based hierarchical systems are not able to capture the acute transition in strain rate sensitivity. If the fluid within the damper is to be filled with a nonlinear viscous fluid, the acute transition could possibly be described, however, a standard nonlinear numerical model could instead be used to describe the behaviour. The reason for pursuing linear fractional viscoelastic systems was to verify whether a linear model could describe the acute transitional behaviour without the need for introducing nonlinearities. Unfortunately as this is not the case, it was decided not to pursue fractional calculus any further for the scope of this project.

Chapter 3

Design and fabrication of the intermediate strain rate apparatus and gas gun

3.1 Introduction

In order to begin intermediate strain rate testing on bone, fabrication, design, and modifications for the intermediate strain rate apparatus and respectful gas gun are required. Originally, the apparatus was designed by Cloete and Oxtoby in 2009 [12], however, in 2013 Stander [57] and Paul [50] began further work on the previously developed prototype. The apparatus to be designed within this project will therefore consist of a reiteration and improvement of the work previously performed.

This chapter will detail the following points:

- A brief history into the design and development of the original intermediate strain rate testing apparatus.
- A discussion with respect to the proposed modifications.
- A further discussion into the development and alterations performed during fabrication of the apparatus.
- The details associated with respect to the design of the accompanying gas gun.

3.2 Original intermediate strain rate apparatus design

As mentioned, the original apparatus concept was designed and presented by Cloete and Oxtoby [12] in 2009. This is shown in Figure 3.1.

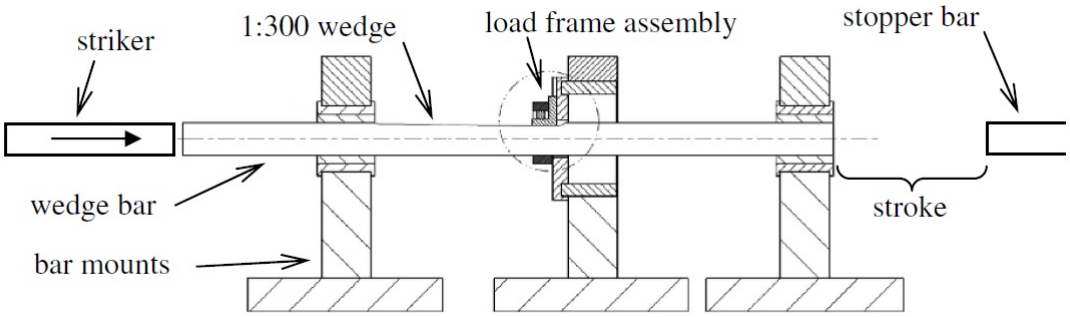

Figure 3.1: A new intermediate strain testing method presented by Cloete and Oxtoby in 2009 [12]

The concept utilises a sliding anvil (which is machined to match the angle of the wedge in the incident bar), a load frame, and a backing plate. The design is to ensure purely vertical compression of the specimen. Issues with this concept arrived as the load frame was not able to provide sufficient damping of the impact vibrations. Even though the apparatus proved the concept that intermediate strain rate testing is possible using this method, the way in which the apparatus was designed required major modification. The next iteration of the concept was performed by Stander and Paul. The new design consisted of a load frame with the load cell being placed within this load frame. A load frame is introduced which will not deform under impact loads and will sufficiently absorb vibrations and noise which may come from the initial impact. The change in concept from Oxtoby to Stander and Paul is demonstrated in Figures 3.2 and 3.3.

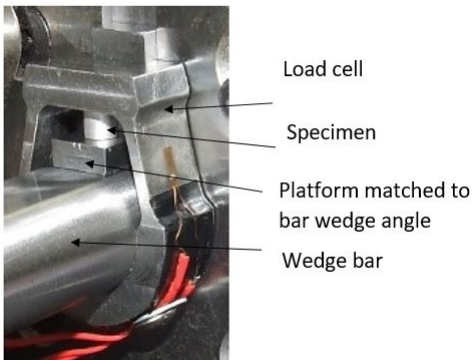

Figure 3.2: Intermediate strain rate apparatus design presented by Oxtoby [12]

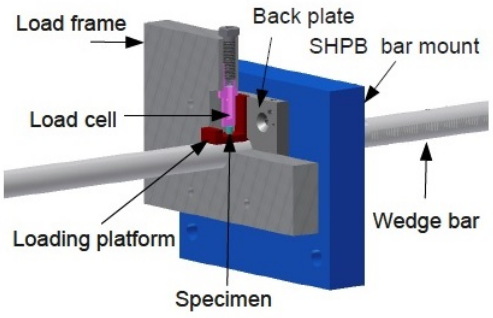

Figure 3.3: Intermediate strain rate apparatus design presented by Stander [57]

However, the prototype produced was based on a short term proof of concept basis and the rigidity of the design played an issue during testing as reported by Stander. As the design works efficiently and has been consistently tested in the current state, the aim of the final concept will be to refine and perfect the work performed by Stander [57].

3.3 Final intermediate strain rate apparatus concept

3.3.1 Introduction

Using the concepts and discussions presented by Oxtoby, Paul, Stander, and Cloete, the following modifications and improvements are discussed and implemented into the final design of the apparatus:

- The apparatus must be constructed upon a single rigid structure which is fastened to the testing bed. This will remove the possibility of undesired vibrations occurring in the load frame during testing as the axial load will now be fully supported.
- The load frame size is to be increased in order to improve damping effects and subsequently lower the overall noise of the recorded data.
- The load frame is to have a support structure of its own which is bolted to the rigid structure, mentioned above, prior to mounting upon the test bed. This is to prevent testing vibrations from directly influencing the data pre, during or post-test as the gas gun and stopper for the stopper bar are mounted to the same test bed.
- The overall testing apparatus is required to be heavy in order to reduce testing vibrations and increase overall rigidity.
- The load cell major body diameter is to be increased. This allows for a necked region to be machined upon which the strain gauges may be placed. Due to the change in diameters, the strain gauges are now protected during installment of the load cell within the load frame.

3.3.2 Detailed design modifications

The following modifications have been made to the final design:

- In order to ensure rigidity of the design, the entire concept was decided to be placed upon a single C beam which would coherently fit onto the I beam bed present within BISRU testing laboratories. In order to prevent torsion of the C beam due to manufacturing, a secondary flat 10 mm beam is placed underneath. This also acts as a raiser for the entire system. This is required in order to level the system with the corresponding gas gun and stopper bar. Furthermore, the addition of this flat beam adds weight and rigidity to the design. Once placed upon the I beam, the rig is leveled using M16x1 fine thread bolts. Once leveled, the rig is fastened against the test bed.
- The load frame is increased by doubling the thickness. This allows for an increased load cell diameter to be utilised. The benefits of increasing the load frame size is to increase the inherent damping ability of the cast iron. The damping ability originates due to the nature of cast iron manufacturing, the microstructural grain arrangement is scattered which prevents internal stress concentrations from occurring at the edges. The scattering of grains allows for the internal stresses generated to be dissipated quickly and effectively.
- The load cell major diameter is increased to allow for a stiffer load cell within the load frame. Subsequently, the minor diameter where the strain gauges are placed is decreased in size. This prevents any damage to the strain gauges during installation or change over of the load cell occurs. This is shown in Figures 3.4 and 3.5.

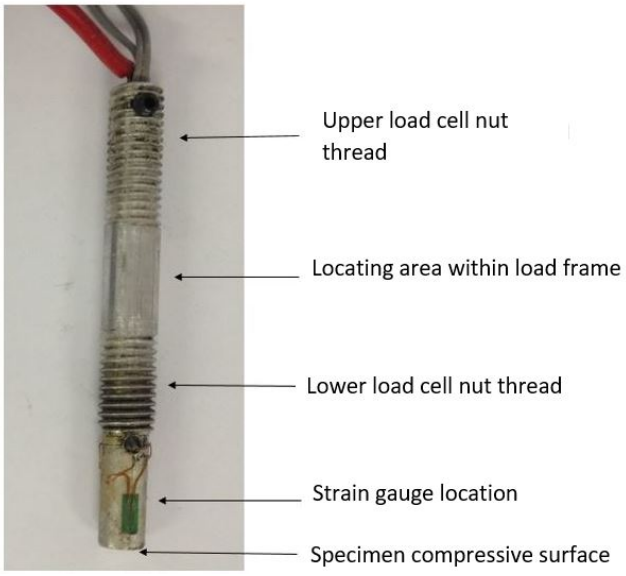

Figure 3.4: Load cell as designed by Paul [50]

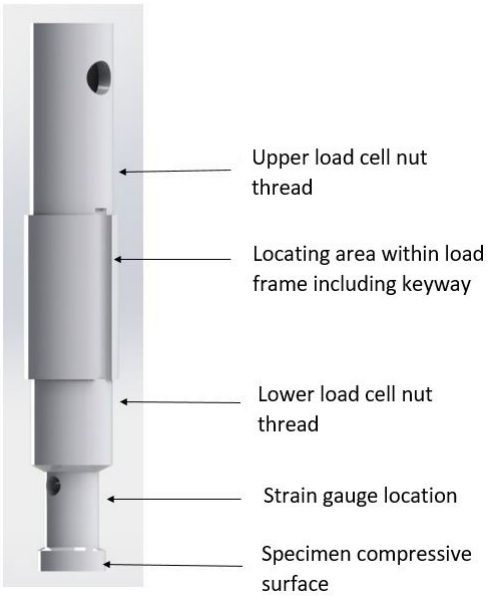

Figure 3.5: Load cell as designed in collaboration with Ms Kelsey Hilton

The generated final concept is presented in Figures 3.7 and 3.8.

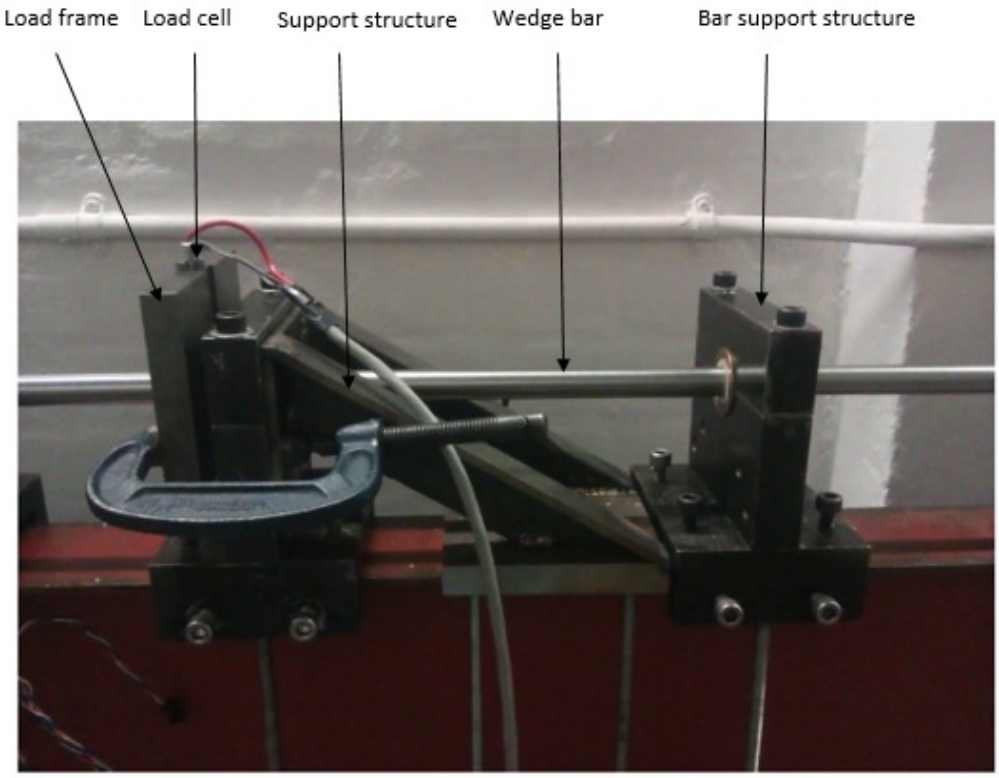

Figure 3.6: Previously used configuration as reported by Paul [50]

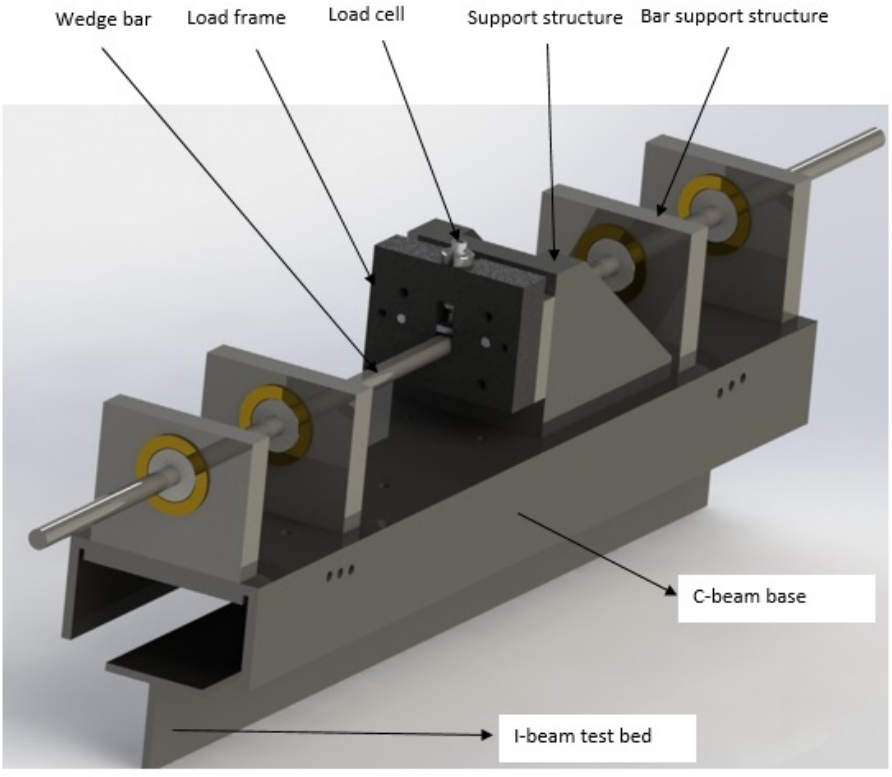

Figure 3.7: Intermediate strain rate apparatus final concept overview

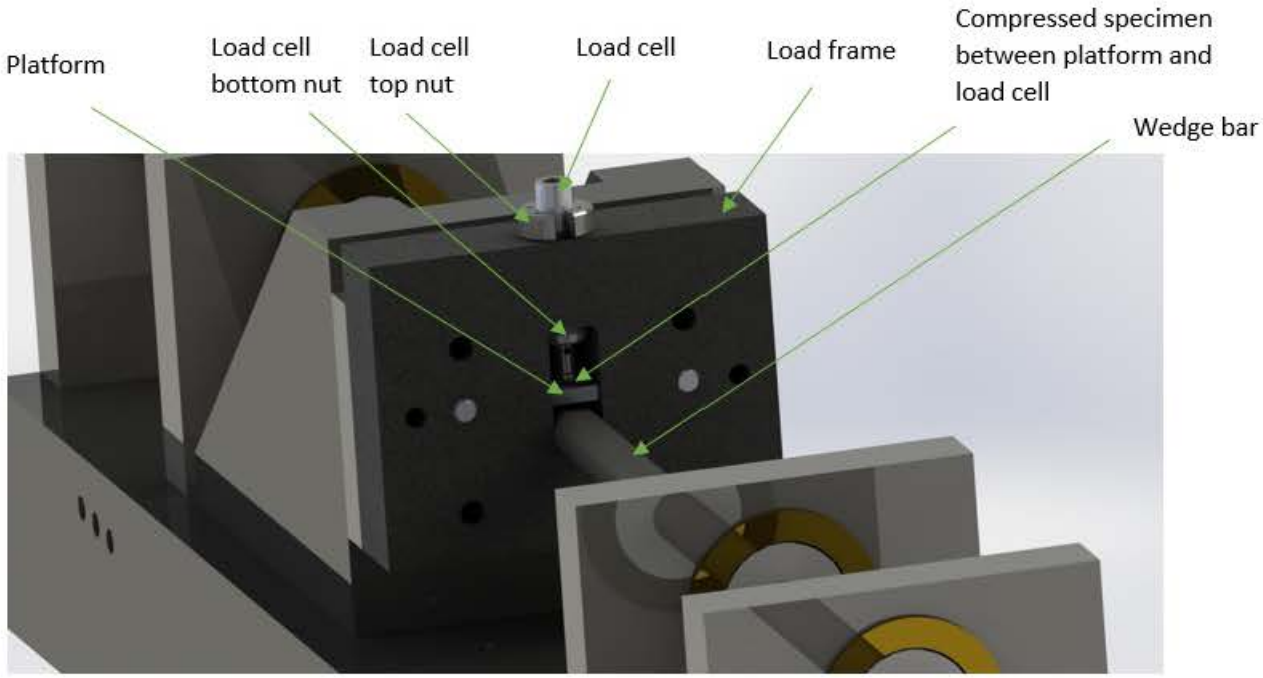

Figure 3.8: View of load cell arrangement within load frame

From Figures 3.7 and 3.8, it is clearly shown that the load frame and subsequent parts are now no longer free standing. The frame is fastened against a support which in turn is clamped to the I beam bed. In order to support various length bars, additional supports are added at set distances from the load frame.

3.3.3 Post fabrication design modifications

As the current design is a reiteration of previous prototypes, the current design itself will need to be re-iterated. Upon construction of the design described, the following issues arose:

- The collars used were taken from the existing apparatus as the wear was originally thought to be negligible. However, during commissioning of the design, these collars were found to be significantly worn which provided a loose sliding fit and subsequently introduced noise into the apparatus.
- The load cell pre-load nut presses against the internal walls of the load frame due to chamfers being machined upon the load frame as a result of machine restrictions.
- The load cell began to rotate during calibration of the pre-load, experienced by the specimen, which subsequently resulted in an inconsistent pre-load setting reading.

In order to clearly gauge the alterations to be performed, Figure 3.9 demonstrates the current load cell/load frame configuration:

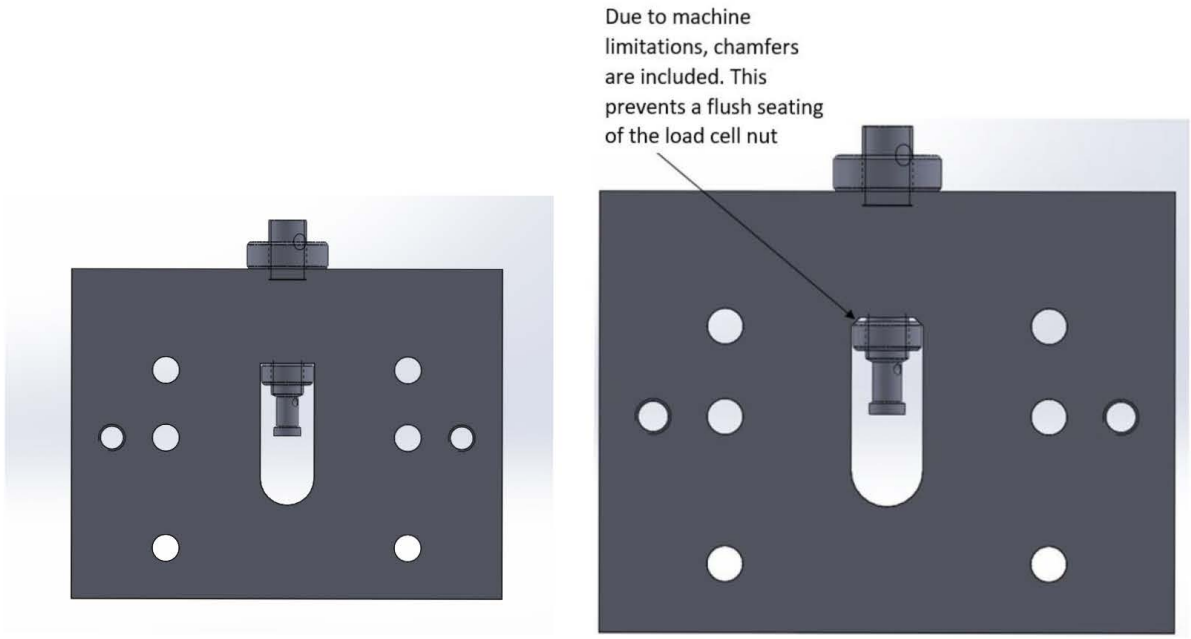

Figure 3.9: Designed vs constructed load frame/cell assembly

The following modifications are therefore performed:

Collars

Due to the Teflon collars used being part of the previous concept, significant wear, approximately 0.5 mm in diameter, is present. This wear results in increased vibration of the bar upon impact and so introduces undesired noise. New collars are machined with close sliding tolerances in order to accommodate smooth movement of the bars used within the set up. Due to the close sliding tolerance, any possible vibrations are removed within the bar allowing for a smoother load cell output reading.

Load cell pre-load nut

The following designs have been generated and modified in collaboration with Kelsey Hilton. Initially, the load cell pre-load nut was designed as follows:

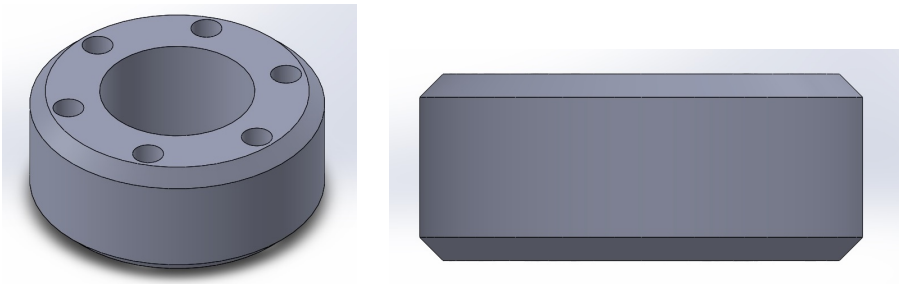

Figure 3.10: Initial pre-load nut design detailing isometric (left) and side (right) views

However, as internal 90 °angles are difficult and expensive to machine, chamfers were added to the load frame. The addition of these chamfers resulted in a decrease of the tightening area for the nut. The current nut is then modified as demonstrated, in Figure 3.11, in order to fit the machining limitation:

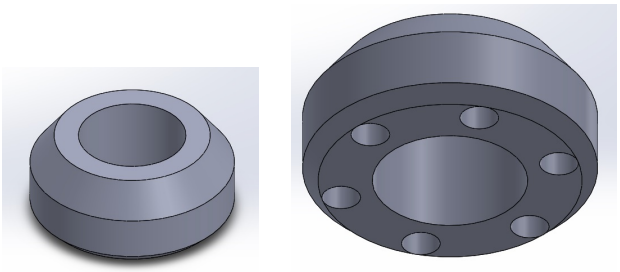

Figure 3.11: Modified pre-load nut design detailing top (left) and bottom (right) isometric views

Load cell rotation

Within the initial design, it was never anticipated that the load cell should rotate during the initial pre-load setting. The decision was based on previous designs not requiring a key for the set up. However, upon completion of the design, the initial pre-load is not sufficient to prevent rotation of the load cell. This rotation impacts the testing by changing the magnitude of pre-load upon the specimen, which in turn contributed to a greater compliance value for the entire system. This prevents repeatability for the compliance tests resulting in the data displaying no distinct pattern among tests. In order to prevent this rotation, a cylindrical key is added to the load cell/frame set up. This is made possible by the initial decision to increase the diameter for the body of the load cell. A 3 mm diameter key is used.

Final design iteration

The final design with all relevant modifications is displayed in Figure 3.12.

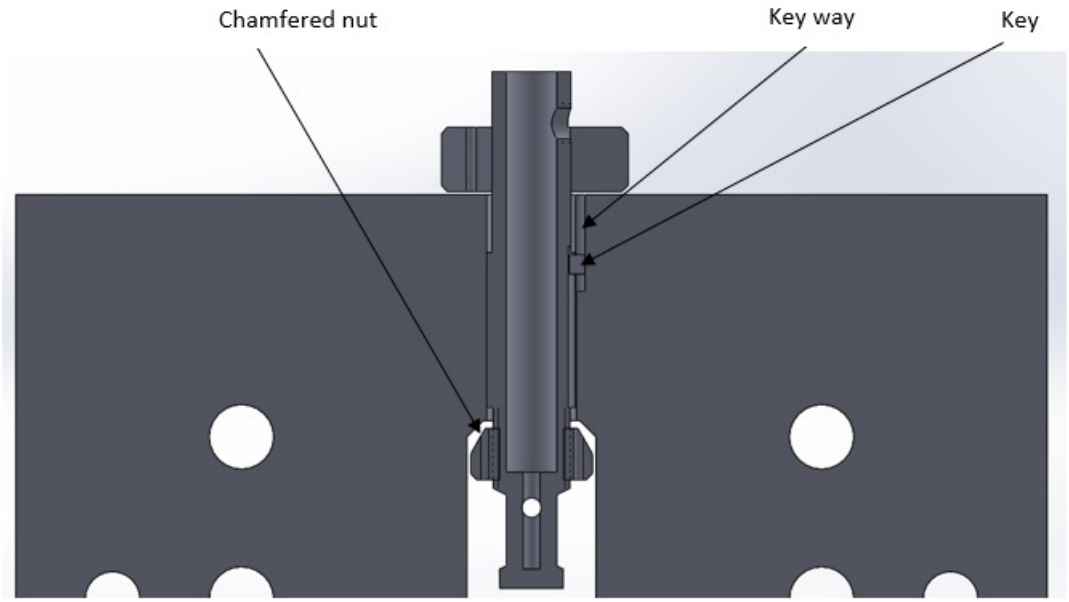

Figure 3.12: Final load frame design with emphasis on the internal key

For comparative purposes, images of the constructed intermediate strain rate testing apparatus are displayed. Final technical drawings may be viewed in appendix A-1.

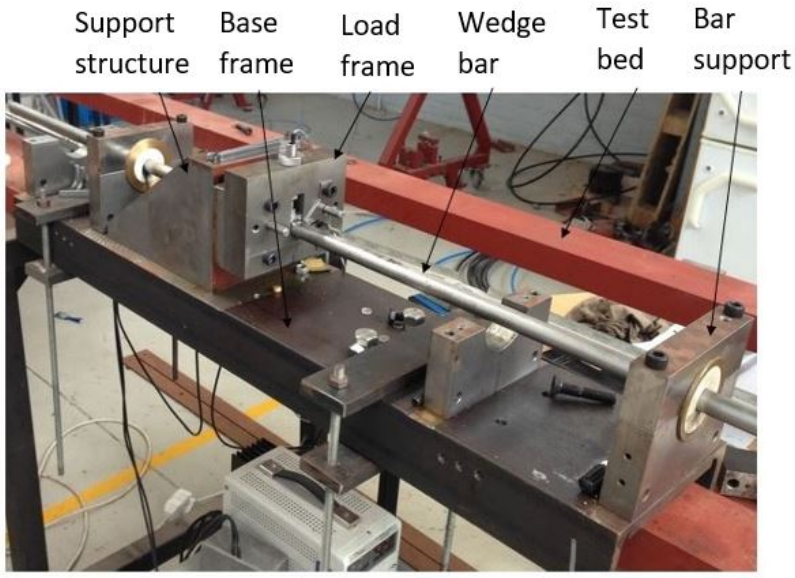

Figure 3.13: Commissioned intermediate strain rate apparatus

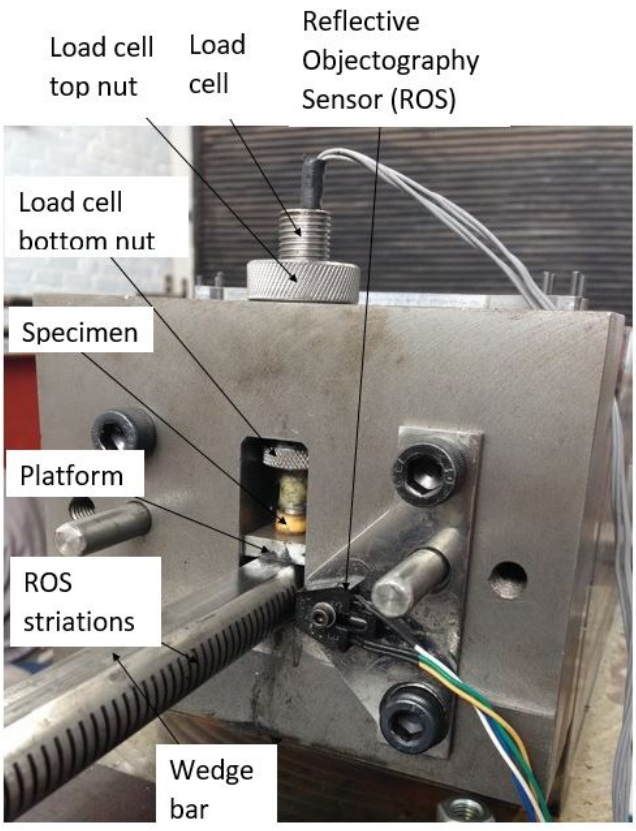

Figure 3.14: A close view of the load frame with the load cell and subsequent features installed

3.4 Gas gun design

3.4.1 Introduction

In order to propel the striker bar at the correct velocity, a gas gun is required which will satisfy the following requirements:

- The gas gun is to propel a 1.5m long, 20mm diameter round bar striker at a velocity of 10m/s using approximately 5 bars of compressed air pressure.
- Allow for safe operation to a maximum pressure of 10 bars.
- The gas gun must be designed with multiple safety aspects installed while allowing for ease of assembly and maintenance.

3.4.2 Design procedure

Previously, a gas gun had been designed by Stander [57], though this catered for pressures ranging over 10 bars. For the purpose of the intermediate strain rate apparatus, the gas gun originally designed is to be modified to perform under the specified conditions.

Modifications performed

The gun dimensions were chosen on the basis of exit velocity (see section, 4.3.2.1, for theoretical velocity calculations). A spread sheet is created which allows for the variation of chamber volumes vs. the barrel exit velocity. Once the correct exit velocity matches the set pressure, the chamber volumes are verified against the Sound Engineering Practice Table within SANS 347:2012, Edition two, Figure 2: Graph for vessels - Non-dangerous gasses.

Modifications performed include:

- Aluminium is to be the material of choice for this gas gun. This was decided due to the low cost of aluminium, ease of manufacturing, ease of purchase, and anti-corrosion and light weight properties. Further, following the SANS 347:2012, edition two, the material can be used for the manufacturing of a pressure vessel provided the hoop stresses do not exceed the yield point.
- Due to the nature of the material being softer than steel, stainless steel tie rods will be machined in order to fasten and hold the entire system together. This is due to the low tensile strength of threaded aluminium .
- A single pressure line will feed both chambers of the gas gun to provide a pressure equilibrium between the chambers. This is performed to prevent differential filling and misfire of the gas gun. The chambers, however, will be filled using two separate valves installed to allow for separate filling in a distinct sequential order. This provides an additional level of safety for the design.
- The valves used will be lockable ball valves in order to provide security when the gun is not operated or supervised.

Final Design

The final design for the gas gun is shown in Figures 3.15, 3.16, and 3.17 with detailed drawings appearing in appendix A-2.

Figure 3.15: Gas gun overview

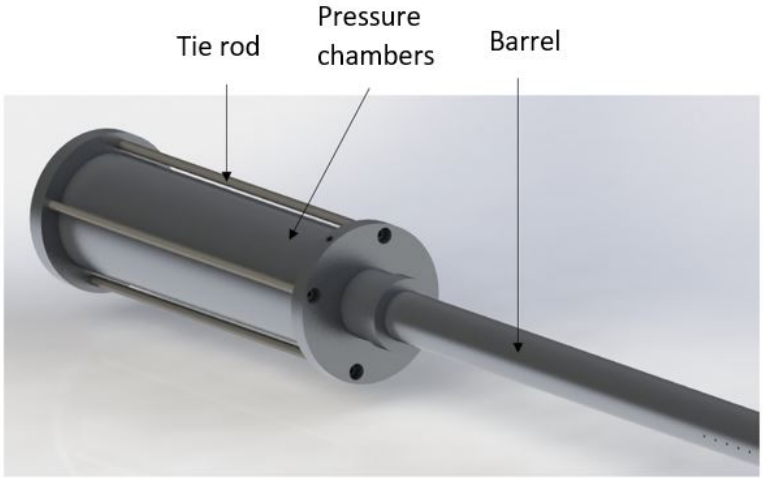

Figure 3.16: Gas gun pressure vessel view

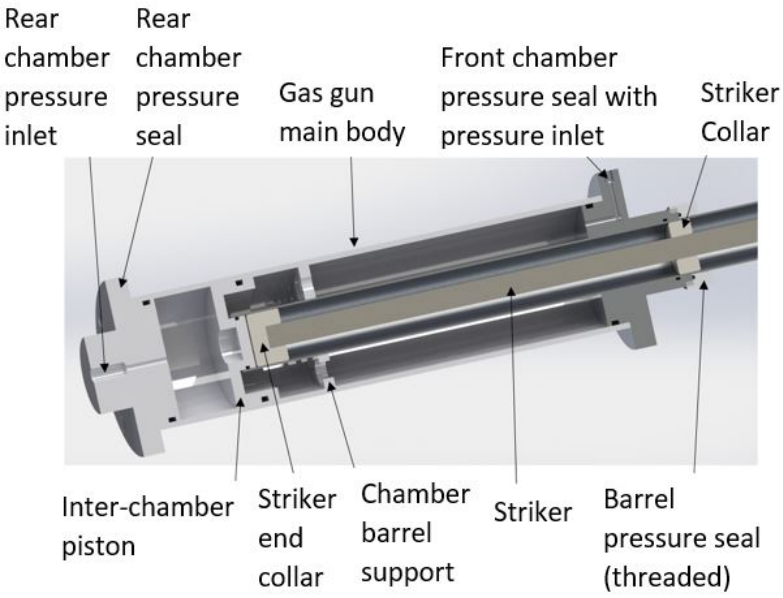

Figure 3.17: Sectioned gas gun pressure vessel view

For comparative purposes, images of the constructed gas gun are displayed:

Figure 3.18: Front length view of the constructed gas gun

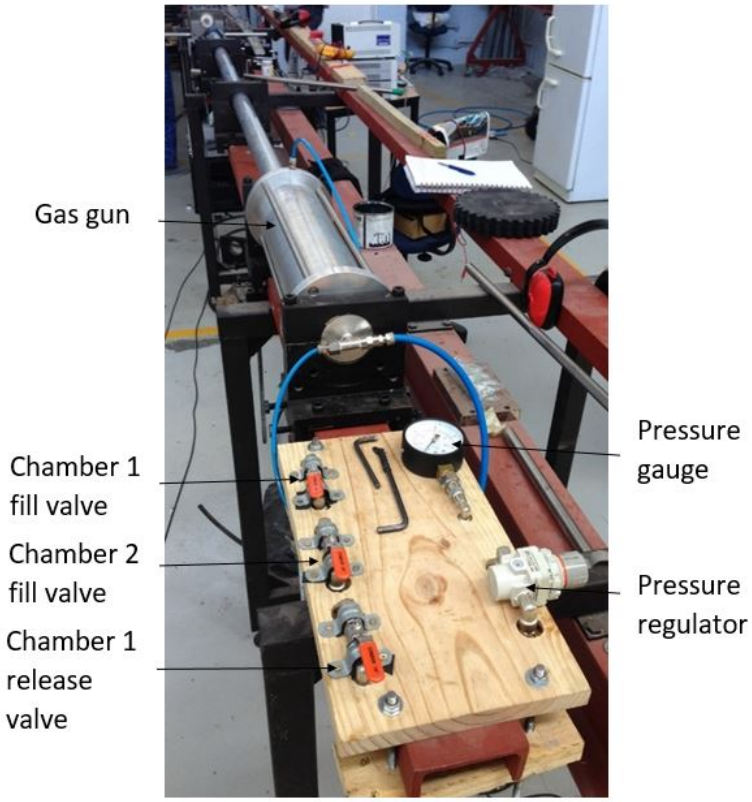

Figure 3.19: Rear length view of the constructed gas gun and accompanying control panel

Design discussion:

- To prevent damage to the O-rings when assembling the chamber ends, slight tapering on the chamber ends was required.
- In order to create a light weight piston, all available excess material is machined off. This allows for slightly higher pressure sensitivity and enables the ability to perform at lower pressures. The piston end of the chamber is also polished to enable smooth movement and prevent any undesired movement past the barrel opening within the chamber.
- In order to achieve the desired velocity, the length from the internal barrel opening until the flutes is calculated to be 1m as per discussion with Mr Trevor Cloete. However, once the striker collar passes these flutes, support for the striker is required. For this purpose, an additional barrel length, equal to that of the striker is added. This prevents the striker from accidentally exiting the gas gun or losing support during testing or post-testing.
- In order to securely mount the barrel to the main body of the gun, welding of the collar to the barrel is required. Welding, above brazing and adhesives, is concluded upon as it creates a secure uniform bond between the two components. For the pressures in discussion, welding is considered as a more reliable bond, however, worries arose as to whether warping would occur of the barrel, but, under preliminary testing on spare barrel lengths, warping did not occur. Welding was therefore decided upon as the means of bonding these two components together.

Chapter 4

Experimental Method

4.1 Introduction

To begin testing the bovine bone specimens, the apparatus is required to be set up and calibrated. This chapter will present the following key points:

- The methodology followed during the preparation, manufacturing and storage of the acquired bovine bone samples.
- The calibration methods performed for each machine component used for testing.
- A description into the analysis methodology applied to the tested specimens to provide accurate results.
- The preliminary testing results and analysis used for calibration of the machinery.

4.2 Specimen preparation

4.2.1 Manufacturing discussion

Two separate deliveries were made for bovine femoral bone due to supply constraints. During manufacturing of the samples from the first delivery, an observation was made by Mr Charles Harris, designated machinist, that the femoral mid diaphysis wall thickness has been decreasing over the time that Mr Charles Harris has been manufacturing specimens for Mr Trevor Cloete. The thickness of the wall of the bovine femoral mid diaphysis, from the same supplier, has decreased from a nominal thickness of approximately 10mm to that of approximately 5mm as shown in Figure 4.1.

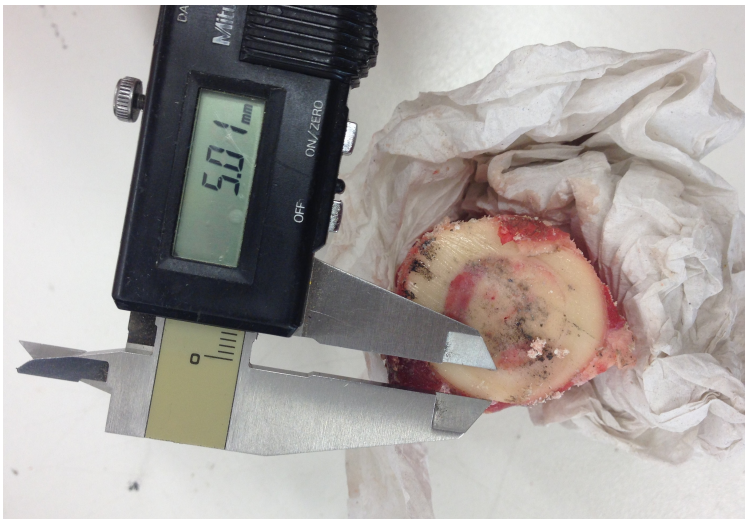

Figure 4.1: Bovine femoral mid diaphysis wall thickness

This may be due to a younger slaughter age of the bovine, the use of different feeding schemes applied, a decrease in physical activity, or a decrease in living conditions.

Due to the decrease in wall thickness, specimens are now only able to be of approximately 4-4.2 mm in diameter and length.

Upon delivery of the second bovine femoral samples, which were noted to be grass-fed bovines, the wall thickness was investigated and found to be in the range of 9-11mm. However, 4-4.2mm specimens are still manufactured to determine if the changes in overall bone dimensions have any effect on the material properties. The reason for the variance in bone wall thickness is not known, however, grass-fed bovine are more likely to walk around opposed to grain-fed bovine. This is based on the assumption that grain-fed bovine are more likely to be confined to feed lots and subsequently are not able to roam. Due to the increase in activity of grass-fed bovine, there bones should naturally strengthen [30]. The variation in bone wall thickness is seen as a positive though as this will allow for a more comprehensive data set to be obtained. This is particularly useful for determining the behaviour of bone irrespective of the source.

Unfortunately it was not possible to attain the time from slaughter until freezing, or the handling procedure, of the bovine prior to purchasing the samples and so effects due to this are unable to be assessed.

4.2.2 Manufacturing of bovine specimens

To begin manufacturing the specimens, the mid diaphysis is firstly cut from the bovine femur and the wall thickness inspected. The bone is then cleaned off of all marrow and connective tissue. This is shown in Figure 4.2.

Figure 4.2: Cleaned bone prior to further machining

Nine such sections are manufactured as three bones are used for each orientation. This allows inter-bone variation to be recorded. Once cleaned as described, the samples are machined into specimens with the respective orientations. In order to extract the specimens from the bulk bone sample, Mr Charles Harris fabricated a custom 4.2 mm core drill, Figure 4.3, to be able to extract samples from the radial and transverse orientations. The need for a custom core drill arises due to the bone machine dust forming a cement like structure when water is introduced as coolant and subsequently accumulating on the teeth of a standard core drill, reducing its effectiveness.

Figure 4.3: Custom fabricated 4.2 mm core drill for the machining of specimens

4.2.2.1 Radial

For the machining of the radial specimens, the cleaned sample is placed into a vice and rotated so that the core drill lies perpendicularly to this axis. The core drill is then used to extract the samples as shown in Figures 4.4 and 4.5.

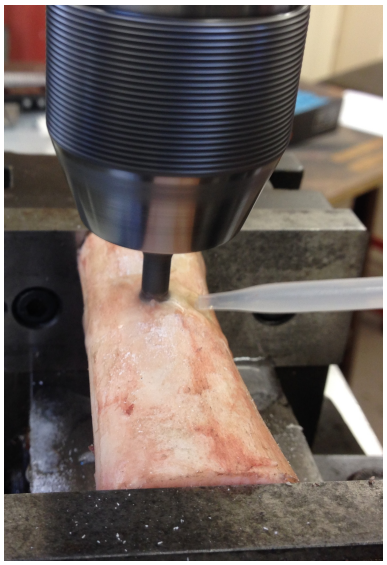

Figure 4.4: Sample core drilling

Figure 4.5: Sample showing where specimens were extracted

The extracted samples are placed into a brass sheath which allows for the lathe to grip the specimen. These are faced off at either end in order to create a clean, flat sided specimen.

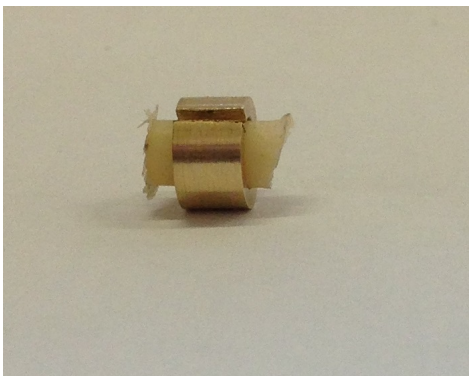

Figure 4.6: Specimen sheath prior to machining

Figure 4.7: Facing of specimens on the lathe

Once faced, the specimens dimensions are recorded and the specimen is placed within the physiological saline solution. These are frozen in the biological freezer at -32°Celsius.

4.2.2.2 Longitudinal

For manufacturing of the longitudinally orientated specimens, the cleaned bone is firstly sliced, using a band saw, into sections. To allow for the lathe to easily grip the section, an end is ground into a circular shape.

Figure 4.8: Longitudinal bone sections with sanded ends

These sections are then placed into the lathe and machined to the correct cylindrical diameter. This is performed in several stages to retain the structural strength of the section during machining as otherwise the cylinder will fracture. This is demonstrated in Figures 4.9 and 4.10.

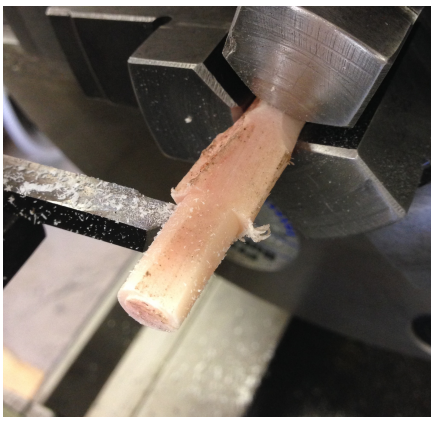

Figure 4.9: Specimen machining in order to obtain a circular shape

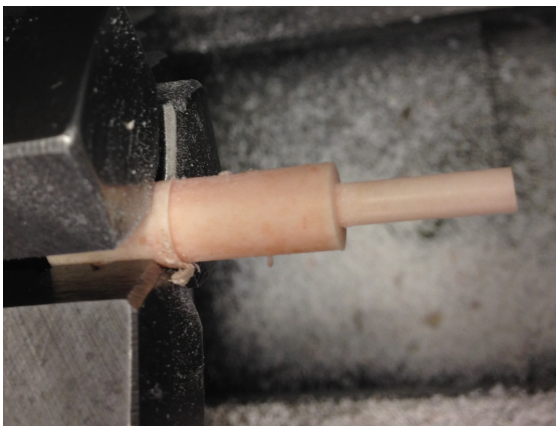

Figure 4.10: Specimen machining in order to obtain correct diameter

Once the required diameter is reached, the specimen is cut using a custom blade fabricated by Mr Charles Harris. The specimens dimensions are measured and the specimen is stored in a physiological saline solution. These are frozen at -32 degrees Celcius in the biological matter freezer.

4.2.2.3 Transverse

In order to machine the transversely orientated specimens, a portion of the cleaned bone is firstly removed in order to access the circumferential thickness. The core drill is used to drill the profiles of the specimens. Once sufficient specimens have been drilled, a portion is cut from the sample in order to retrieve these specimens. This is demonstrated in Figures 4.11 - 4.13.

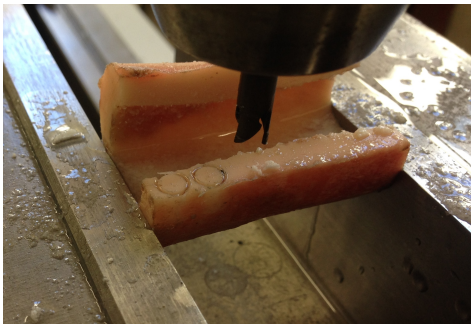

Figure 4.11: Core drilling of the sample showing cut out section

Figure 4.12: Sample cutting in order to retrieve cored specimens

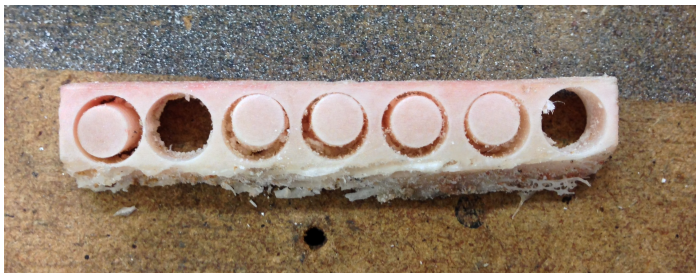

Figure 4.13: Cut sample section demonstrating specimen retrieval

The specimens obtained are placed into a brass sheath and machined as performed in the radial specimen orientation manufacturing, shown in Figures 4.6 and 4.7. The specimens are stored in a physiological saline solution and frozen at -32 degrees Celsius in the biological matter freezer.

4.3 Testing apparatus

To perform the required testing at the designated strain rates, the following equipment is to be used:

- Zwick quasi-static mechanical testing apparatus - for quasi static tests ranging 0.001/s - 0.1 /s strain rate
- Intermediate strain rate apparatus - for intermediate strain rate testing ranging 1/s - 50 /s strain rate

4.3.1 Quasi-static mechanical testing apparatus (Zwick) - quasi static strain rate

The Zwick quasi-static testing apparatus, manufactured by the Roell Group, is used in conducting tests within the quasi static regime. As stated in the literature review, multiple authors have used variations of this machine to generate accurate stress/strain data.

4.3.1.1 Pretest set up and calibration

Previously, when utilising the Zwick quasi-static mechanical testing apparatus, Bekker *et.al* [7] and Paul [50] utilised the 200kN load cell. However, such a high rated load cell is unnecessary as bone tends to fracture at forces less than 5kN [50]. Using a load cell rated significantly higher than the specimen fracture strength may skew the data as the load cell will not be sensitive enough. For the purpose of the testing performed, the Zwick quasi-static mechanical testing apparatus is fitted with a 10kN load cell. A shield is placed in position around the testing anvil to provide protection from biological material scattering in the event of a violent fracture. The specimen is placed upon a tungsten carbide platform which aids in the position and removal of the specimens. Tungsten carbide is selected in particular as the deformation of the material will be well within the elastic regime and of negligible magnitude under the forces in discussion. The test set up is demonstrated in Figure 4.14.

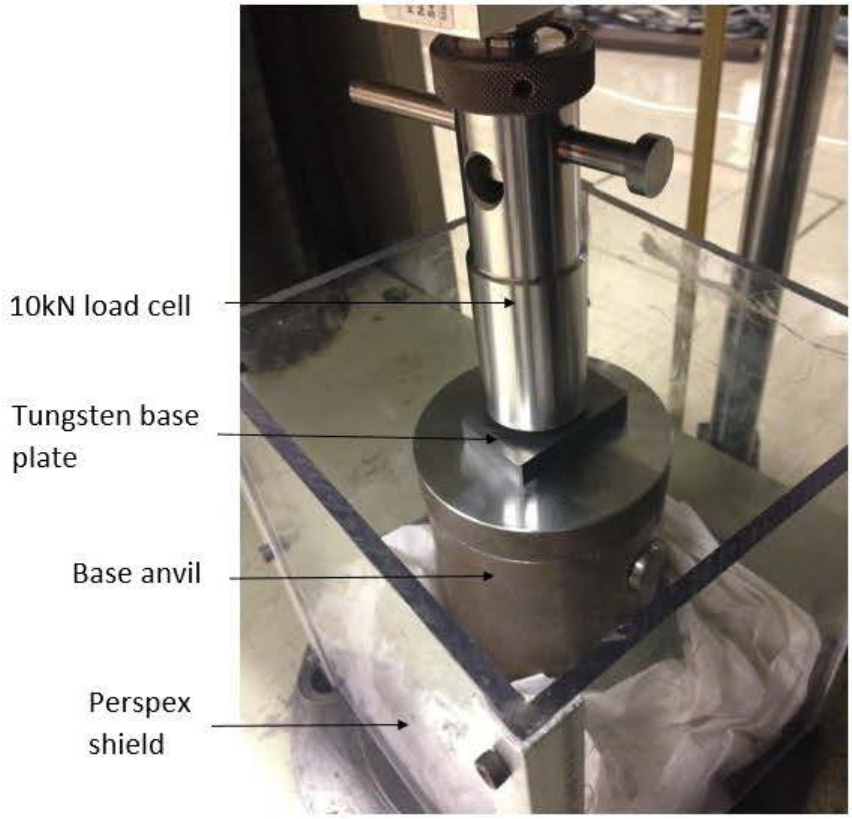

Figure 4.14: Zwick quasi-static mechanical testing apparatus set up

In Figure 4.14, the base anvil is shown with the clear Perspex shield in place. The space between the base anvil and shield is filled with absorbent tissue to prevent biological contamination of the machine in the event of serious fracture. Beneath the load cell, the tungsten carbide platform may be seen.

Compliance

Prior to testing, the compliance value for the Zwick quasi-static mechanical testing apparatus set up is required. Tungsten carbide is used as the base plate for the specimens due to its rigid nature. Repeated compression tests are run on the base plate which generates a linear trend as shown in Figure 4.15.

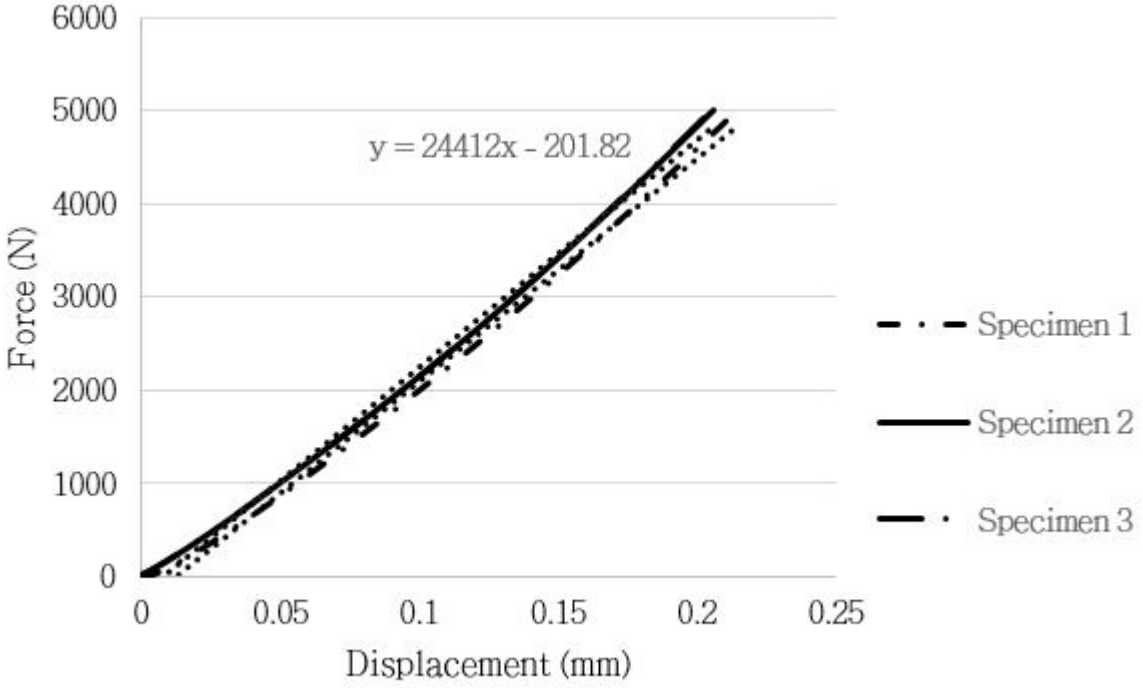

Figure 4.15: Example of the Zwick quasi-static compliance tests performed and the linear trend lines applied

The gradient of each test is calculated and an average value is taken for calculation purposes.

- 16.2 kN/mm - Radial testing (testing session 1)
- 25.4 kN/mm - Longitudinal and transverse testing (testing session 2)
- 25.8 kN/mm - Longitudinal testing (testing session 3)
- 26.9 kN/mm - Radial and transverse testing (testing session 4)

The results show the variance in compliance over the testing sessions and so it is important to consider the compliance of each individual testing session. The lower compliance value recorded on session one may be attributed to a less stiff test setup. However, after compliance removal is performed, the recorded data from session one corresponds with the data recorded on session four.

4.3.1.2 Data analysis

Analysis of the data is performed using Matlab R2014b student edition provided by the University of Cape Town. Raw data captured by the Zwick quasi-static mechanical testing apparatus software is processed in the following steps:

1. Raw data is contracted in order to eliminate post failure characteristics.
2. Smoothing is performed using a five point moving average method.
3. The gradient between the data values is determined.
4. The maximum gradient is identified with a 10 % window in order to determine the average gradient of the linear portion of the data. A value of 10 % is decided upon as this provides enough data for an accurate linear regression.
5. The linear regression is performed on the data which coincides with the 10 % window from maximum gradient as stated above.
6. The x intercept is calculated for the linear regression and applied to the data in order to zero the data. This allows for the initial take up zone to be removed.
7. The compliance is removed and the apparent modulus is calculated from the linear portion of the data.

This is displayed visually in Figures 4.16 and 4.17.

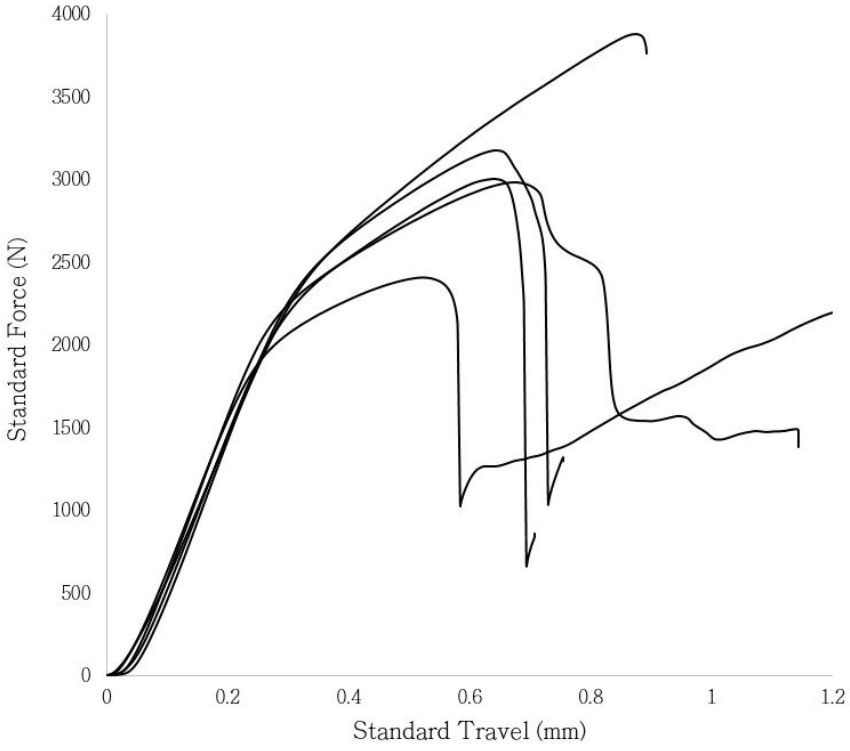

Figure 4.16: Example of recorded raw data within radial orientation at a strain rate of 0.01/s

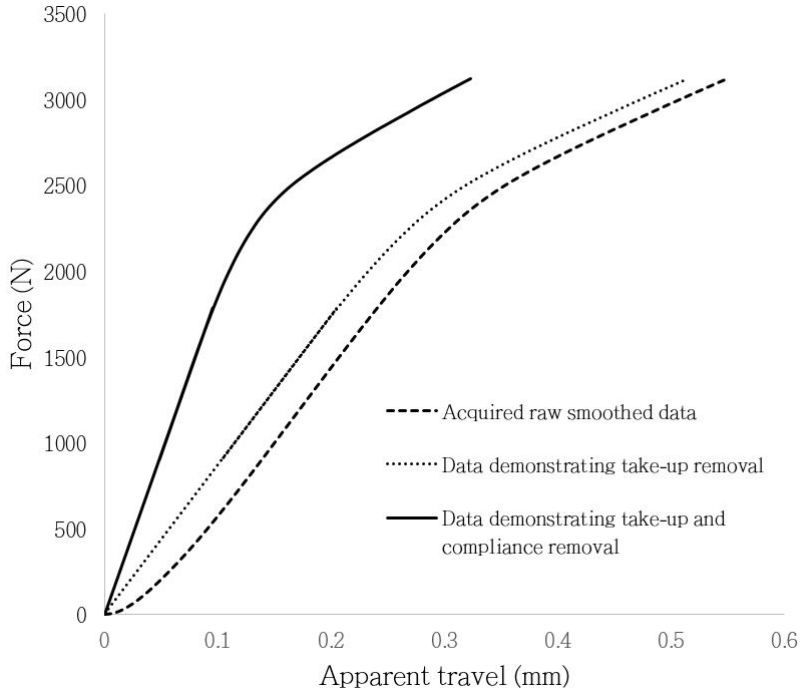

Figure 4.17: Example of the analysis performed for removing compliance

4.3.2 Intermediate strain rate apparatus

4.3.2.1 Calibration

Load cell

Prior to any initial testing the load cell, designed in collaboration with a MSc Eng student within BISRU UCT (Kelsey Hilton) is calibrated. This is attained using the Zwick quasi-static mechanical testing apparatus force control mechanism. The test performed uses a manufactured block of tool steel to fasten the load cell in place as it would be within the load frame. A sacrificial specimen of PVC is placed between the 10kN machine load cell and custom built load cell. Prior to calibration, the bridge and excitation voltage is recorded. In order to power the amplifier, the amplifier power supply voltage is always set to 8 V whereas the excitation/bridge voltage used for the strain gauges may not exceed 4 V and 0.04 A. For calibration the Table 4.1 demonstrates the parameters used:

Table 4.1: Parameters used for custom load cell calibration

Amplifier Gain	500
Amplifier Voltage	8.02 V
Excitation/Bridge Voltage	1.63 V
Elasticity Modulus of Material	195 GPa
Strain Gauge Factor - Kgf	2.12

Using these parameters, the raw data generated from the constructed load cell is smoothed and amplified using Matlab until the graph replicates that of the quasi-static mechanical testing apparatus recorded values. Five tests are conducted and the average calibration factor is taken for use within the analysis of the results. This yields an experimental calibration factor of 7206 N/V. If different parameters are utilised, the calibration factor will change. However, it should be noted that the strain measured by the strain gauge bridge is proportional to the output voltage and bridge excitation voltage. Therefore it is possible to express the calibration as a factor of this ratio allowing for freedom to adjust the excitation voltage without needing to recalibrate. Figure 4.18 is an example of the comparison between the two recorded load cell signals:

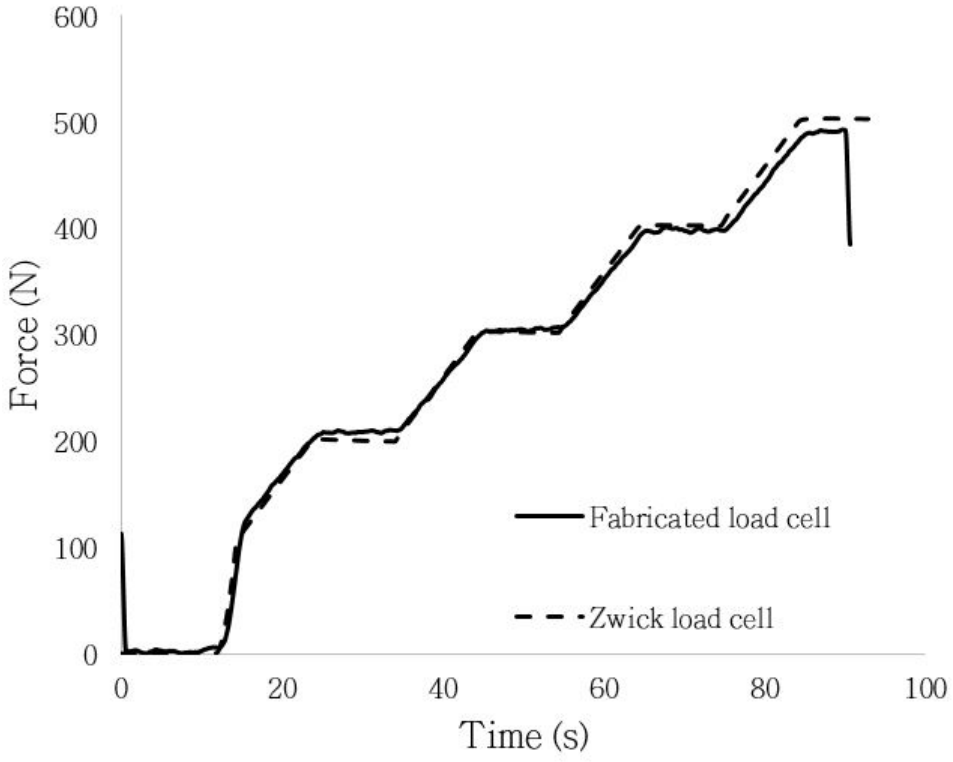

Figure 4.18: Fabricated load cell calibration example

Using the determined parameters, the theoretical load cell calibration factor is calculated using the equation reported by Stander [57]:

$$K = \frac{4.E.A}{Gain.K_{gf}.N.V_{BV}} = 9404.25N/V \tag{4.1}$$

where A is the strain gauged cross sectional area, K_{gf} is the strain gauge factor, E is the load cell material elasticity modulus, Gain is a constant set on the amplifier used, N is the number of strain gauges applied, V_{BV} is the recorded bridge voltage. The theoretical load cell calibration factor is significantly higher than that experimentally determined which may be attributed to the incorrect manufacturing of the load cell dimensions. For the analysis of the data generated, the experimental calibration factor will be implemented.

Striker and incident wedge bar velocity

In order to propel the incident wedge bar, a matching striker bar is required. As the impedances and dimensions of these bars are equal, theoretically, the striker should transfer all momentum to the incident wedge bar. In order to achieve consistent testing, the reliability of the gas gun exit velocity is investigated. This is performed by firing the gas gun at various pressures and measuring the striker speed by means of a light trap. Knowing the distance between the light gates for the light trap and the activation time of each trap, the striker bar exit gun velocity is calculated.
Theoretically, the exit gun velocity is calculated on the assumption of an adiabatic polytropic system with air being the ideal gas. Formulae (4.2) and (4.3) are therefore applied:

$$\frac{P_{barrel}}{P_{(Chamber)}} = \left[\frac{V_{(Chamber)}}{V_{(Chamber)} + V_{(Barrel)}}\right]^{\gamma} \tag{4.2}$$

$$V_{Exit} = \sqrt{\frac{2P_{(Barrel)}A_{(Bar-collar)}L_{(Barrel)}}{m_{(Bar)}}} \tag{4.3}$$

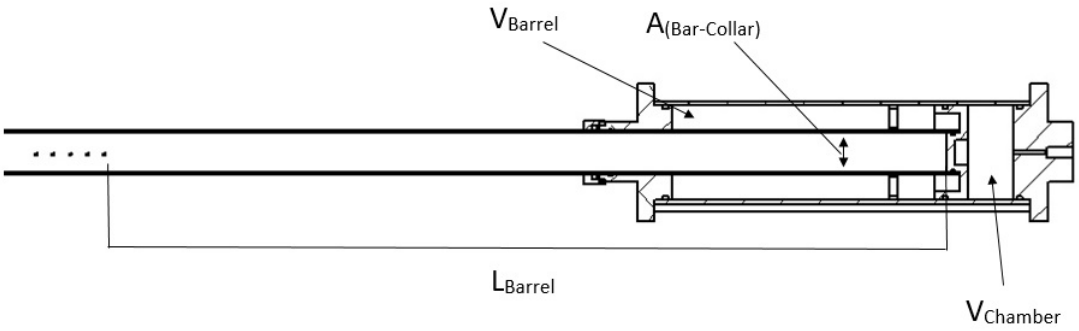

Figure 4.19: Schematic detailing gas gun dimensions as shown in (4.2) and (4.3)

Where the barrel length is from the beginning, where the piston blocks the entrance, until the venting flutes begin. The area of the bar end collar is the surface area which will be in contact with the pressure upon fire. For air, γ, the adiabatic polytropic coefficient is set at 1.4, and m_{Bar} is the mass of the striker. An example for the theoretical vs experimental barrel exit velocity variation is shown in Figure 4.20.

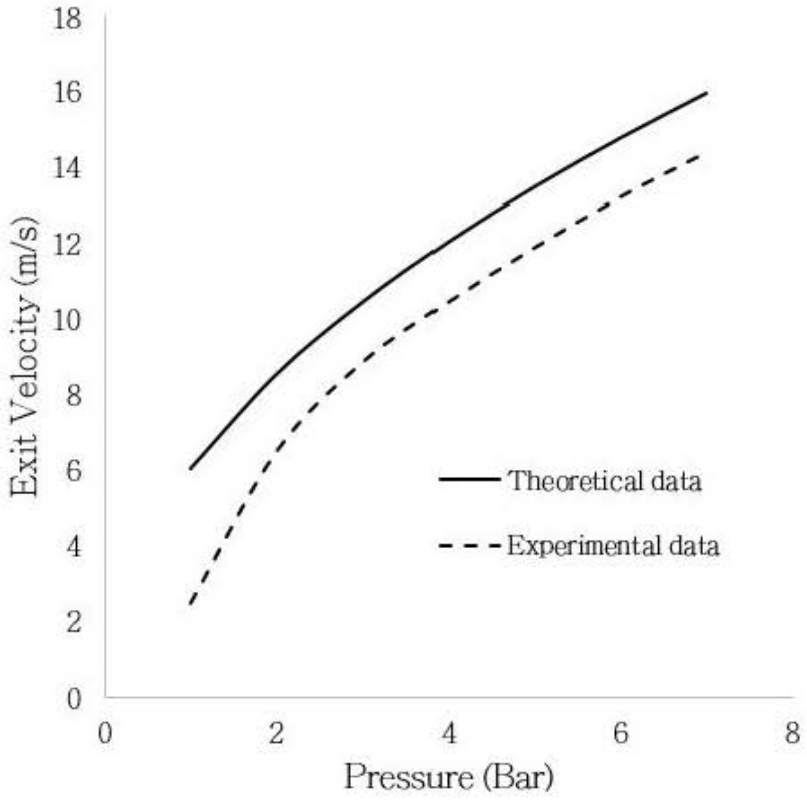

Figure 4.20: Comparison between theoretical and experimental striker exit barrel velocities for a 1:500 wedge bar

As the theoretical model does not account for friction and energy losses, the difference displayed between the theoretical and experimental velocity may be attributed to these losses. As the difference between the theoretical and experimental data appears to be constant, except for very low pressures within the longer bars, the gas gun striker velocity is consistent and acceptable for testing.

4.3.2.2 Compliance

Previously, Stander [57] utilised numerical calculations via finite element methods to determine the combined stiffness/compliance of the system. This accumulated to an amount of 194 kN/mm. Visually, the current set up appears to be stiffer than that of Standers, however, experimental validation is to be performed as Stander, Paul, and Oxtoby never performed experimental compliance validation.

Load cell

The load cell was first component tested for compliance. This is performed by observing the compliance of the Zwick quasi-static mechanical testing apparatus with the testing apparatus in place. The load cell is then installed and the compliance test is re-initiated. The system is seen as a set of springs arranged in a series layout. This means that the total deflection is the sum of the individual deflections experienced per component. With the force being equal per "spring", the force may then be divided throughout the entire system. Formula (4.6) is therefore derived:

$$\delta_{total} = \delta_{zwick} + \delta_{loadcell} \tag{4.4}$$

$$F_{total} = F_{zwick} = F_{loadcell} \tag{4.5}$$

$$\frac{1}{K_{total}} = \frac{1}{K_{zwick}} + \frac{1}{K_{loadcell}} \tag{4.6}$$

Taking the mean compliance from running tests purely on the test set up and again with the load cell included, the stiffness of the load cell is determine to be 65.893 kN/mm. This is considerably less than Standers load cell which presented a stiffness of 369 kN/mm, however, the stiffness determined within Standers work is theoretical and was never confirmed experimentally.

Wedge bar mechanism

For the entire system, the load cell is not the only component which complies. The incident wedge bar and platform can further add to the compliance of the set up. For the following, the wedge bar itself and corresponding platform is used as a single entity.

The compliance is calculated by setting a datum and measuring the displacement of the bar from this datum point. The bar is moved using consistent 10-20 mm increments which are used to infer the theoretical vertical displacement. Theoretically, the system should not move as the sacrificial specimen (stainless steel) is deemed to be incompressible (the theoretical compliance of a 8mm diameter, 5mm height is 2.5 μm) and so any movement of the system is therefore directly measured as the compliance of the machine.

Figure 4.21 details an example of the compliance behaviour within the respective intermediate strain rate apparatus configuration:

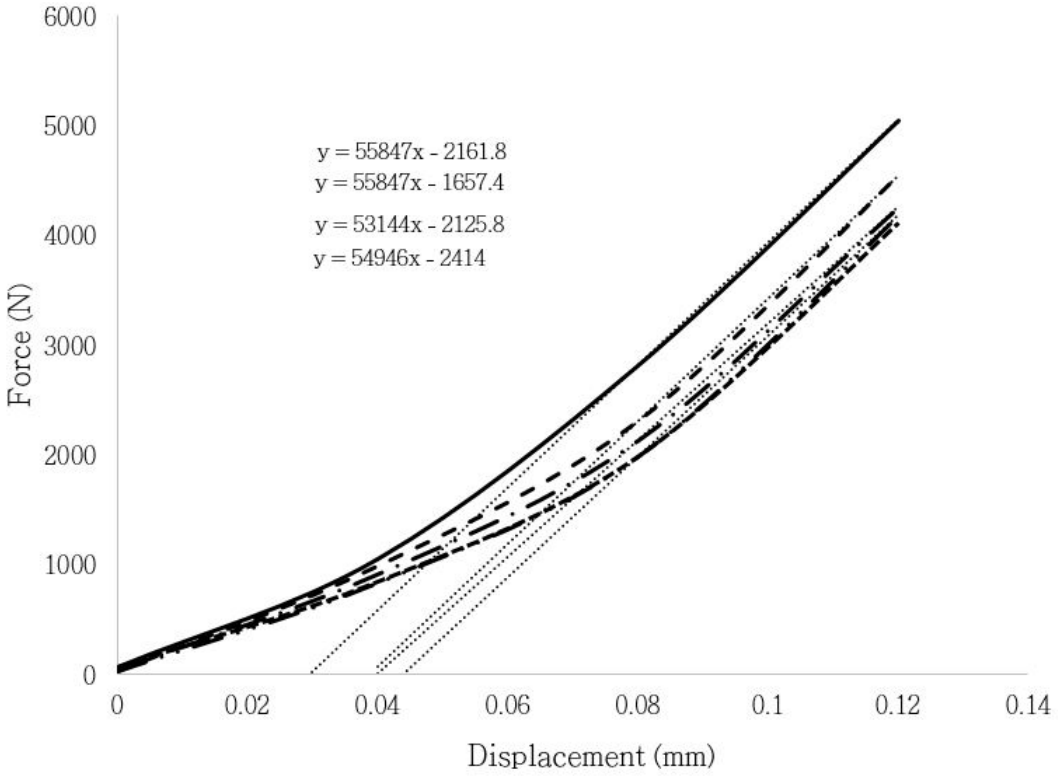

Figure 4.21: 1:250 bar compliance representation

Figure 4.21 clearly demonstrates that a distinct take up zone exists followed by a linear path. This is also apparent for the 1:500 bar. The compliance is calculated by looking at the linear section post take up; a linear trend line is used in order to gauge the gradient of each linear section. The compliance value is calculated by taking the average of these gradients. This is demonstrated below per bar:

- 1:500 bar - 55.6 kN/mm
- 1:250 bar - 61.6 kN/mm

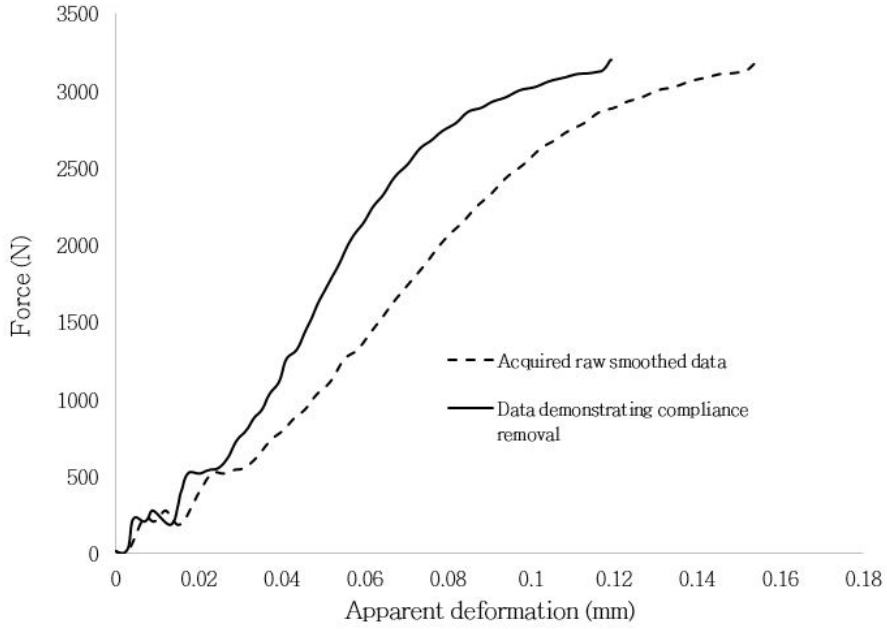

Figure 4.22: Example of raw data vs raw data with compliance removed for the intermediate strain rate regime in order to visualise the significance of the compliance

The vertical displacement of the system also verified by two separate and different methods. A vernier calliper measures the vertical rise of the sliding platform directly, which the specimen is placed upon, and a clock gauge measures the rise of the bar as shown in Figure 4.23. Using these methods, it was found that the bar initially displaces 20μm - 30μm prior to operating as per design. This is assumed to be the bar seating itself within the key way prior to accurately measuring the correct load.

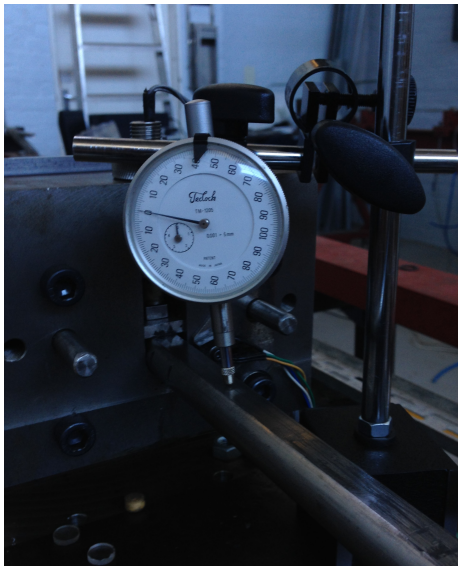

Figure 4.23: Image demonstrating the use of a clock gauge to measure micron vertical displacement within the wedge bar

Summary

Compliance within a machine is undesirable, however, for this machine, the compliance may be attributed to the following factors:

- The surface between the wedge bar and platform is difficult to machine perfectly as this is performed using milling. For this reason, the seating may not be perfect which in turn will add additional compliance.
- The load cell is fastened using two counter turning nuts, if these nuts do not lie flush with the load frame during fastening, this will further add to the compliance of the system.
- A required sliding fit has been added to the bar and load frame. A close sliding fit is required in order to aid in misalignment and prevent seizure from occurring during testing. Using a clock gauge with micron accuracy during compliance testing, it is recorded that the bar displaces an initial 20 - 30 microns during take up and then begin to perform as required. Unfortunately this is difficult to overcome and so the system will always have an inherent compliance as the bar cannot be modelled as a rigid structure.
- The load cell as discussed previously has an inherent compliance of 65.9 kN/mm. During testing, this value will be the maximum attainable compliance within the system if a completely rigid load path is assumed. For the purpose of future designs, a stiffer load cell will result in a better compliance value.

To achieve a machine with zero compliance is deemed near impossible. However, for the purpose of this final prototype, the compliance values are acceptable and simple to deduct from the data. This is due to the compliance tests showing repeatability and linearity post take up.

4.3.2.3 Preliminary testing

In order to receive data from the relevant wedge bar components, the components are attached to a picoscope which is connected to a laptop. The sampling rate was set to record at 2 Ms/s (million samples per second).
Preliminary testing of the wedge bar was performed on specimens machined from Perspex(PMMA). These tests were performed in order to gauge whether the system performed as required both mechanically and electronically. This is performed by comparing the recorded data to that of Stander [57]. The tests performed by Stander were for a strain rate of 6.5/s whereas the current tests performed are at a rate of 3.5/s. As the components used are distinctly different, from different designs and users, the average gradient of the recorded data is investigated for analysis. It is determined that these gradients lie within a 5% variation of one another which is acceptable for comparison. After completion of the comparison tests, bone may now begin to be tested. Figure 4.24 demonstrates this comparison:

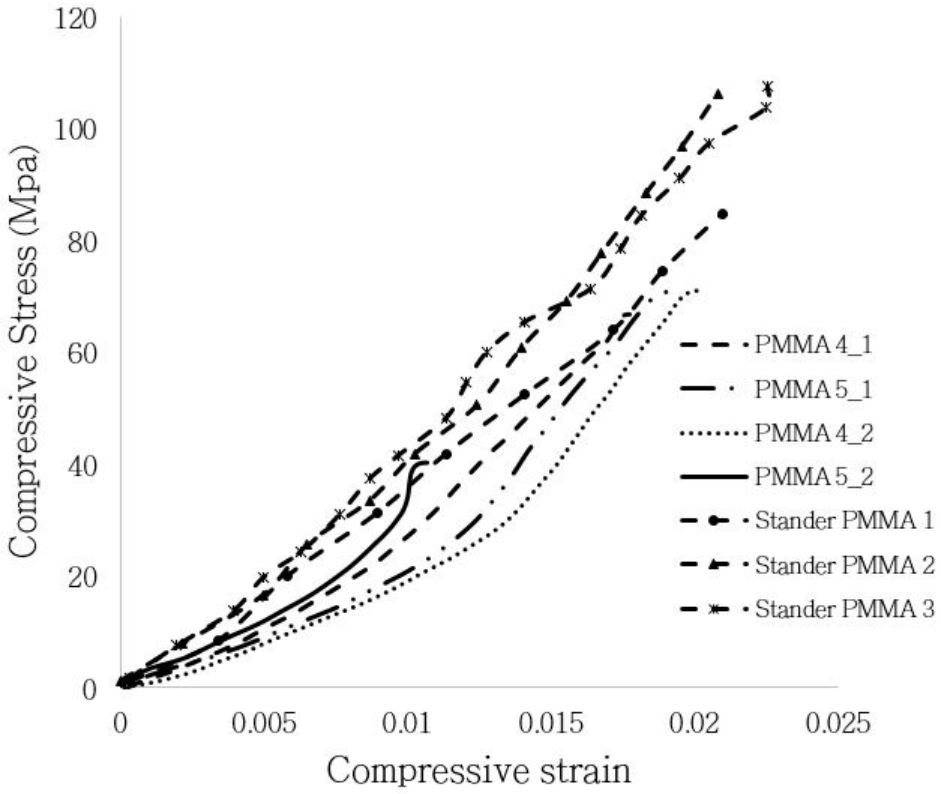

Figure 4.24: Comparison between Standers work and current data for PMMA

As the apparatus is required to perform at a constant strain rate during testing, this is investigated and displayed in Figure 4.25:

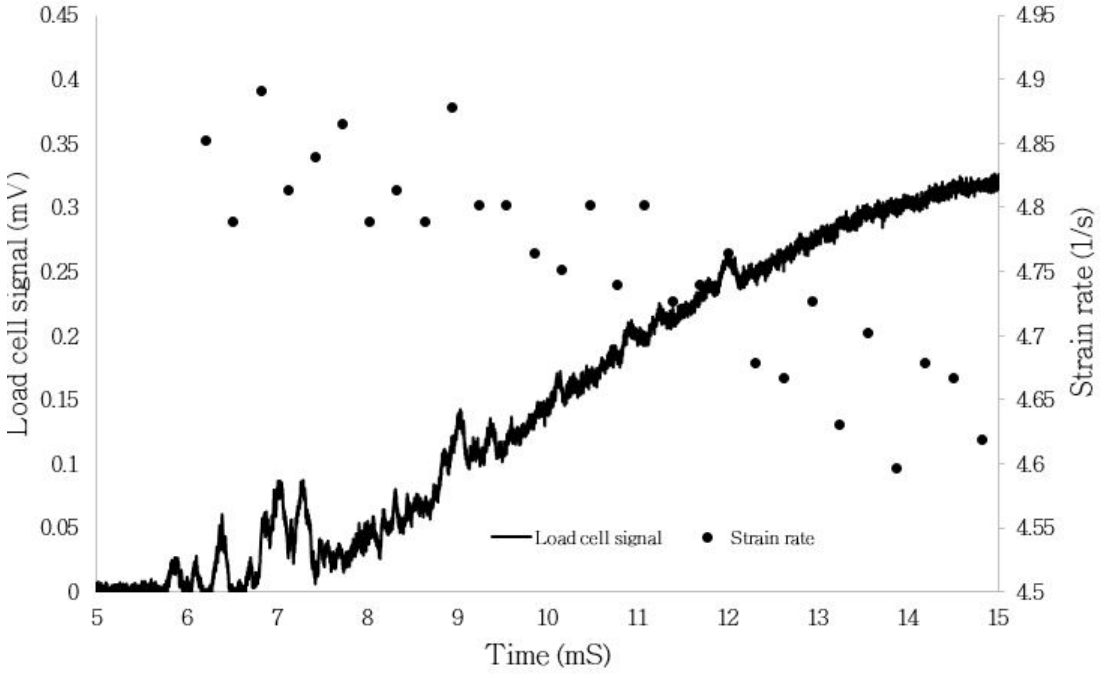

Figure 4.25: Demonstration of constant strain rate during test duration

Figure 4.25 displays the region of impact during testing with the strain rate behaviour superimposed. The strain rate at impact is shown to be approximately 4.85/s and decreases to approximately 4.65/s when maximum stress is reached prior to fracture. As the variance in strain rate is less than 5%, the strain rate is taken as being constant over the testing period. Further investigation for high strain rates yielded similar results with variation decreasing further due to the decrease in testing time.

4.3.2.4 Data analysis

Analysis of the intermediate data is performed using Matlab R2014b student edition provided by the University of Cape Town. The following list highlights the major functions of the code:

- Raw data is contracted in order to eliminate post failure characteristics.
- Smoothing is performed using a moving average analysis in order to eliminate any high frequency noise.
- The peaks of the reflective objectography sensor(ROS) data are identified and counted in order to infer the horizontal and respective vertical displacement.
- The vertical strain rate is calculated.
- The compliance is removed from the data set.
- The maximum gradient is calculated and a linear regression is taken using data points which lie within 10 % of the maximum gradient in order accurately gauge the apparent modulus.

Chapter 5

Experimental Results

5.1 Introduction

Bovine bone is classified to be a highly anisotropic material [47, 60, 42, 59, 6], the testing performed is upon the three defined orientations labelled as transverse, radial, and longitudinal, see Figure 5.1. The data acquired will be analysed and compared to literature where applicable. This chapter will detail and include the following key points:

- The presentation and discussion with respect to the quasi-static and intermediate strain rate testing performed.
- A discussion into the analysis performed with respect to the data acquired and respectful observations made.

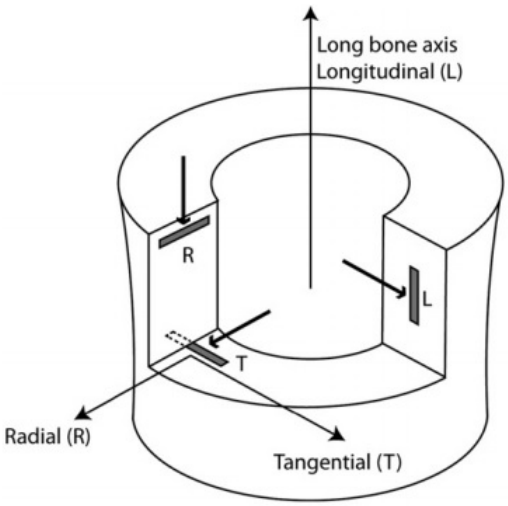

Figure 5.1: Orientations tested [59]

The following is to be taken into consideration within the results presented: bone one and two specimens are attributed to the thin walled bone supply whereas bone three is attributed to the thicker bone wall supply.

5.2 Quasi-static testing

5.2.1 Introduction

Quasi static testing was performed using the UCT Zwick quasi-static mechanical testing apparatus manufactured by the Roell Group. The testing performed consisted of the transverse, longitudinal, and radial orientations. Ten specimens per strain rate were tested at strain rates of 0.001/s, 0.01/s, 0.1/s in order to compare the results with that of literature. This amounts to a total of 90 specimens tested in the quasi-static regime.
Even though a slight variance is present within the results, the tests are seen as repeatable due to the stress-strain curves following a distinct pattern per orientation tested. This may be attributed to variation in the microstructure of the bone as discovered by Mayya *et.al.* [1]. Farther variance is due to multiple bones being used from which the specimens are machined. It is to be noted that nine bones are used for the manufacturing of quasi-static specimens where each orientation is machined from three distinct bones. Within each orientation, the three bones spoken of are three distinct bones which have been allocated to the specific orientation in discussion, this includes specimens for intermediate strain rate testing.

5.2.2 Radial

Figure 5.2 demonstrates the analysed radial quasi static data set:

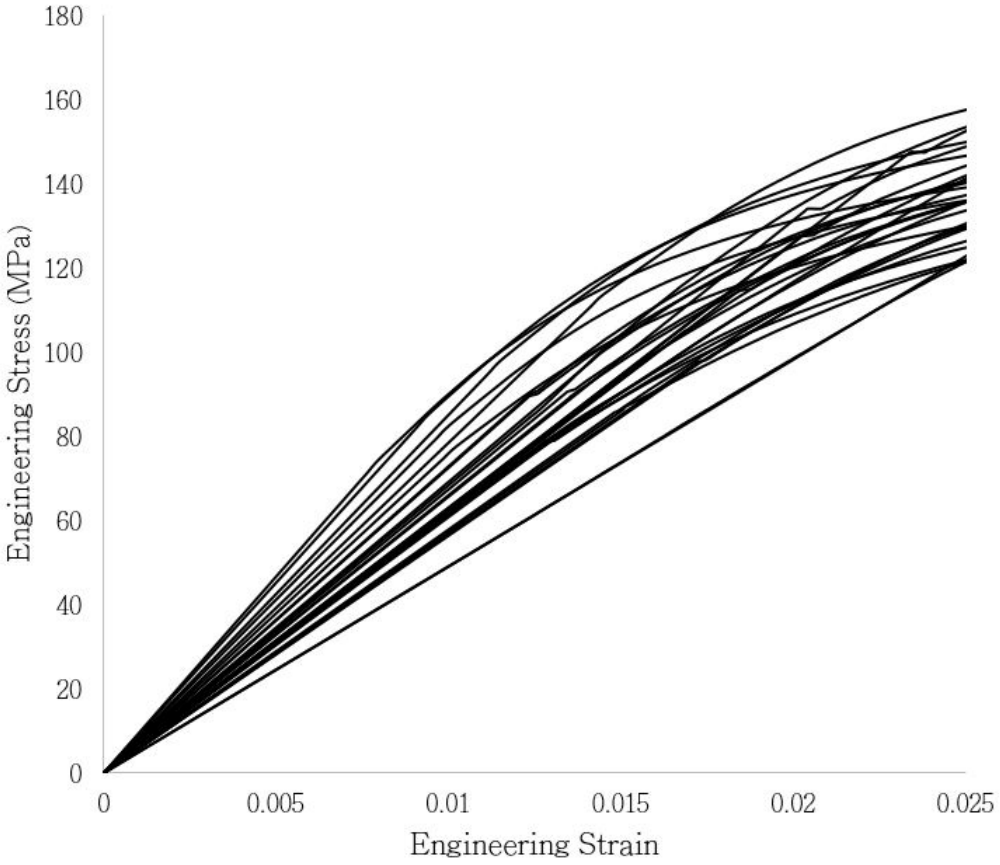

Figure 5.2: Analysed radial quasi static-dataset

The test data displayed no clear differentiation between bones. If the specimens themselves were observed using light microscopy, the specimens from one bone sample behaved in a manner that displayed a form of shearing fracture whereas the other bone displayed hardly any fracture. All tests conducted were taken until a artefact of fracture presented itself upon the stress strain curve.

This is demonstrated in Figures 5.3 - 5.6.

Bone one

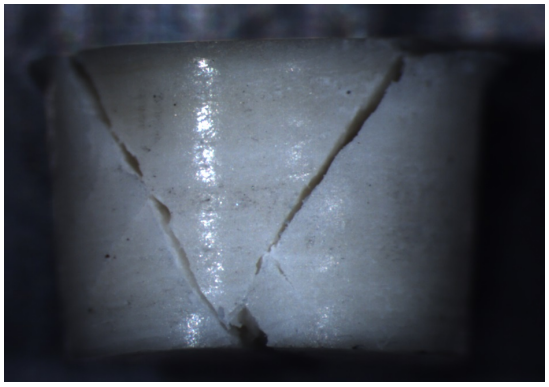

Figure 5.3: Radial specimen 2 fracture - 0.001/s strain rate

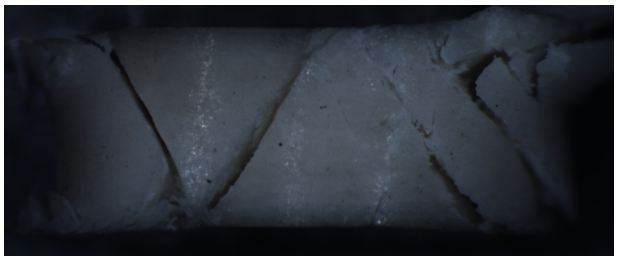

Figure 5.4: Radial specimen 3 fracture - 0.001/s strain rate

Bone two

Figure 5.5: Radial specimen 32 fracture - 0.001/s strain rate

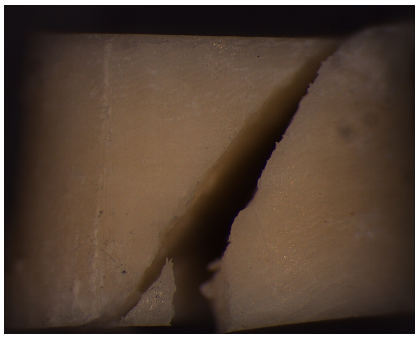

Figure 5.6: Radial specimen 42 fracture - 0.1/s strain rate

The fractures demonstrated for bone one are present in all radial quasi static tests performed. Depending on the length of the test, the fracture will begin to propagate as displayed in Figure 5.4. The second bone fracture is difficult to attain with the bone displaying micro-cracking rather than severe fracture. Only within the higher strain rates was full fracture attained. Imaging of the specimens at this stage cannot yet explain the difference in behaviour. Another observation made within Figure 5.2 is the distinct change in linearity. This cannot be explained as of yet.

5.2.3 Longitudinal

Figure 5.7 demonstrates the analysed longitudinal quasi-static data set:

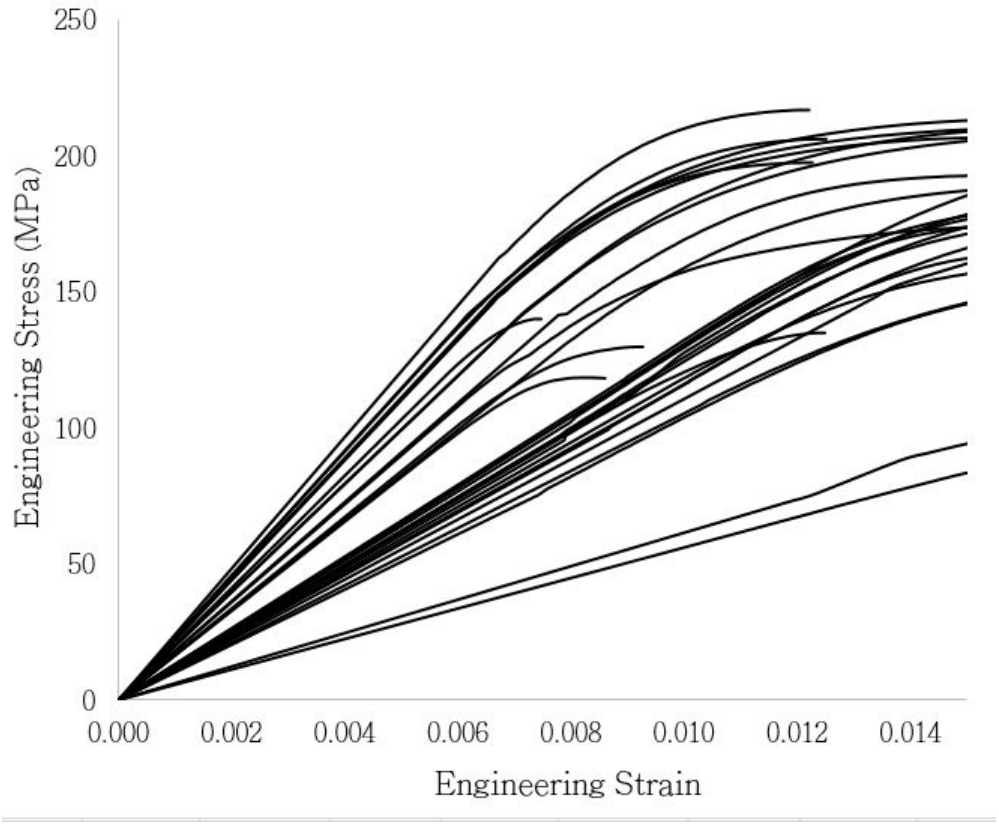

Figure 5.7: Analysed longitudinal quasi-static dataset

Figure 5.7 displays what appears to be two distinct groupings with two specimens diverging significantly from these. As two different bones were used, the groupings are attributed to these bones. This is confirmed by separating the data per bone tested as demonstrated in Figure 5.8 and 5.9.

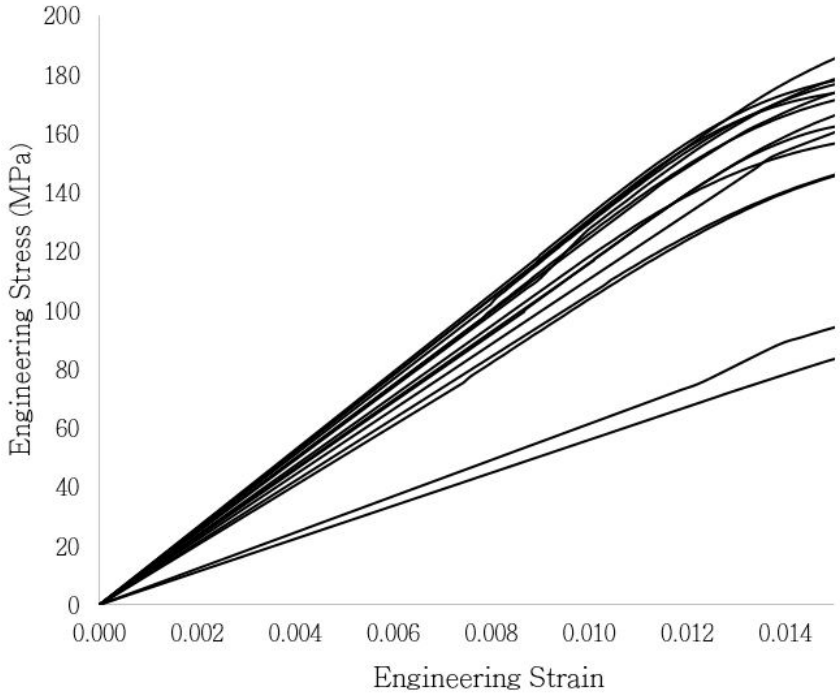

Figure 5.8: Quasi static longitudinal data for bone one

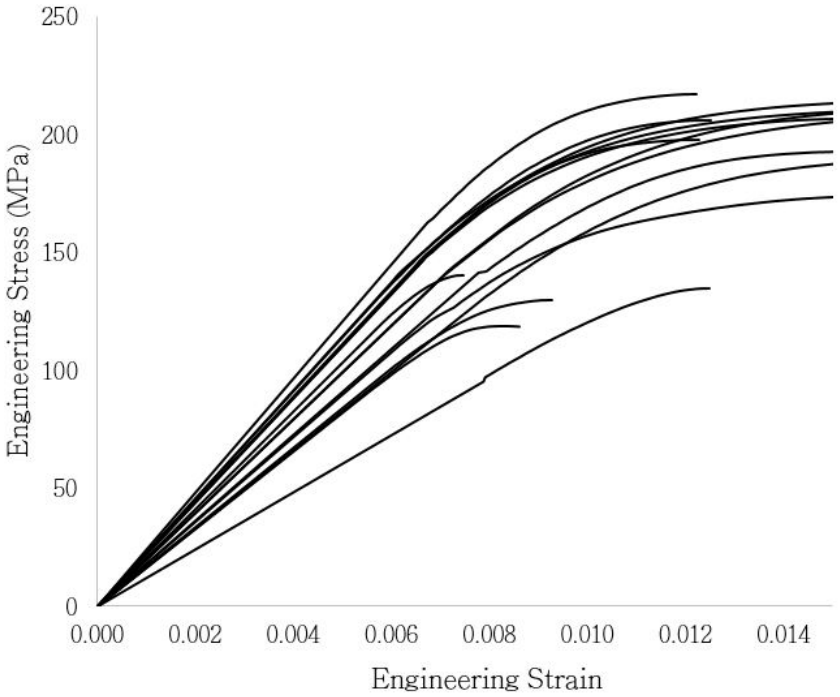

Figure 5.9: Quasi static longitudinal data for bone two

Specimen 15 and 16, otherwise recorded as the significantly divergent specimens, are further investigated in order to determine the reason for this variance. Light microscopy is used which identifies the specimens as being heavily vascularised compared to other specimens. This is demonstrated in Figure 5.10 and 5.11.

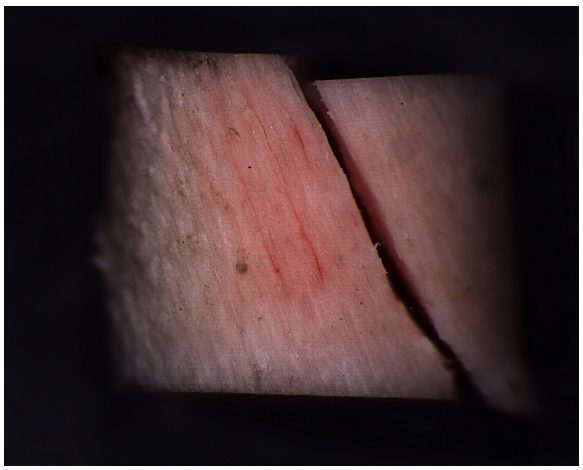

Figure 5.10: Longitudinal specimen 15 fracture - 0.1/s strain rate

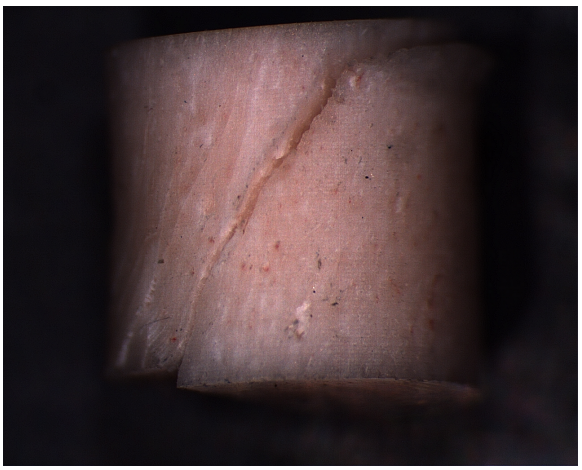

Figure 5.11: Longitudinal specimen 16 fracture - 0.1/s strain rate

For the purpose of data acquisition and comparison with literature, these specimens may be omitted as sufficient specimens have been tested.

Observing the fractures presented by each bone, both bones display similar fractures, however, fractures observed in the second bone appear less severe (shown in Figure 5.14 and 5.15) with the specimen physically appearing stiffer.

Bone one

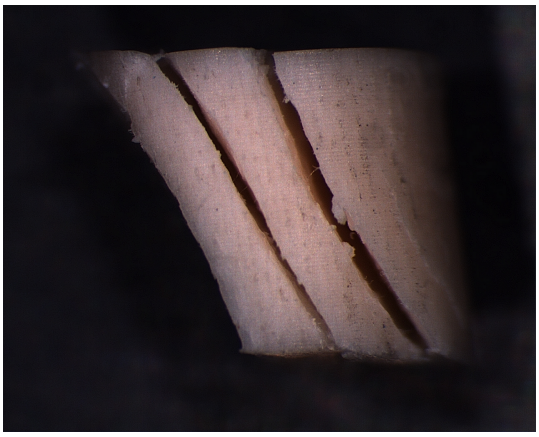

Figure 5.12: Longitudinal specimen 7 fracture - 0.01/s strain rate

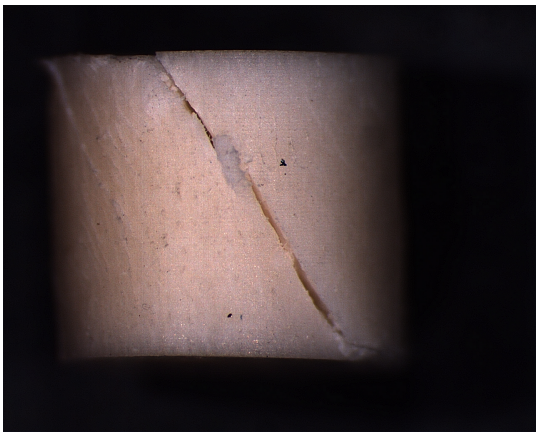

Figure 5.13: Longitudinal specimen 14 fracture - 0.1/s strain rate

Bone two

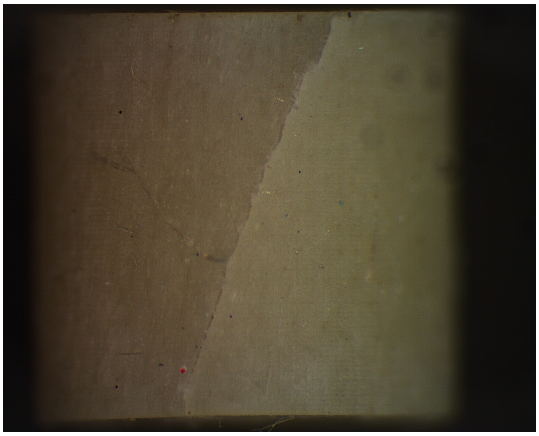

Figure 5.14: Longitudinal specimen 31 fracture - 0.001/s strain rate

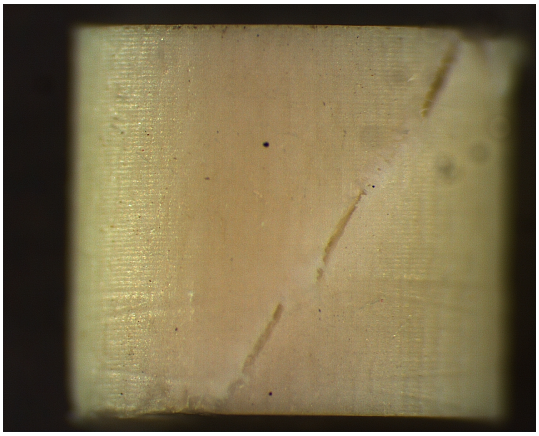

Figure 5.15: Longitudinal specimen 44 fracture - 0.1/s strain rate

It is clear to see that in the longitudinal testing orientation, bone two is noticeably stiffer than bone one. As intrinsic factors cannot be controlled and extrinsic factors not being able to be assumed as constant, there is no distinct nor justifiable reason as to the strength variation between bones. Both bones were produced from a single supplier, however, these bones may not necessarily be from the same bovine.

5.2.4 Transverse

Figure 5.16 demonstrates the analysed transverse quasi-static data set:

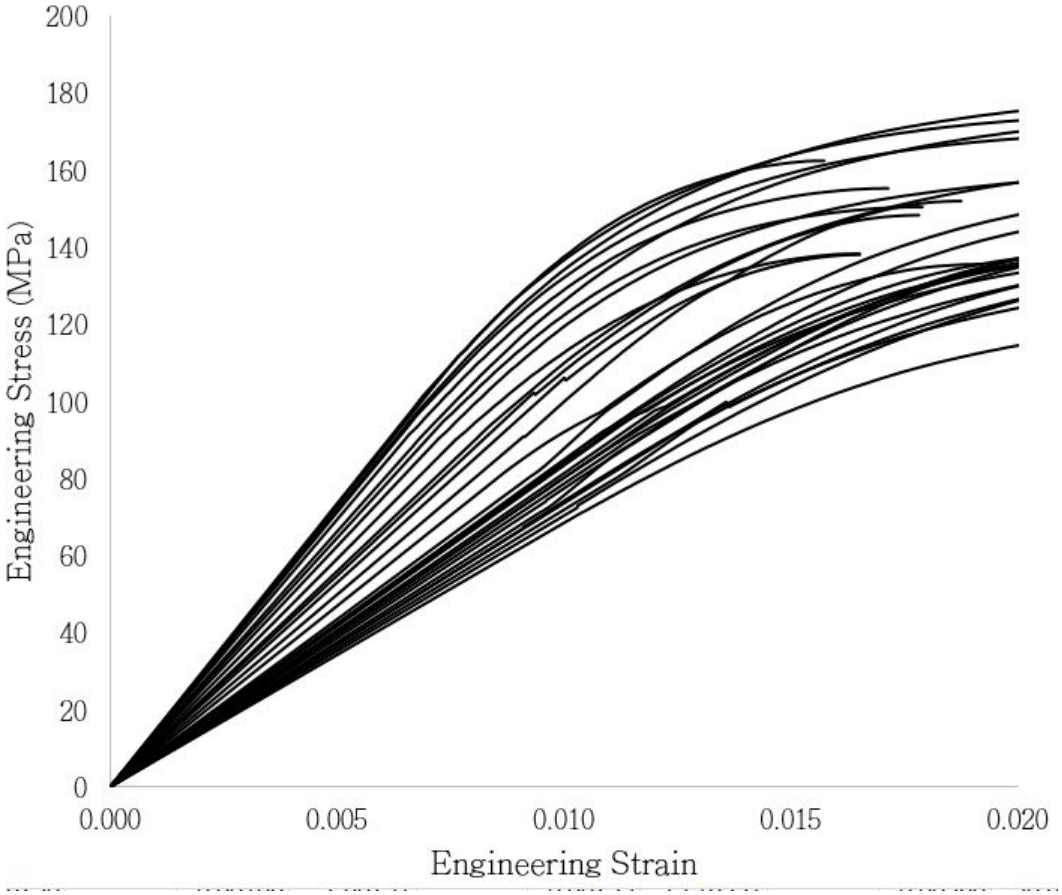

Figure 5.16: Analysed transverse quasi-static dataset

The specimens displayed a stress/strain curve which coincides to a characteristic combination of both radially and longitudinally orientated behaviour. As discussed within the longitudinal orientation, bone two again displays distinctly stiffer behaviour. Fractures upon the specimens appear to produce a shattered glass appearance. As the strain rate increases, fracture of the specimen is achieved, however, the distinct shattering fracture pattern is still present within the specimen with the overall fracture following the lines of these micro fractures. This is shown in Figure 5.17 - 5.20.

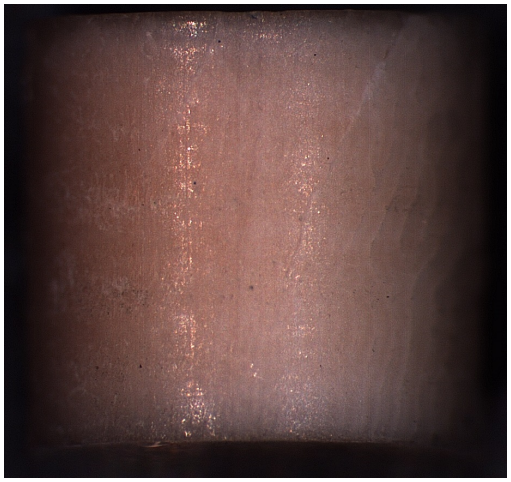

Figure 5.17: Transverse specimen 6 fracture - 0.01/s strain rate

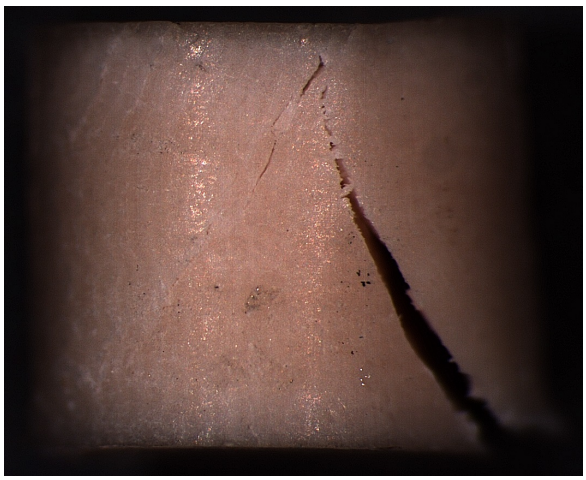

Figure 5.18: Transverse specimen 11 fracture - 0.1/s strain rate

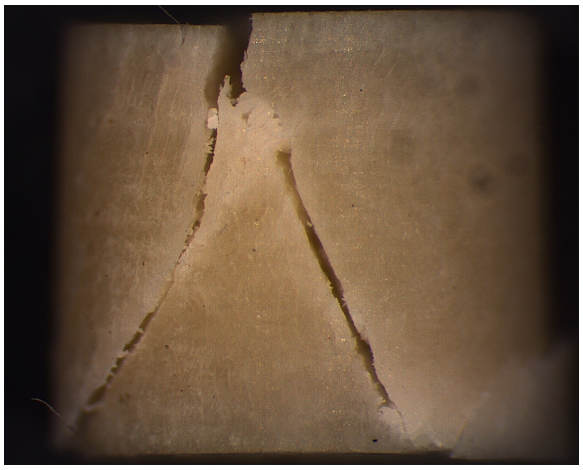

Figure 5.19: Transverse specimen 36 fracture - 0.1/s strain rate

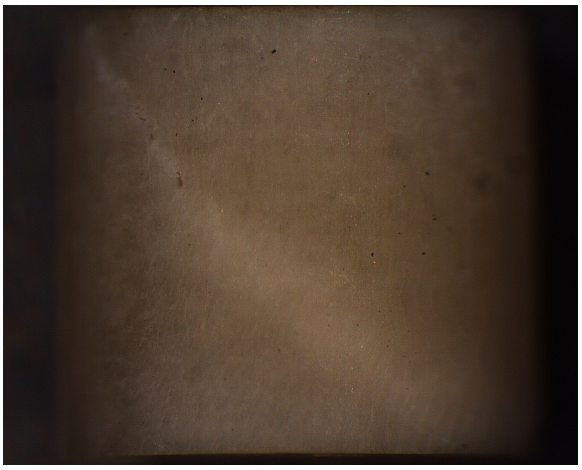

Figure 5.20: Transverse specimen 37 fracture - 0.1/s strain rate

Transverse specimens appear to not separate completely during fracture. Specimens machined from bone two appear to also fracture less severely than those of bone one. As displayed in Figure 5.20, bone two specimens appear to fracture more internally than externally. The reason for the variance in fracture can only be attributed to the increased stiffness displayed by bone two as all tests were conducted in the same manner.

5.2.5 Data evaluation and comparison

To further analyse the data acquired and compare it to literature, the apparent modulus is investigated. The recorded apparent modulus of the tested specimens, per orientation, is shown in Figure 5.21 - 5.23 with each figure displaying the variance from the three respective bones.

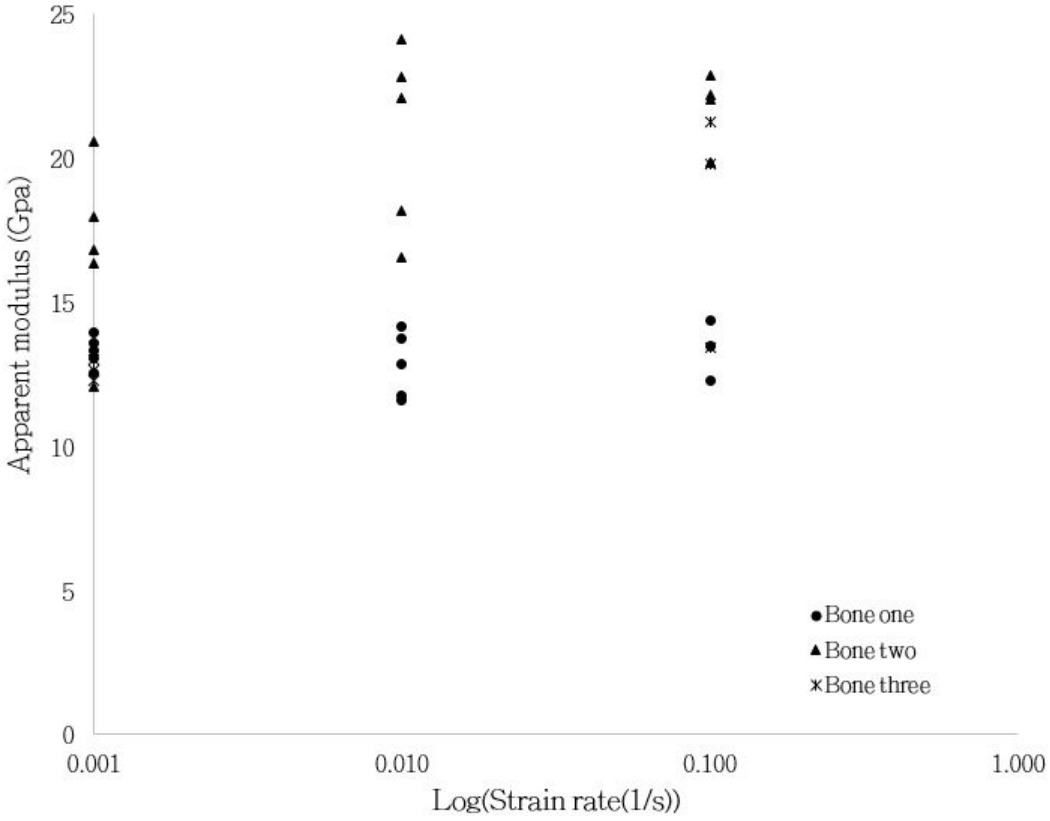

Figure 5.21: Analysed quasi-static longitudinal dataset

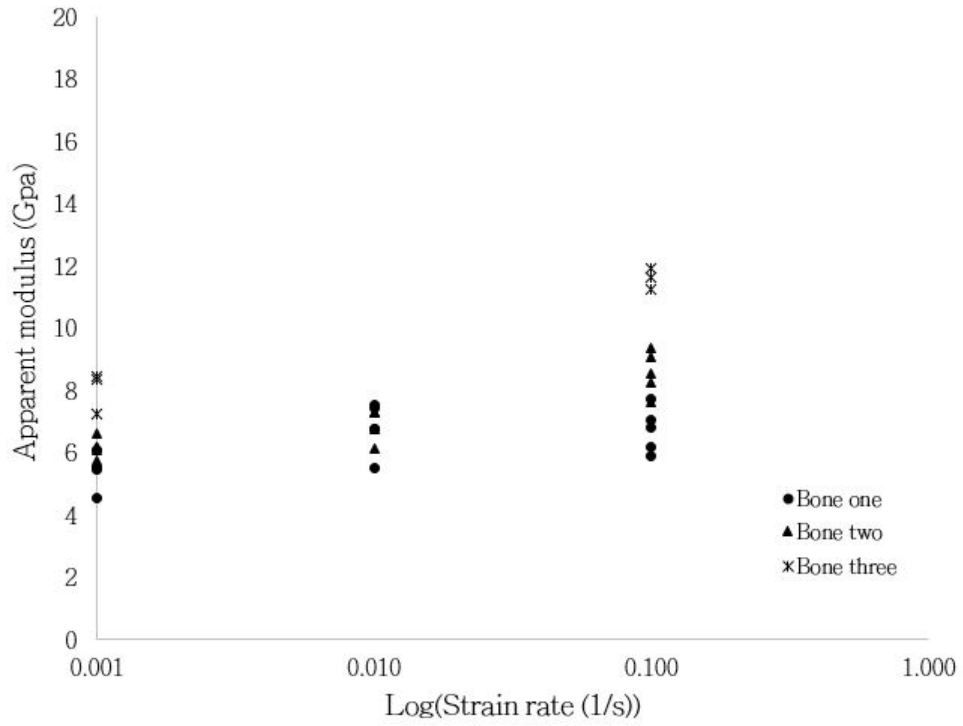

Figure 5.22: Analysed quasi-static radial dataset

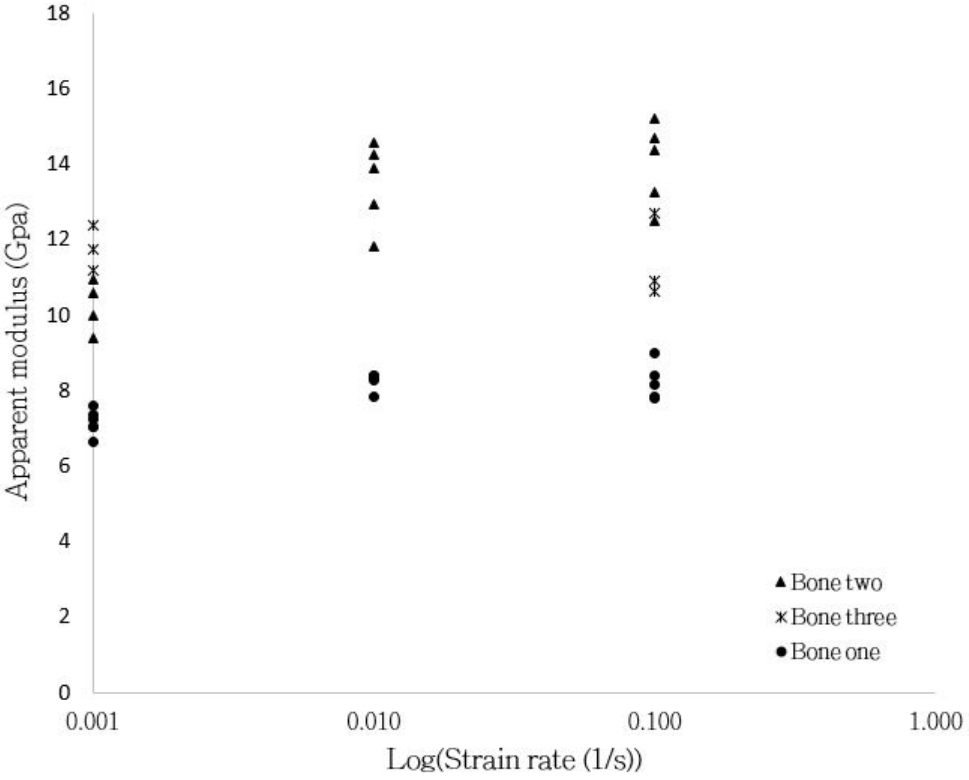

Figure 5.23: Analysed quasi-static transverse dataset

If the evaluated data is compared to that of literature, the following graphical data cluster may be created for the apparent longitudinal moduli:

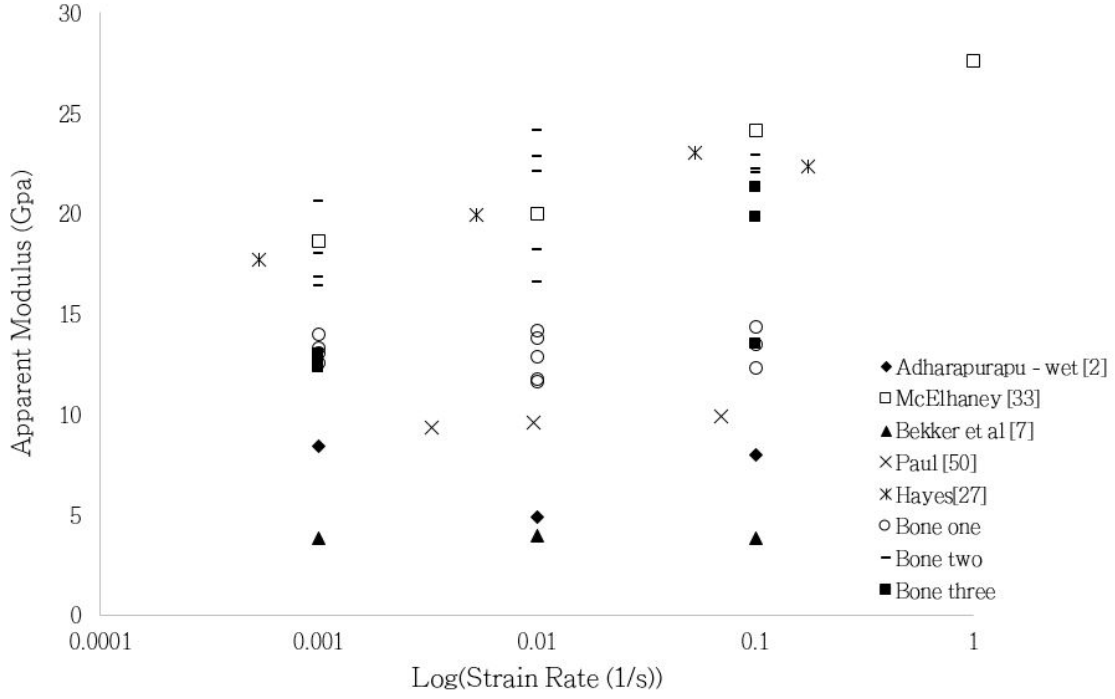

Figure 5.24: Comparison between current work and available literature for the longitudinal direction

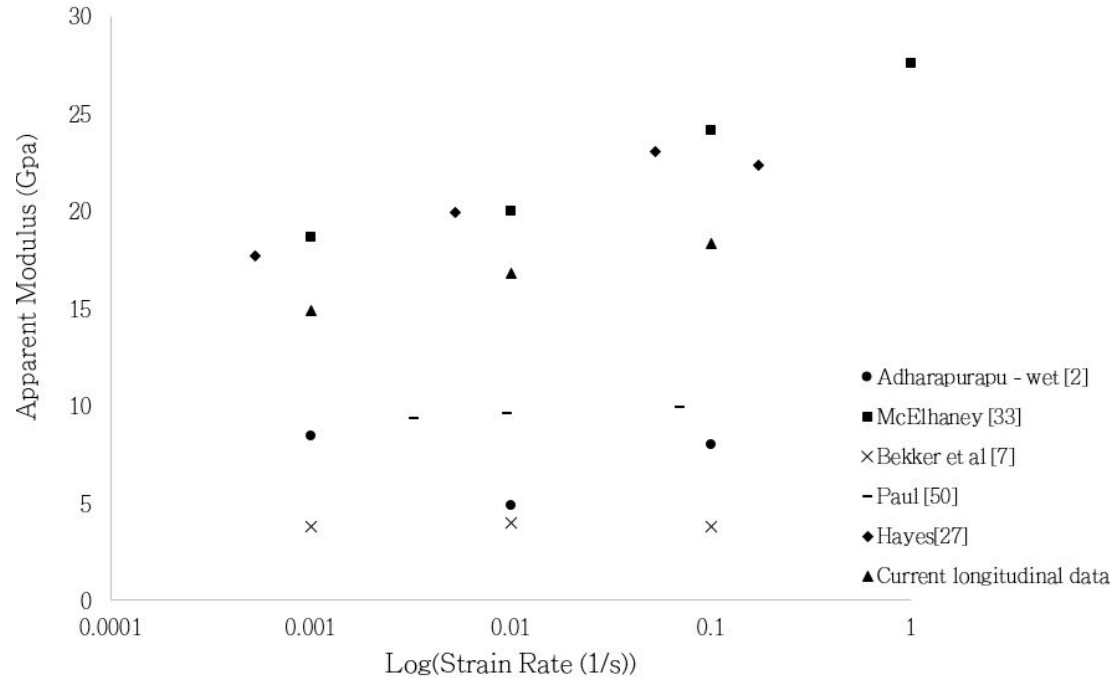

Figure 5.25: Comparison between current work and available literature using average values for the longitudinal direction

Figure 5.25 clearly demonstrates an initial similarity between the work of McElhaney [33] and Hayes [27] and current data, however, the data obtained from the literature does not appear to be consistent. The comparison between the work of McElhaney and the current data is useful as McElhaney proceeded to fit strain gauges to the specimens directly in order to measure accurate readings. Upon investigation of the previous work performed, it was discovered that Paul and Bekker did not account for the compliance in the machinery when testing. This may be a reason as to why the data appears to display such low values. There is also no indication whether other authors accounted for such compliance and what the actual scatter within their data was.

Observing the data for the three directions tested, there is a quantitative stiffness differentiation present.

5.3 Intermediate strain rate

5.3.1 Introduction

Intermediate regime testing is performed using the fabricated intermediate strain rate testing apparatus. Preliminary tests have been performed on PMMA (Perspex) in order to calibrate and confirm that the apparatus is functioning correctly. This is achieved by comparing the results to the work of Stander. For the purpose of intermediate regime data acquisition, the samples are tested at rates between 3/s to 17/s. To demonstrate any form of strain rate sensitivity which may be present, quasi-static data will be incorporated as part of this section.

5.3.2 Bar analysis

Prior to any testing performed, each incident wedge bar is analysed in order to gauge the level of noise introduced during testing. The tests are performed on PMMA(Perspex) at various strain rates. The bar ratios used are 1:500, 1:250 and, 1:200 of which the 1:500 and 1:250 ratios are machined onto 1.5m bar lengths whereas the 1:200 ratio is machined as a cantilevered bar of 600mm in length.

Using the 1.5m bar lengths for both ratios yielded positive results. The noise generated does not appear to be sufficient enough to obscure the data. Using these ratios, a maximum strain rate of 17/s may be achieved. If the 1:200 bar is used, a maximum strain rate of 29/s may be achieved, however, there is significant noise within the signal. A signal comparison between the 1:500 (smooth signal) and 1:200 (noisy signal) bar is demonstrated in Figure 5.26.

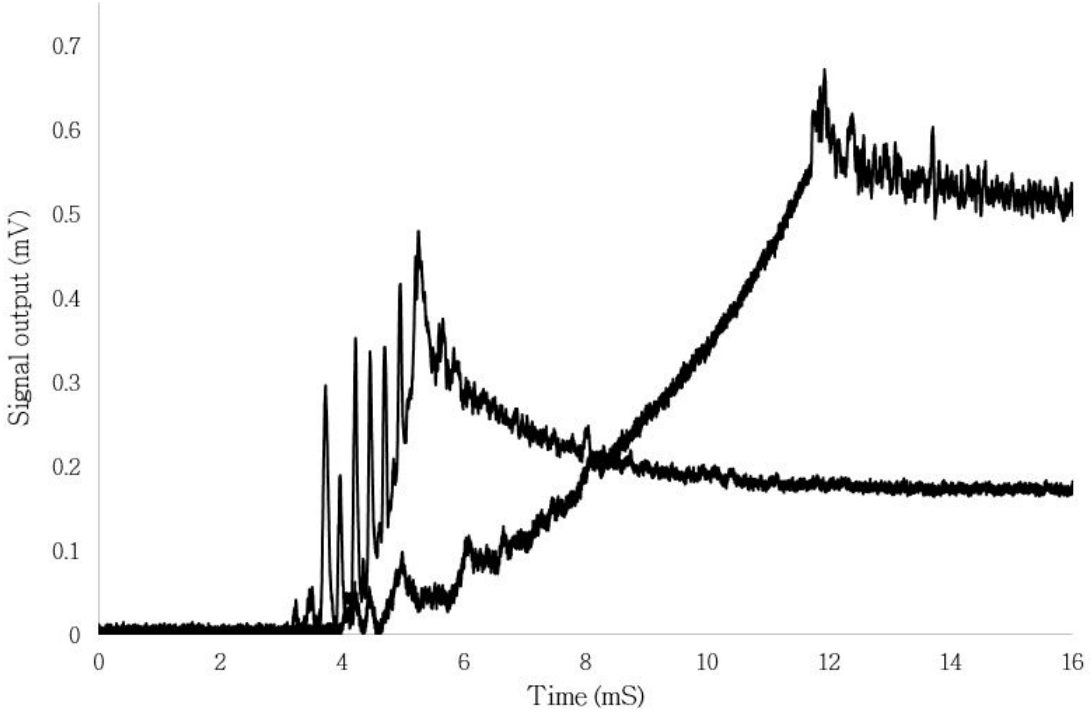

Figure 5.26: Comparison of noise for the 1:500 (smooth) and 1:200 (noisy) bars

Due to the low mass for the 1:200 bar, the initial acceleration is significantly higher upon impact.

This introduces the noise displayed in Figure 5.26. The noise presented may be due to impact vibrations, or the capturing method not being fast enough to capture data at these strain rates. Introducing a sacrificial foam specimen at the point of impact between the incident wedge bar and striker bar decreases the noise by approximately half, however, this tends to increase the noise slightly within the recovery period. The noise is reduced as the sacrificial specimen allows for vibration damping upon impact by reducing the acceleration rate, however, the noise is still inadequate and accurate readings are unable to be attained.

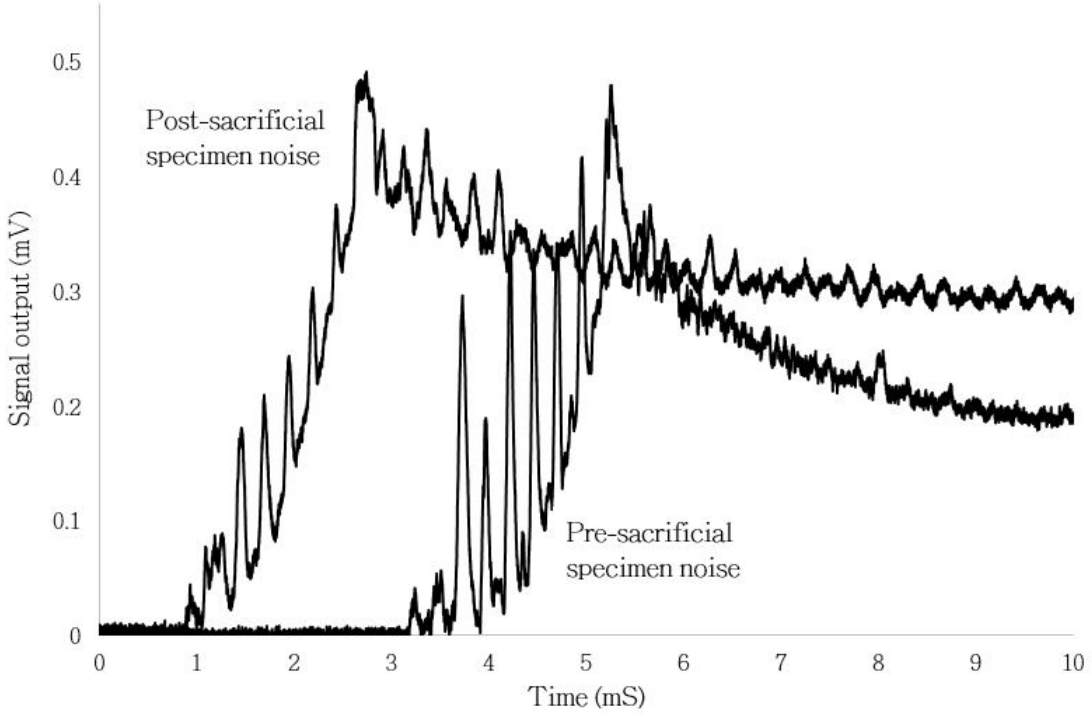

Figure 5.27: Noise reduction due to sacrificial specimen

For the purpose of testing cortical bone at intermediate strain rates, only the 1:250 and 1:500 wedge bars shall be used as the strain rates attained are within the regime which demonstrates the transitional behaviour between high and low strain regimes, as described by Paul[50].

5.3.3 Intermediate strain rate experimental data

For the purpose of the data analysis, the quasi-static data is included within the intermediate data to gauge the presence of any strain rate sensitivity. The apparent modulus is chosen to be reported upon as this proves more consistent than the previously reported compressive strength. The apparent modulus will also be used within the new numerical model discussed in chapter 7. Figures 5.28 - 5.30 demonstrate the scatter present within the tested directions:

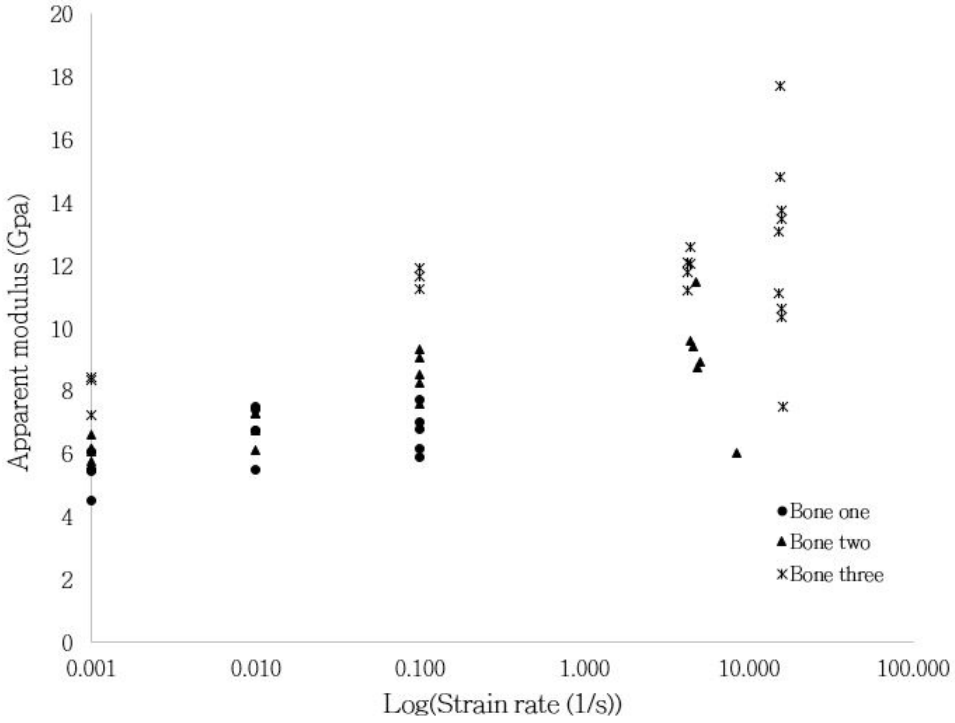

Figure 5.28: Scatter present within the radial direction

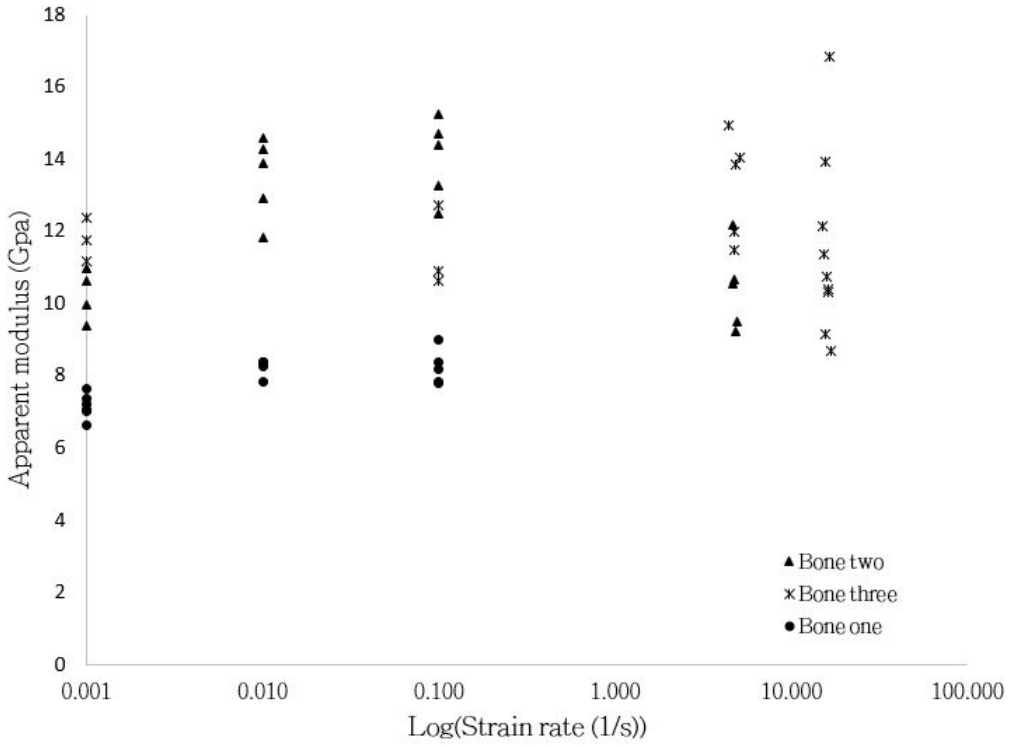

Figure 5.29: Scatter present within the transverse direction

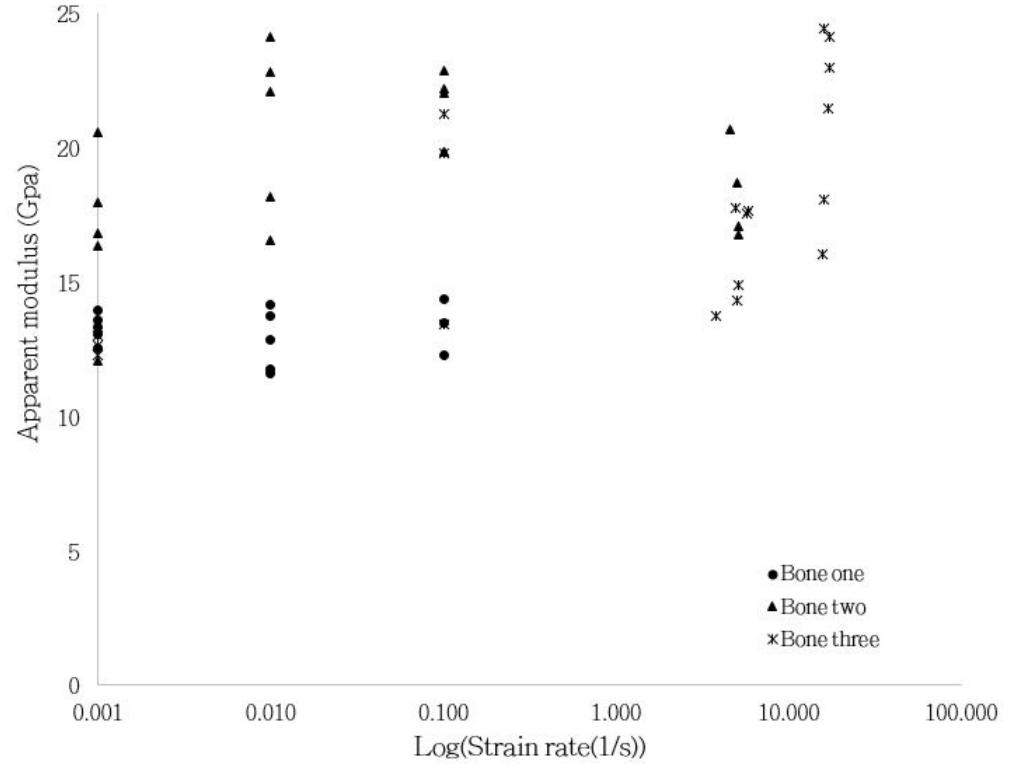

Figure 5.30: Scatter present within the longitudinal direction

From these plots, it is observed that there is a form of strain rate sensitivity present which is best represented by the longitudinal, as discovered by Paul [50], and radial orientations. In order to compare these results with literature, averages are taken. The transversely orientated data, however, does not demonstrate any statistically significant signs of strain rate sensitivity and consequently no averages are presented. The longitudinal and radial averages are shown in Figure 5.31 with a further diagram, Figure 5.32, demonstrating the longitudinal direction compared to the data found within literature:

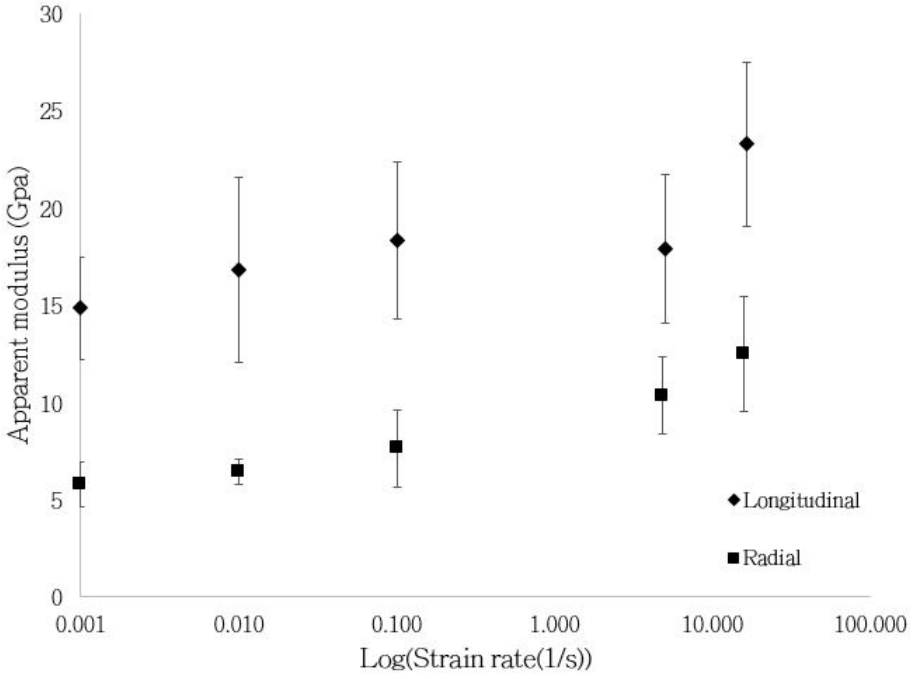

Figure 5.31: Apparent modulii average values for the longitudinal and radial directions

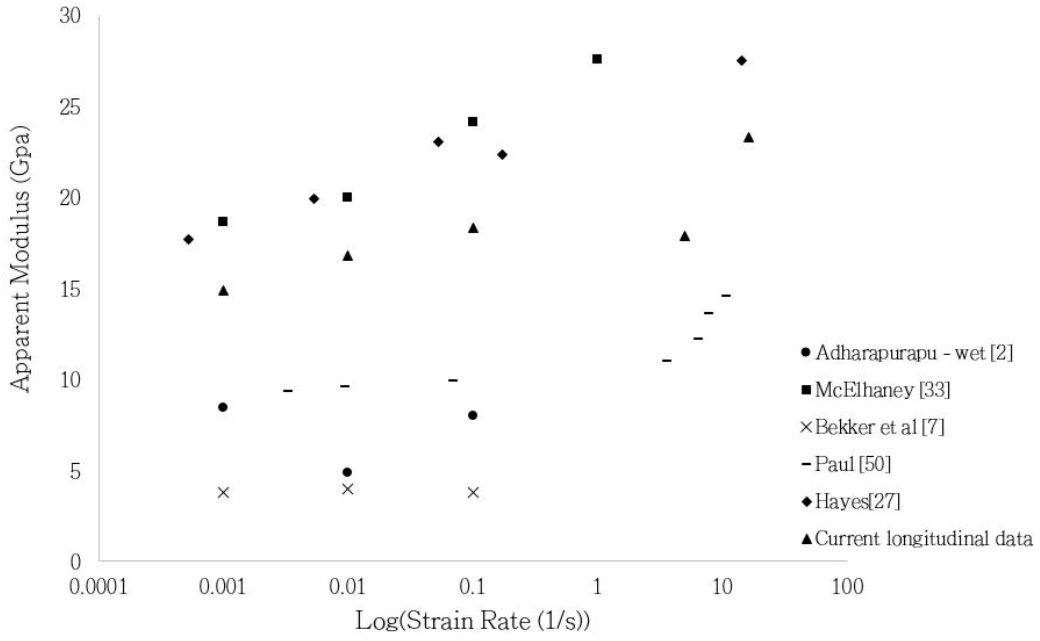

Figure 5.32: Comparison between current longitudinal data and literature

From the average values, the strain rate sensitivity may be clearly seen. However, the average values represent a large level of scatter which is not discussed in the literature. The averages per bone tested are demonstrated in Figure 5.33.

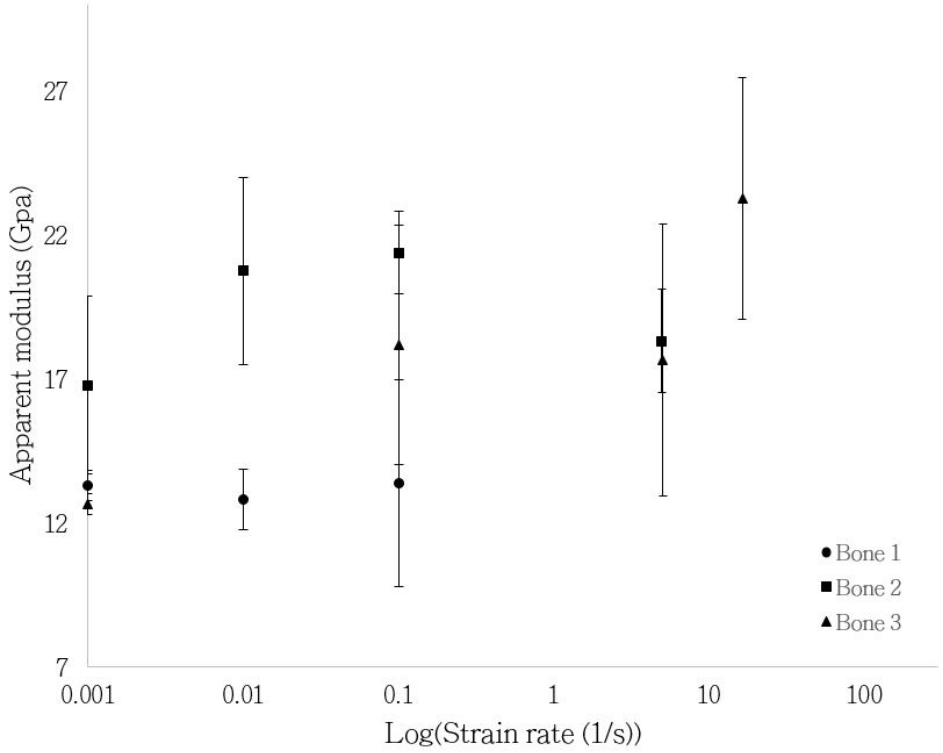

Figure 5.33: Longitudinal modulus averages per bone per strain rate

Due to the high inter-bone variation, an investigation into the density of the specimens was performed and compared to that of Zioupos *et.al.*[31]:

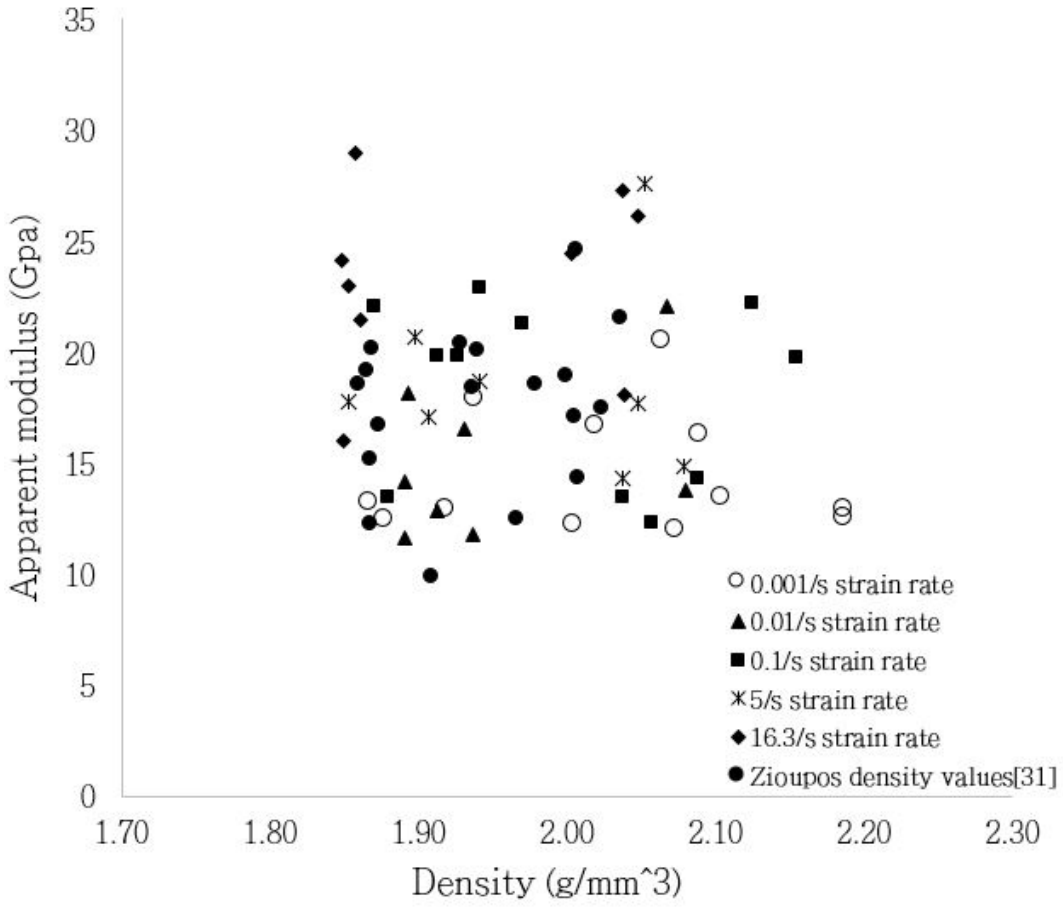

Figure 5.34: Density values per strain rate from current longitudinal data set in comparison with Zioupos *et. al.* [31]

Figure 5.34 displays no direct correlation between the apparent modulus and density as the scatter is too large. Observing scatter per strain rate yielded no further results and so currently this scatter cannot be explained. For future comparisons, the density vs log strain rate is shown for the transverse (Figure 5.35) and radial (Figure 5.36) orientations.

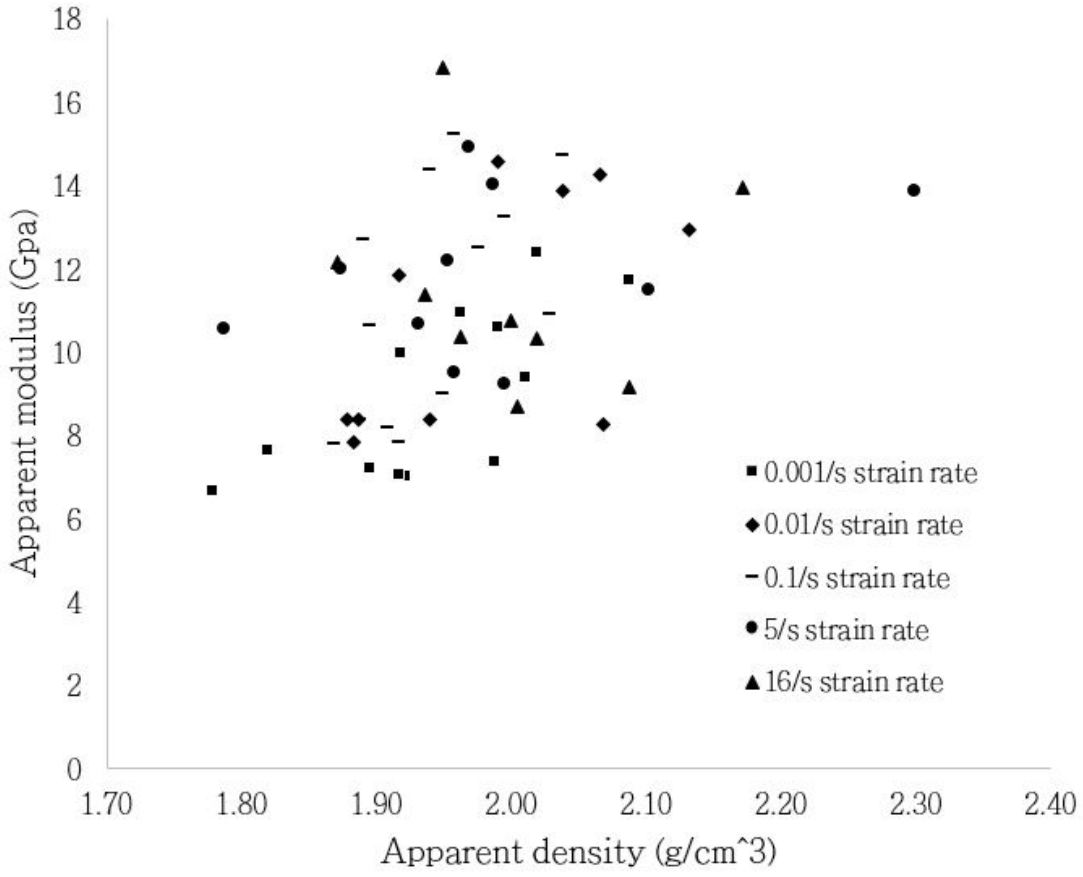

Figure 5.35: Transverse apparent modulus vs apparent density comparison

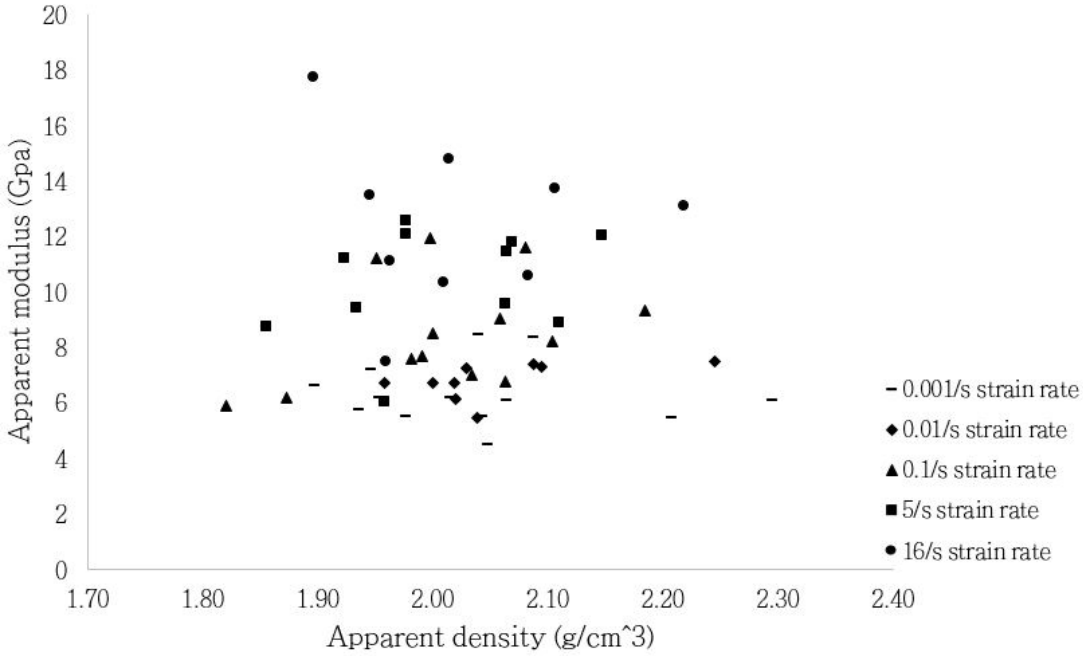

Figure 5.36: Radial apparent modulus vs apparent density comparison

5.4 Fracture

Once intermediate strain rate testing had begun, it was observed that specimens tested at higher strain rates fractured differently to those tested quasi-statically. The following observations were made:

- Quasi-static regime specimens appear to produce fluid during the tests. The fluid appears to seep from the specimens side wall.
- During intermediate regime tests, specimens which remained intact post-test displayed very little fluid seeping or none at all from the side walls.
- Quasi-static regime tests appear to display distinct 45 ° or 60 ° fractures which are displayed throughout each direction. Intermediate tests appear to fragment showing no distinct fracture pattern regardless of the direction. As found within quasi-static tests, the radial specimens once again displayed a distinct change in stiffness during the testing duration.

As a result of the observations made, imaging of the fractures was approached to determine whether a difference can be viewed at a microstructual level between different strain rate regime fractures. All required preparation, for imaging, and other significant phenomena will be discussed within chapter 6.

Quasi-static regime fractures appeared to follow no distinct pattern. Fracture propagators appear to follow the inherent lamella layout though the major fractures appear to run directly through the lamella. This is demonstrated in Figure 5.37 - 5.40.

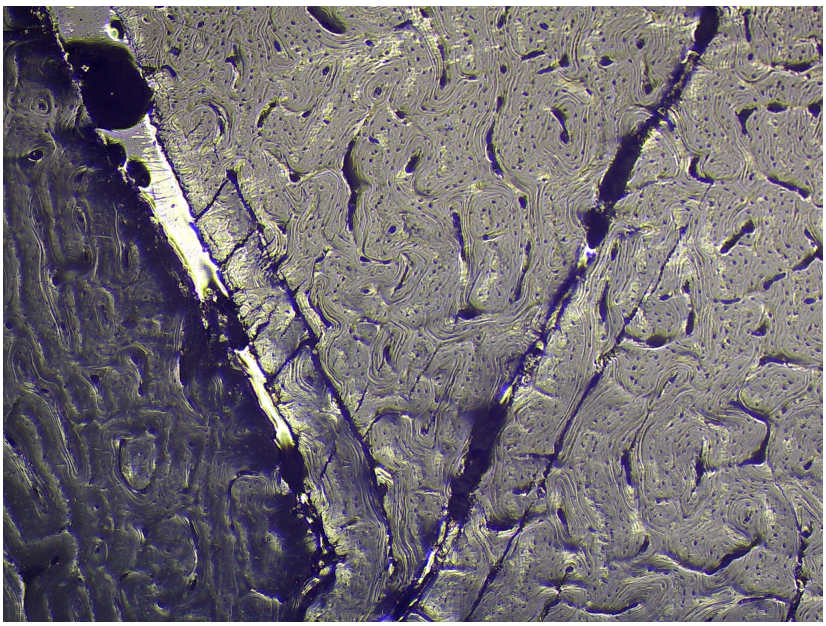

Figure 5.37: Quasi-static transverse lamella view for a fractured specimen at 5x magnification

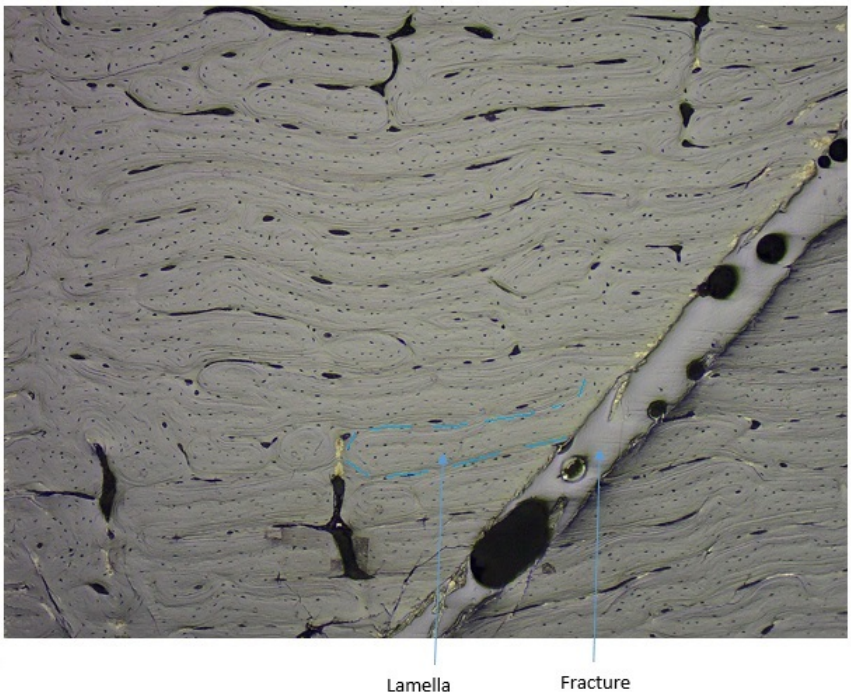

Figure 5.38: Quasi-static radial lamella view for a fractured specimen at 5x magnification

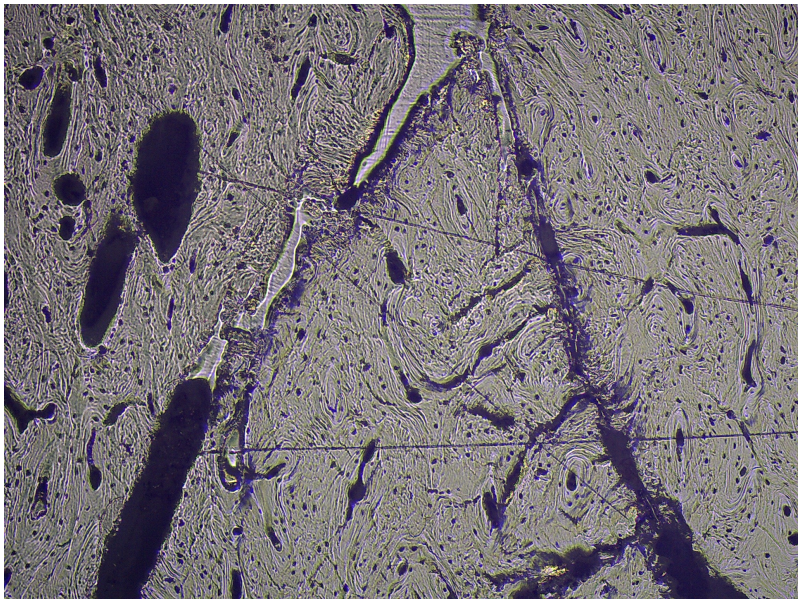

Figure 5.39: Quasi-static longitudinal lamella view for a fractured specimen at 5x magnification

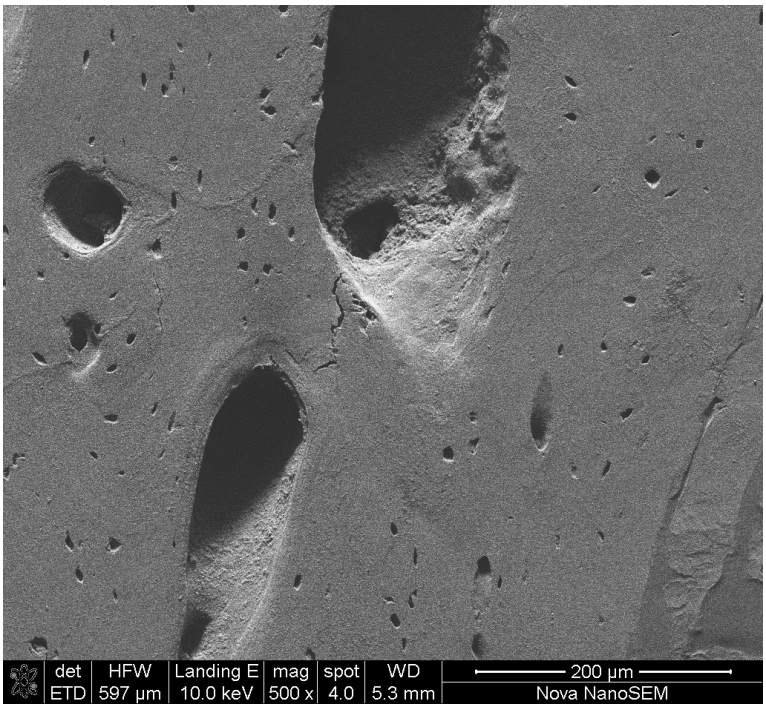

Figure 5.40: Demonstration of a major Haversian channel in the longitudinal direction as seen in Figure 5.39 which appears to remain intact during quasi-static fracture

Within the intermediate regime, specimens chosen displayed only partial internal fracture or the fracture present was not sufficient to fragment the specimen. Fracture propagators were once again observed to follow the lamella pattern within the bone, however, the major fracture now also displays a tendency to follow a pathway between Haversian channels. This is distinctly different to quasi-static fractures. Haversian channels will be discussed within the imaging chapter. These fractures are demonstrated in Figure 5.41 and 5.42.

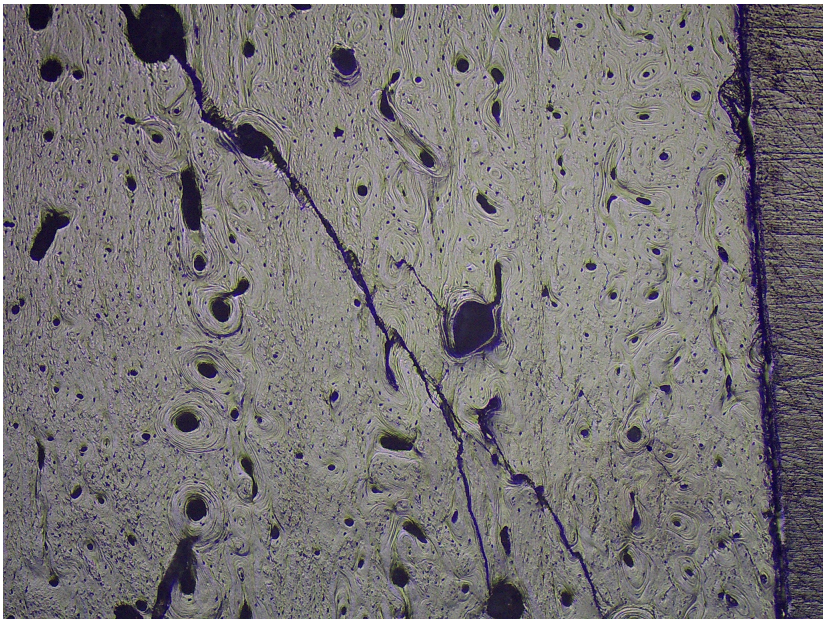

Figure 5.41: Transverse specimen fractured within the intermediate strain rate regime at 5x magnification

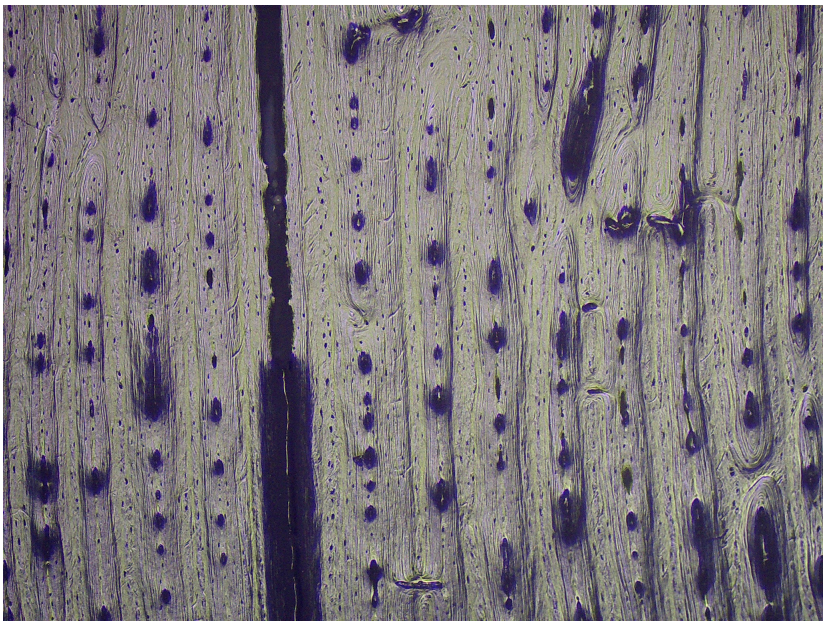

Figure 5.42: Longitudinal specimen fractured within the intermediate strain rate regime at 5x magnification

It is postulated that during quasi-static testing there is sufficient time for the specimen to compress which allows for any fluid trapped within the bone to escape. Once a certain point is reached, the specimen will fracture displaying a form of solid shear fracture. Within the intermediate regime there appears to be insufficient time for any internal fluid to escape due to the compression which results in the fracture displaying a tendency to follow the path of least resistance.

5.5 Discussion

As originally presented by Paul [50], the strain rate sensitivity is once again displayed within the longitudinal direction. The longitudinal results also appear to be representing the data presented initially by McElhaney [33] and Hayes [27], which is seen as an accomplishment due to McElhaney [33] placing strain gauges directly upon the specimen, measuring the true properties of those specimens. However, these papers make no mention of the level of scatter present within the research, nor is there any mention of any compliance being accounted for or inter-bone variation. The scatter present within each bone may be accounted for by increasing the order of accuracy in measurement for the specimens. Currently a vernier calliper was seen as sufficient, however, from the current data this is deemed to be insufficient as the calculation for the apparent modulus is highly dependent on the dimensions of the specimen in question. Further scatter may be accounted for with the construction of a stiffer load cell configuration as the compliance appears to form a large section of the data which may lead to further inaccuracies.

Previously, Bekker [7] and Paul [50] failed to remove compliance from their data sets. Within this chapter, compliance was extensively measured for each set up and removed. It was found that compliance does indeed play a major role in determining the true material properties and so must be accounted for in future studies.

For the longitudinal data, three separate bones were used, with recorded data on the circumferential position of these specimens due to machining limitations. The data between bones proved to vary significantly yet analysing the behaviour of each bone, the behaviour appears to be consistent, simply lying within different strength scales. From this it is possible to visualise the inherent strain rate sensitivity. However, further tests are required using a variety of bones in order to create a comprehensive data set which truly represents this strain rate sensitivity.

Anisotropic behaviour between the directions is proven with the transverse direction displaying no statistically significant signs of strain rate sensitivity. The radial orientation appears to follow a similar trend to the longitudinal orientation with the data obtained from three different bones producing very little scatter.

As all the data recorded has been appropriately verified with compliance effects being removed, this data set now represents true material data which may be used in comparison with future data sets.

Previously, imaging of the fractures has only been performed extensively by Bekker though no conclusions or postulates were able to be made within the work performed by Bekker [7]. Within the current work, it is possible to see a distinctly different fracture pattern between the quasi-static and intermediate specimens though further analysis is required in order to test the postulate stated.

Within the intermediate strain rate testing, the average vector length for the data recorded ranges in excess of 60 000 points at a 2MS/s sampling rate. At higher strain rates, noise does become an issue and it is believed that the use of fast fourier transforms may reduce this noise. However, more points would be required which the Picoscope is not able to achieve due to hardware limitations. It is therefore proposed that with the next edition of the wedge bar prototype, a high speed data card is considered and that other noise reduction methods are investigated.

Chapter 6

Imaging

6.1 Introduction

This chapter details the imaging performed and preparation required in order to gauge an idea of the specimen surface microscopy.

During testing of the specimens, fractures and behaviours displayed became difficult to explain or elaborate on. Imaging of the samples may be used as a further type of analysis where surface and internal structures may be studied in order to gain vital information about the specimens micro structure. This is, however, dependent on the method of imaging used.

The Electron Microscope Unit was also approached in order to develop another level of detail and understanding for the surface structure of specimens.

Key points covered in the following chapter include:

- A description to the various methods of imaging used.
- The methodology for the preparation of the specimens.
- Surface imaging and microstructual displays for each orientation manufactured.

The imaging techniques used in this chapter are light microscopy, inverse light microscopy, and SEM. This is because each method is able to capture a different aspect of the microstructure for the specimen as described below:

- Light microscopy - General surface overview
- Inverse light microscopy - Cellular/Haversian level structure
- SEM - High definition surface overview with nano scale resolution

6.2 Preparation of the specimens

Initial drying and sterilization

Due to the SEM requiring dry and sterilized specimens, the specimens are firstly placed into an ethanol solution for up to two hours in order to rid the specimen of any bio contaminates which may be present. The specimens are then placed in an oven at 60-80 °C and left to dry for three hours. Once dry, the specimens are then placed in glass vials and stored.

Resin casting

To view fractured specimens or even remove micron thick layers off the surface, specimens may require to be set in a rigid support structure. The need for a support structure is to allow for simple and even sanding or polishing which may be performed. Commonly, casting resin is used for simplicity and easy handling, with a Methyl Ethyl Ketone Peroxide (M.E.K.P.) catalyst to initiate the curing process. A further benefit of resin casting is that multiple specimens may be cast and compared simultaneously. The dried and disinfected specimens are placed within a casting container and the mixed resin is syringed into the mould. The use of a syringe is preferred as pouring the resin may shift or change the orientation of the specimens. Once cured, the non-specimen end of the resin is sanded to ensure a flat base for alignment within the SEM. Due to the manner of casting, resin will generally always create a thin layer over the specimen. This is sanded off using a sanding table until the specimens are clearly present. A finer sand paper is used, starting from 1200 grit size and progressively moving to 4000 grit size, depending on the amount of bone one wishes to remove. Once the sanding is complete, a 0.04 micron silca polishing suspension is used to remove any remaining sanding scars which may obscure the imaging to be performed. The surface smoothness is verified using a light microscope and, if possible, an inverse light microscope.

6.3 Imaging

6.3.1 Unfractured frozen specimens SEM

A specimen from each orientation is selected, unfractured, and prepared without resin or sanding. These are coated with gold palladium and placed within the SEM in order to begin to gauge an idea of the raw machined surface structure. Figure 6.1 and 6.2 displays these images.

Longitudinal

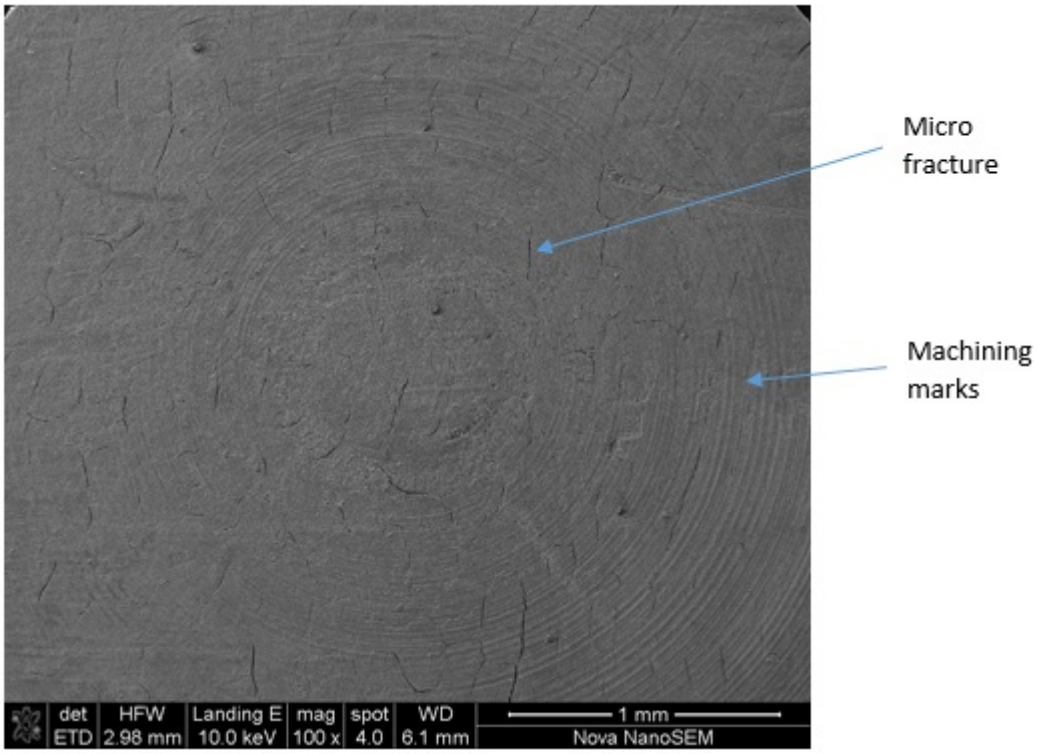

Figure 6.1: Longitudinal specimen surface overview

From this, the machining marks performed by the blade slicing the specimens post-machining are clearly observed. Secondly, the surface appears to have a high density of irregular micro fractures present. These are investigated further in Figure 6.2.

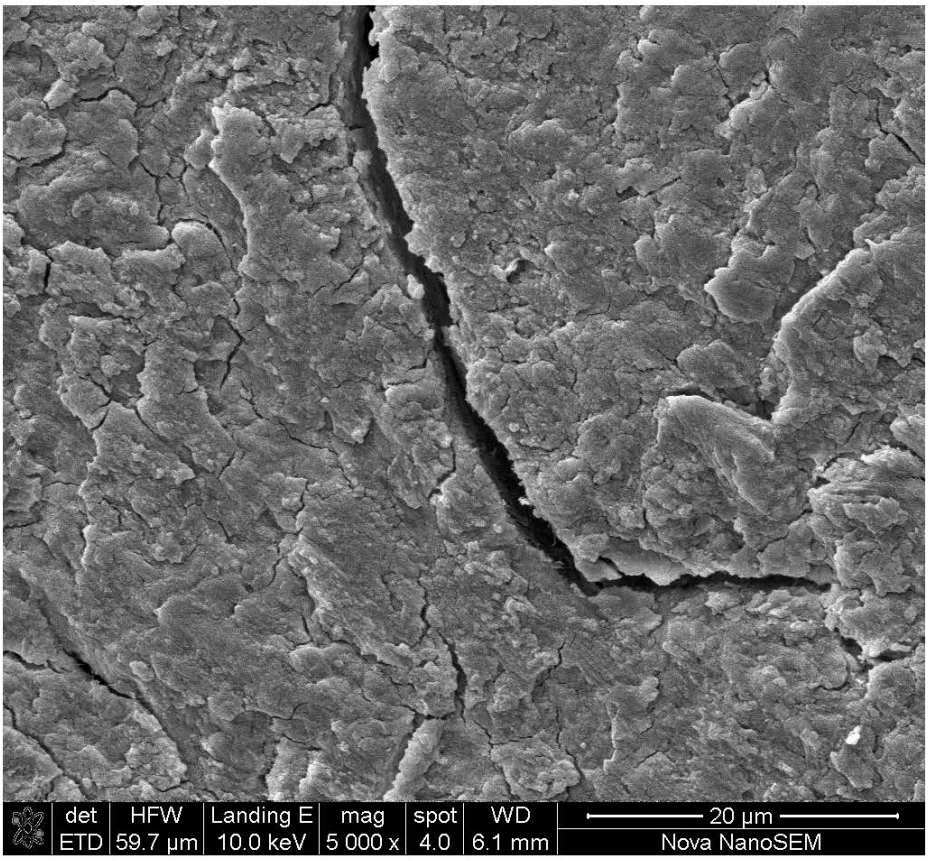

Figure 6.2: Longitudinal specimen surface 5000x magnification

It is now clearly visible that the surface of the specimen appears to be highly irregular, however, this should not influence the mechanical properties as the rough surface, only a few microns thick, should be compressed during the initial take up/pre loading zone. What is of great concern are the cracks present. These range between 1-10 μm. Whether these cracks are introduced during machining or freezing is not known at this stage.

Radial

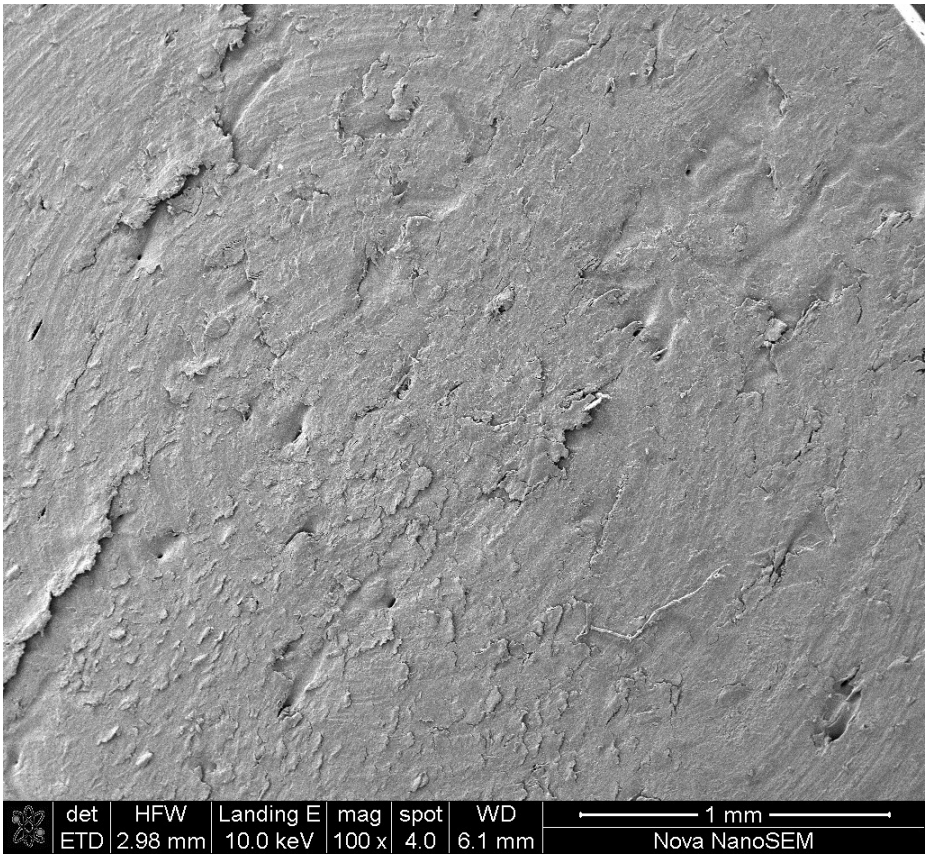

Figure 6.3: Radial specimen surface overview

As the radial samples were core drilled from the sample bone and then machined to size, the lathe does not have the same sharpness as the blade used in cutting longitudinal specimens. Due to the machining tool being less sharp, there is a presence of tears as material is removed. This may in turn weaken the bone by introducing unnecessary fractures. Figure 6.4 and 6.5 displays these tears at a greater magnification.

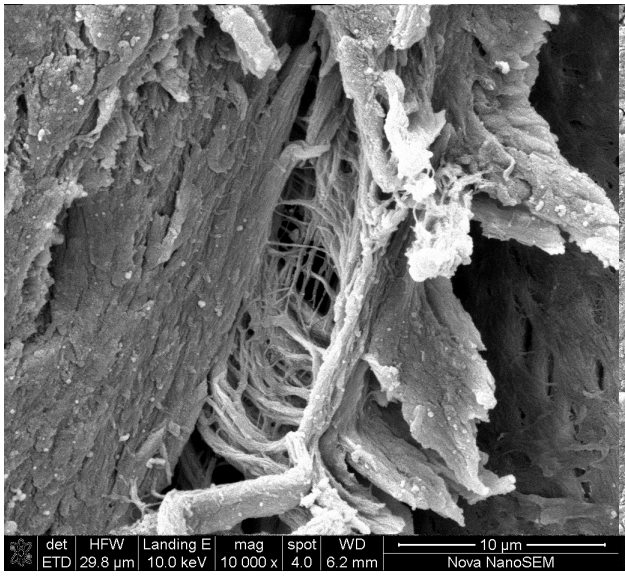

Figure 6.4: Radial internal magnification of a tear pattern

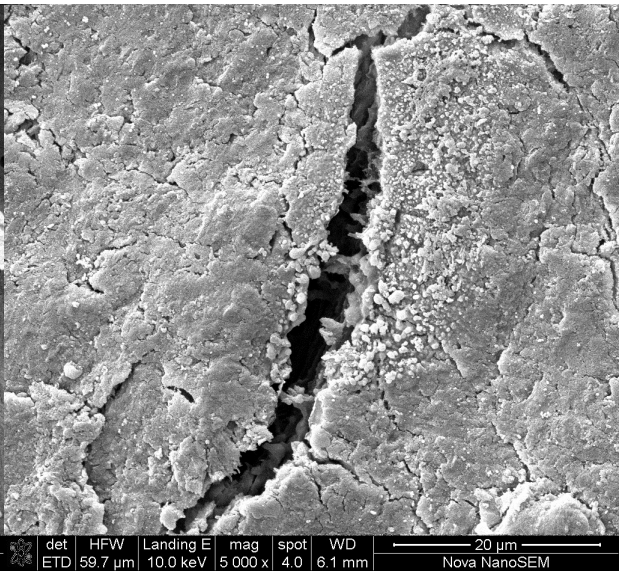

Figure 6.5: Radial micro fracture overview

From Figures 6.4 and 6.5, the possible presence of tearing occurring is very likely as we can begin to see the bone fibres splitting and de-laminating from one another. This may be further propagated by freezing of the specimens. Further investigation of the surface focuses on a pit-like structure present on the surface. When focusing on these structures, these are verified, using the work of Pazzaglia *et.al.* [51, 52] and Figueiredo *et.al.* [19], to be the Haversian channels in the bone. The channels are further investigated with the Figure 6.6 and 6.7 displaying images of the complex interwoven wall formation.

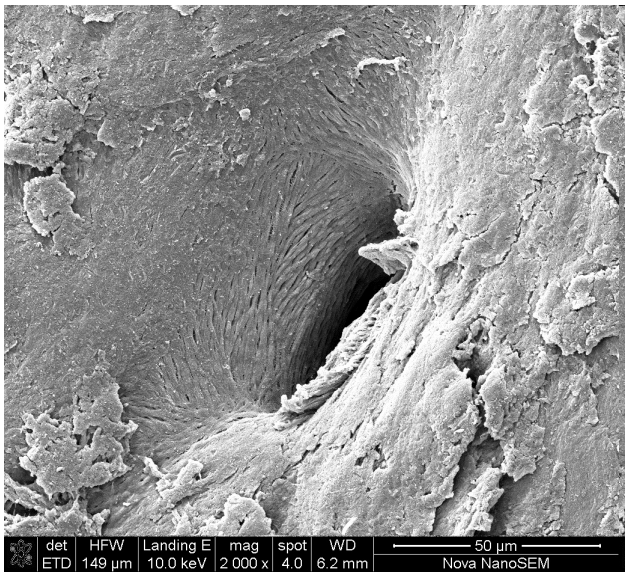

Figure 6.6: Large radial specimen vasculature

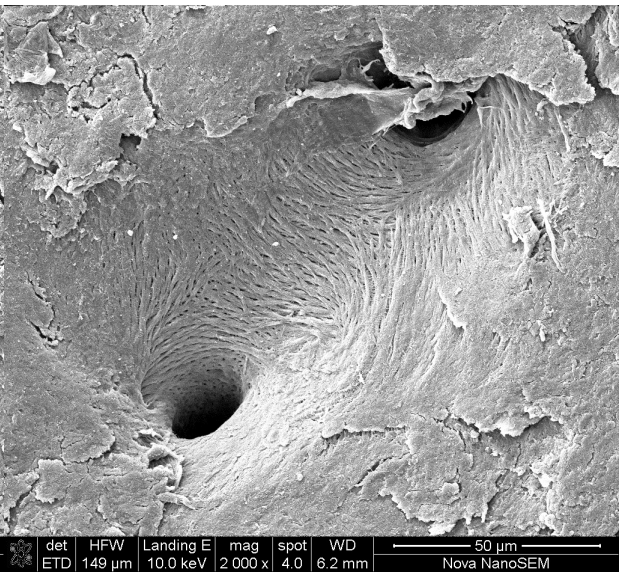

Figure 6.7: Radial specimen vasculature demonstrating the complex woven wall structure between two small canals

Figure 6.8: Opened vascular channel using a Phenom Pro X SEM which does not require a gold paladium coating allowing for depth of view

Figures 6.6, 6.7, and 6.8 begin to display the complexity of the inherent vascular systems found within cortical bone. Such systems may aid to the strain rate sensitive behaviour characteristics. As the diameters of these channels range between approximately 20 μm - 100μm, these may play an important role in the propagation of fracture during testing.

Transverse

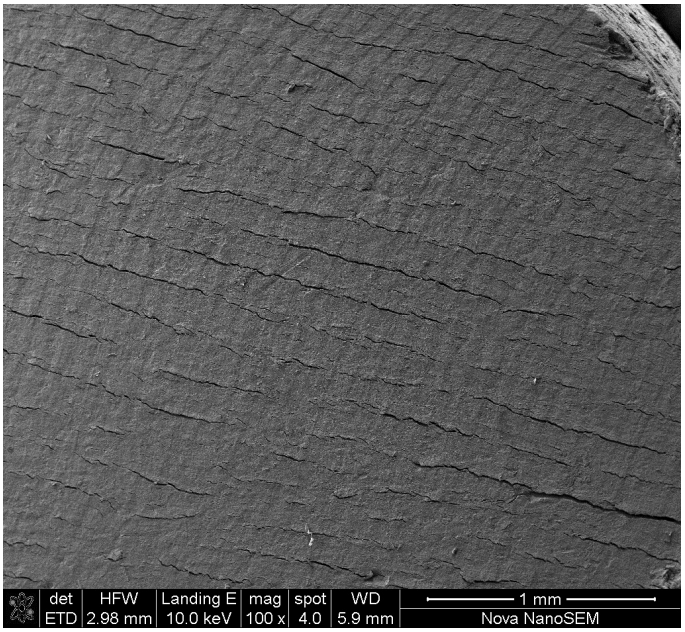

Figure 6.9: Transverse specimen surface overview

The cracks present in the transverse specimen appear to be highly uniform, running in parallel lines along the diameter. As the specimens are machined on a lathe in order to achieve the correct length post-coring, these machining lines are visibly present. It is highly unlikely, though, that machining could achieve such uniformly distributed cracks. At a closer view of the cracks, a form of de-lamination occurring is observed. The high density of cracks occurring may significantly increase the variability of fracture within the bone due to the numerous crack propagation paths present.

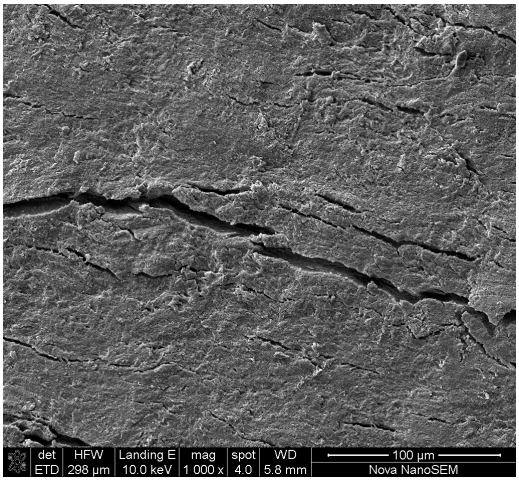

Figure 6.10: Transverse specimen crack overview

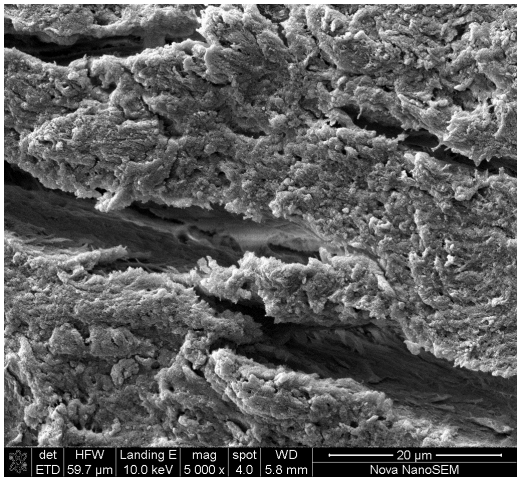

Figure 6.11: Transverse specimen internal crack view

Specimens are then set in resin and refined. The purpose of refining specimens is to remove any machining marks and irregularities. This will help gauge the true form of the surface. For this, the specimens were set in resin and machined until a smooth surface was present.

Figures 6.12 - 6.17 display images, at a 5x magnification, which are taken in order to develop an understanding into the microsctructural variance per orientation, viewed both from the top and side of the specimen.

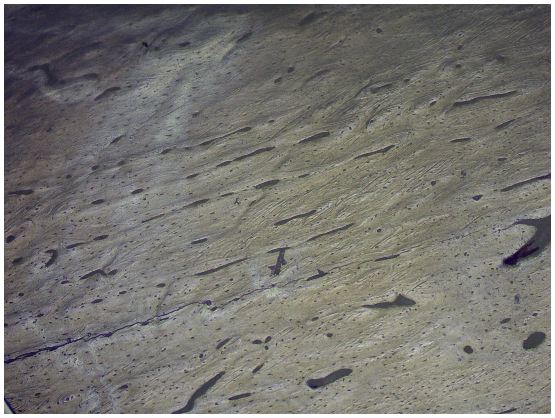

Figure 6.12: Top view of a transversely orientated specimen

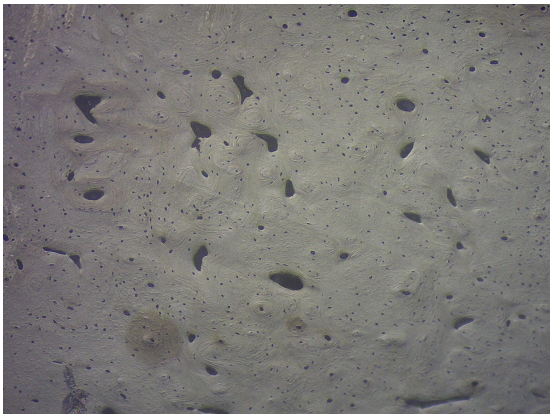

Figure 6.13: Internal Side view of a transversely orientated specimen sliced in half

Figure 6.14: Top view of a longitudinally orientated specimen

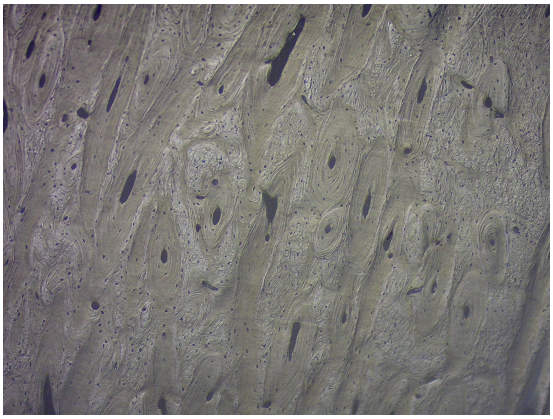

Figure 6.15: Internal Side view of a longitudinally orientated specimen sliced in half

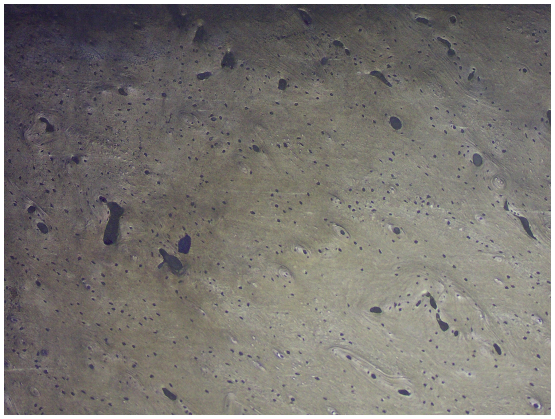

Figure 6.16: Top view of a radially orientated specimen

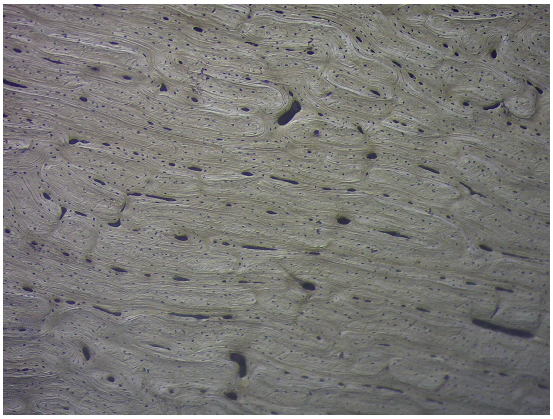

Figure 6.17: Internal Side view of a radially orientated specimen sliced in half

Based on the observations made on the variation in microstructure for each orientation, Figure 6.18 is generated to provide an approximate idea of the bovine specimen microstructural architecture. The true architecture, however, is highly complex as already demonstrated and so this image purely serves as a template to display the basic layout of a specimen.

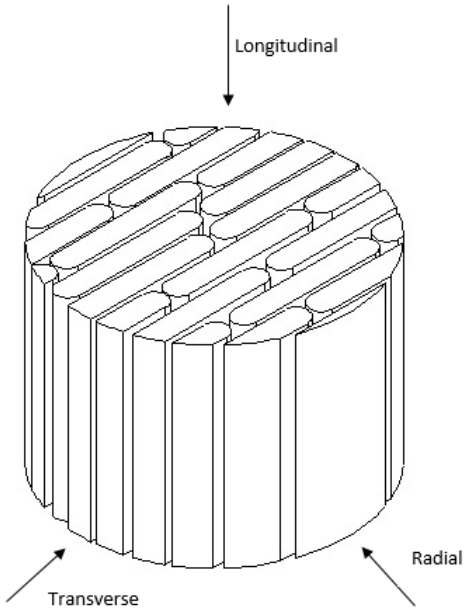

Figure 6.18: Modeled microstructural approximation of the bovine specimen architecture and testing orientation descriptions

6.3.2 Unfractured non frozen specimens SEM

In order to determine whether freezing may initiate pre-testing fractures as seen in Figures 6.1, 6.3, 6.9, machined specimens are placed within ethanol and dried as previously described. No further sanding or polishing is performed as raw specimens are to be observed. These are placed within the SEM and the surface is analysed.

Longitudinal

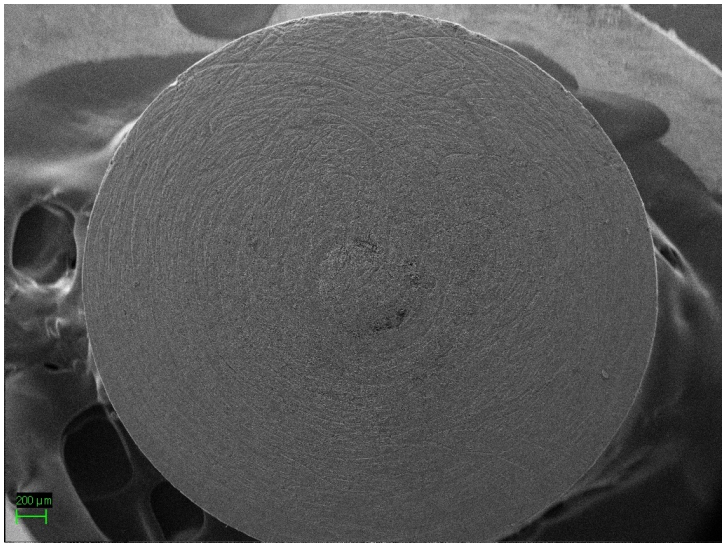

Figure 6.19: Surface structure of a longitudinal specimen prior to freezing

Observing the longitudinally orientated specimen, there is a significant decrease in surface fractures, however, there is an increase in surface roughness due to natural manufacturing variation. Under further observation of the surface structure, very few apparent fractures are present, with those present being significantly smaller than in the frozen specimens.

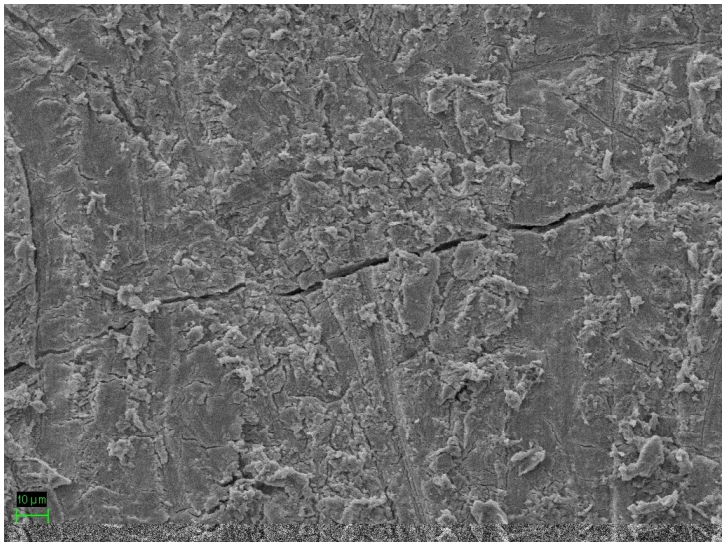

Figure 6.20: Longitudinal surface fracture demonstration

Radial

The radial specimen also demonstrates a significant decrease in fractures with only imperfections present being in the form of Haversian channels, found naturally within bone, and the machining marks which are difficult to remove on biological material.

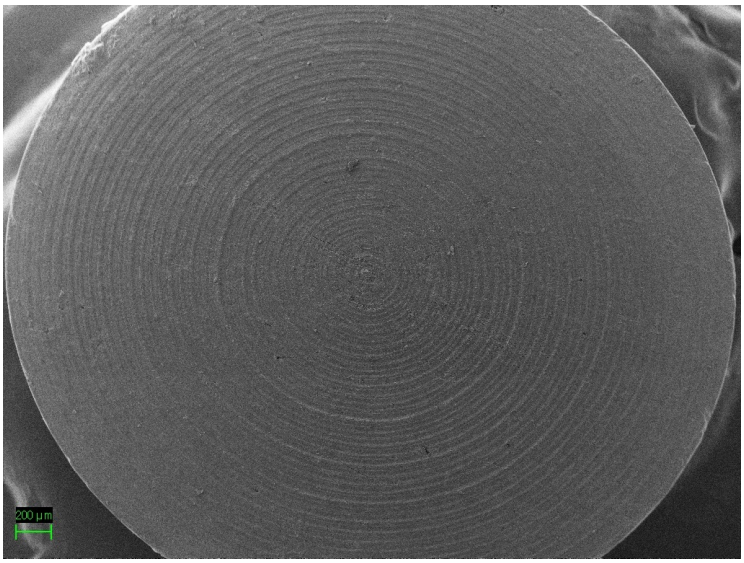

Figure 6.21: Surface structure of a radial specimen prior to freezing

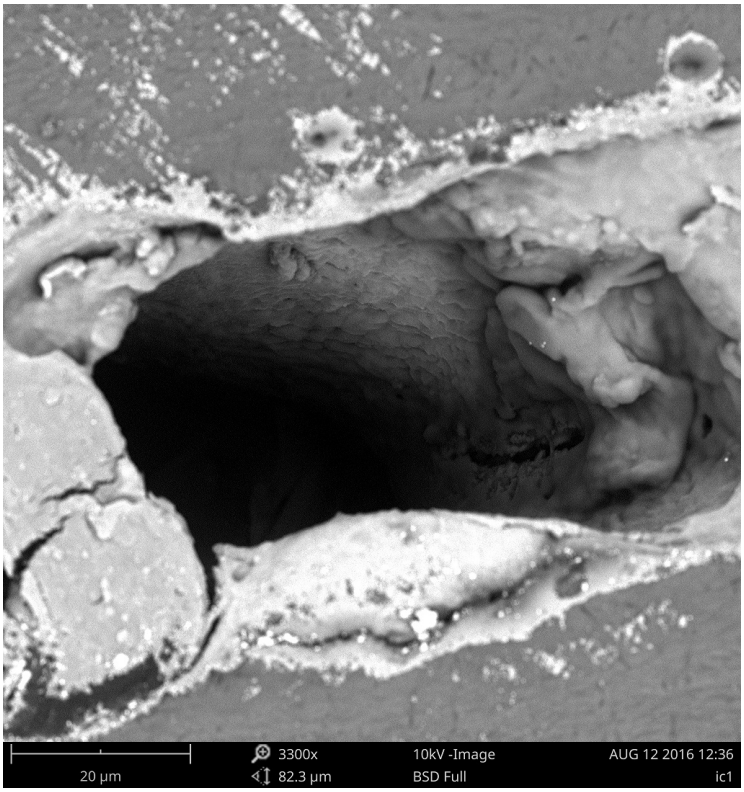

Figure 6.22: Radial surface vascular channel presence

Transverse

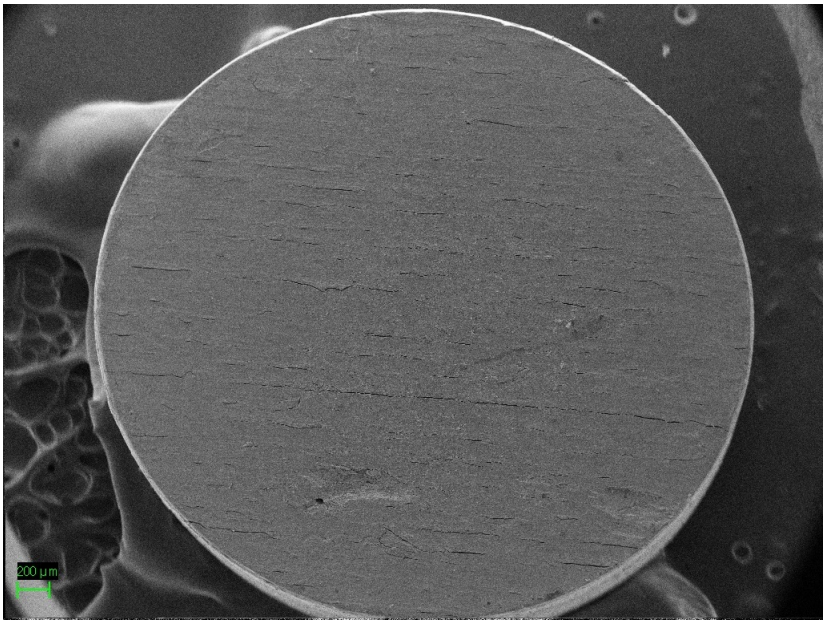

Figure 6.23: Surface structure of a transverse specimen prior to freezing

Observing the transverse specimen, the presence of the parallel fractures is still present. This may suggest that these fractures do not originate due to freezing, but instead may be subject to the manufacturing method, or simply be an inherent feature of the bone. Focusing on these fractures displays what appears to be a form of de-lamination as previously seen within the frozen specimen. The fractures also appear to be running within the pattern of the lamella found on the surface. This is demonstrated in the following figure:

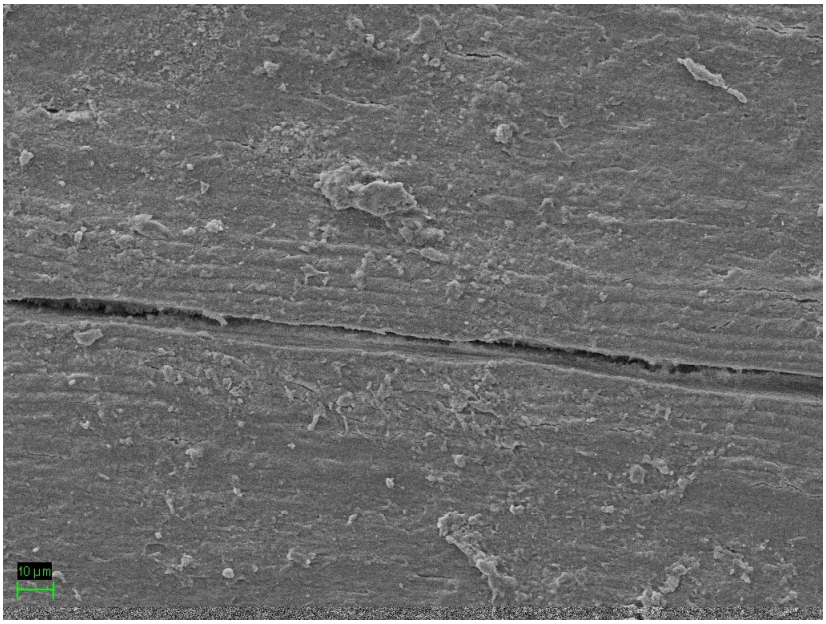

Figure 6.24: Transverse fracture structure

6.4 Summary

In this chapter a number of postulates have been presented, these are summarised as:

- Bone is a highly porous material with a large presence of Haversian channels ranging from 5μm to 100μm. The presence of these Haversian channels does not appear to weaken the material as seen in section 5.3.3.
- Freezing of the bone appears to induce micro fractures within the radial and longitudinal orientations. This may be due to liquid expansion during freezing, forcing the bone fibers to separate.
- Haversian channels appear to lie in the spaces between the lamella. A postulate is made which suggests that freezing may initiate the separation of lamella due to liquid expansion within the Haversian channels.

Chapter 7

Numerical Model

7.1 Introduction

The long term goal of the broader research project is to use measured data to formulate mathematical models that capture the deformation, stress, and fracture of cortical bone. These models would ultimately be used for analysis and prediction of behaviour. As a first attempt, only the stress/strain behaviour is modelled. This is limited to one dimension, and the model is later developed into the other directions.

The following chapter will detail the following key aspects:

- A discussion about the previous model developed.
- The modifications performed in order to correct the errors discovered.
- The presentation of a new phenomenological model which is able to capture the longitudinal orientation behaviour.
- Further adjustments of the current phenomenological model in order to capture the behaviour of the radial orientation.

As stated in the literature review, fractional calculus and Ricatti equations were investigated, however, the investigations showed that the approaches would not easily capture the required behaviour. As a result, further investigation was not attempted. All models were subject to a least squares analysis in order to generate a best fit relationship. All coefficients are rounded up to a single decimal place.

7.2 Paul *et.al.* Model

7.2.1 Preliminary investigation

Previously, Paul *et.al.*, [50] created a phenomenological model which fitted the experimental data seemingly perfectly. However, upon performing a unit analysis, the units do not balance correctly. A further issue is that the integral provided does not produce the correct analytical solution. This error is introduced in incorrect integration of the nonlinear Maxwell element. In order to gauge the error introduced, a numerical approximation, using forward Euler, is applied to the integral shown in equation (7.1).

$$\sigma_{Maxwell} = \int_0^t E\varepsilon(\dot{\tau})^m e^{\frac{-E}{\eta}(t-\tau)} d\tau \tag{7.1}$$

The solution to equation (7.1) is compared to that of the analytical solution in equation (7.2)

$$\sigma_{Maxwell} = \eta\dot{\varepsilon}^m \left[1 - exp\left[\frac{-E\varepsilon}{\eta\dot{\varepsilon}^m}\right]\right] \tag{7.2}$$

Visually, this comparison is shown in Figure 7.1 for the case m = 2. For both the following figures, all modulus and strain values are set to unity:

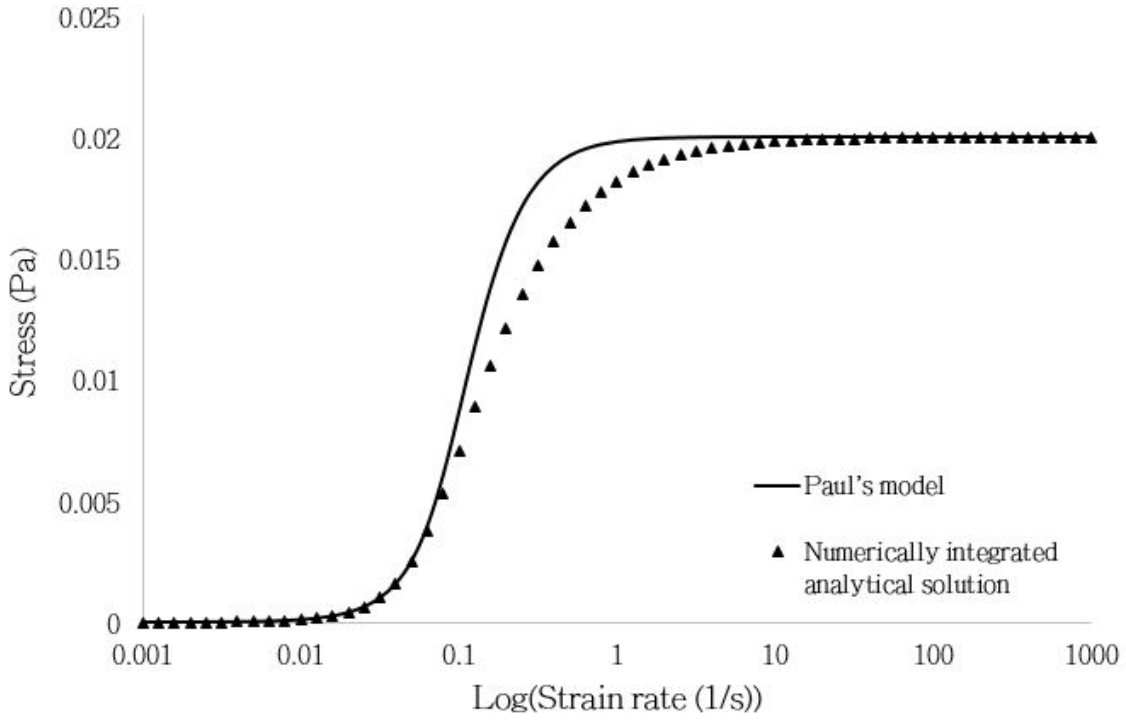

Figure 7.1: Numerical vs analytical comparison for a Maxwell element with viscous power 2

It can clearly be seen that the constant strain rate equation by Paul provides a much steeper transitional period. For the case where m = 2.9, the rate of transition (gradient on the graph) is similar in both approaches, but the onset of the transition in not correctly captured.

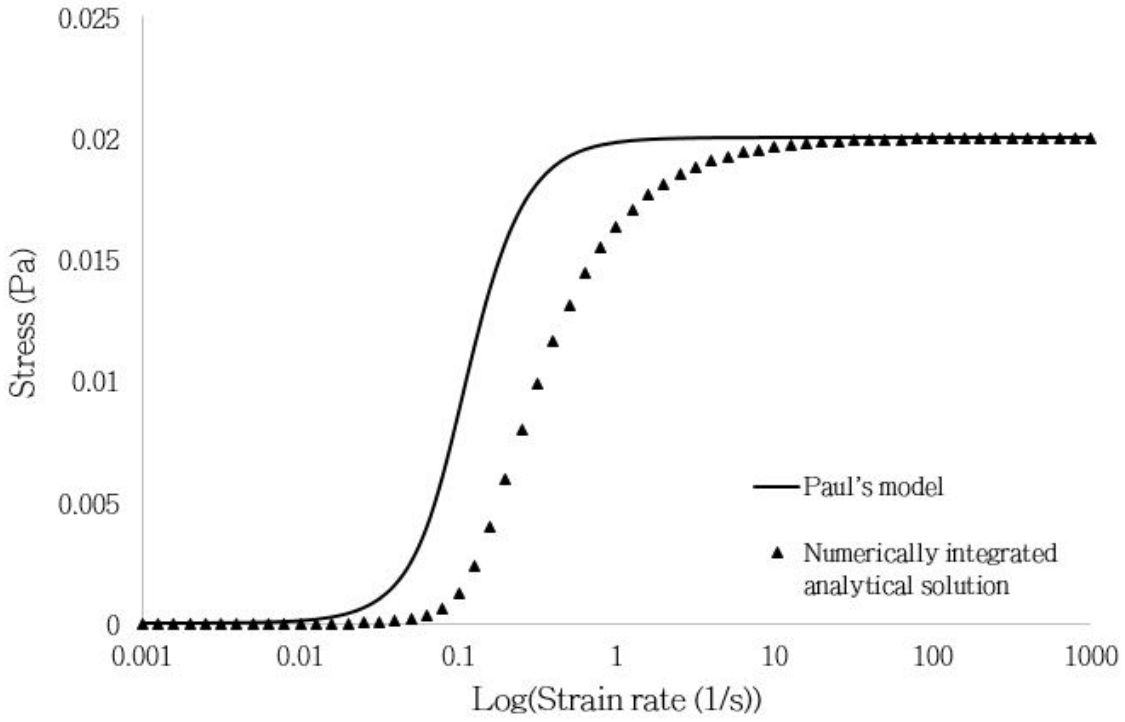

Figure 7.2: Numerical vs analytical comparison for a Maxwell element with viscous power 2.9

Within the model presented by Paul for bone, a coefficient of three is used. In order to match the steepness achieved within the model reported by Paul, using the non linear Maxwell element, the exponent will need to be significantly higher than three. For these reasons, a different model, whether phenomenological or an actual material representation, is required. Furthermore, the processing time and power required to solve high coefficient nonlinear equations increases exponentially and is not feasible.

7.2.2 Model Modifications

Focusing on the Maxwell integral as seen in equation (7.1), is is assumed that the damping coefficient is governed by a power law function. In order to prevent this coefficient's units from being dependent on the exponent, a non dimensionalising term is added in the form of a reference strain rate. This allows for the coefficient to possess the unit of MPa. The modified power law is presented in equation (7.3).

$$\eta = \mu\left(\frac{\dot{\varepsilon}}{\dot{\varepsilon_o}}\right)^{m-1} \tag{7.3}$$

where μ is a modified viscosity coefficient with units Pa and m is the power law parameter.

The modified power law viscosity is substituted into the Maxwell integral instead of the actual constitutive equation and the following phenomenological integral of Maxwell form is achieved:

$$\sigma(t) = \int_0^t E\varepsilon(\dot{\tau})e^{\frac{E}{\mu}\left(\frac{\dot{\varepsilon_o}}{\dot{\varepsilon}}\right)^{m-1}\left(\tau - t\right)}d\tau \tag{7.4}$$

While no specific physical rationale exists for the assumption of power law behaviour (m-1 term), this approximation is introduced as it correctly captures the changing rate dependence, and yields the analytically tractable equation (7.5).

$$\sigma = \mu\left(\frac{\dot{\varepsilon}}{\dot{\varepsilon_o}}\right)^{m-1}\dot{\varepsilon}\left[1 - e^{-\left(\frac{E\varepsilon}{\mu\dot{\varepsilon}}\right)\left(\frac{\dot{\varepsilon_o}}{\dot{\varepsilon}}\right)^{m-1}}\right] \tag{7.5}$$

Comparing the phenomenological model of Paul to the modified one, it is found that the models behave identically. This is confirmed by varying the values of the coefficients and powers. If the reference strain rate is varied, the onset of the regime change with respect to strain rate will change horizontally, which is highly beneficial. The plot comparing these two methods is shown in Figure 7.3 for equivalent coefficients, and when the reference strain rate is varied in Figure 7.4.

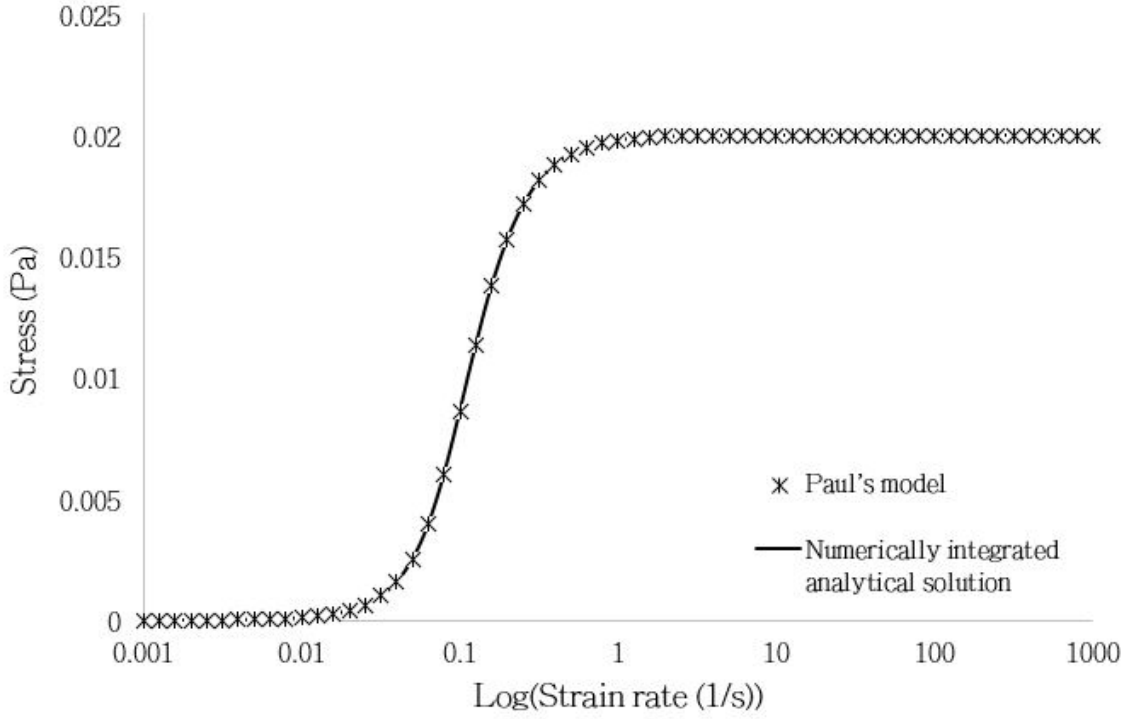

Figure 7.3: Comparison between phenomenological models for equivalent powers, for the case m = 2, and unity values for all other coefficients and reference strain rate

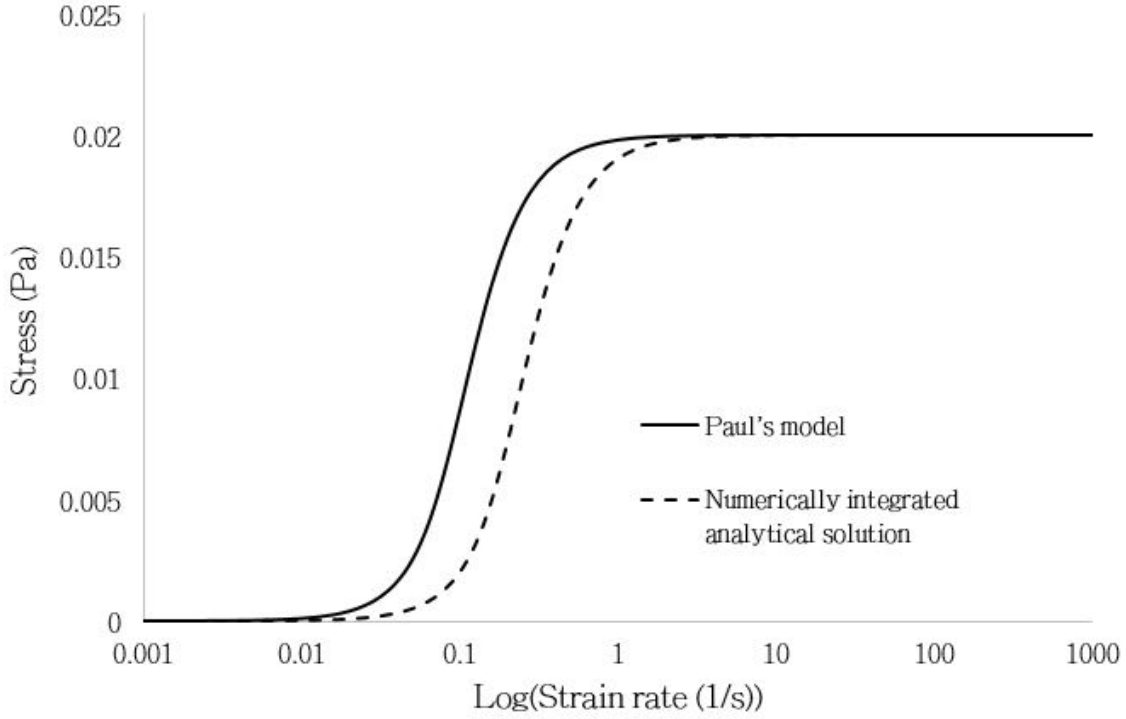

Figure 7.4: Delayed onset of transition from low to high regimes for the case of reference strain rate, $\dot{\varepsilon_0} = 5$

7.3 New phenomenological model

Using the nonlinear Maxwell element presented in 7.2, two new phenomenological models for bovine cortical bone are developed. These models are based on two arguments of springs and nonlinear dampers.

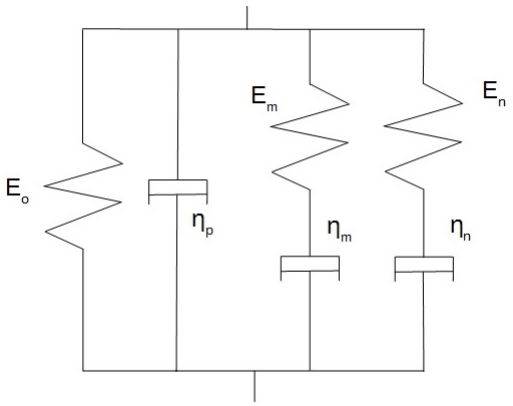

Figure 7.5: Model one

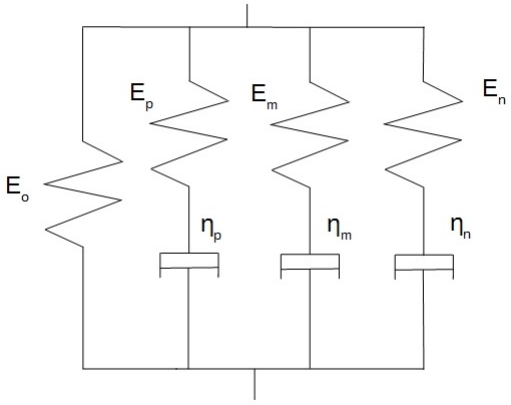

Figure 7.6: Model two

The model presented in Figure 7.5 consists of a Kelvin Voigt and two Maxwell elements in parallel while the second one is three nonlinear Maxwell elements combined with a spring to provide base stiffness. Originally, Shim *et.al.* [56] incorporated a damper into his model when trying to capture the behaviour of bone. This is included in order to capture the initial linear jump in stress prior to the nonlinear behaviour as demonstrated in Figure 7.7.

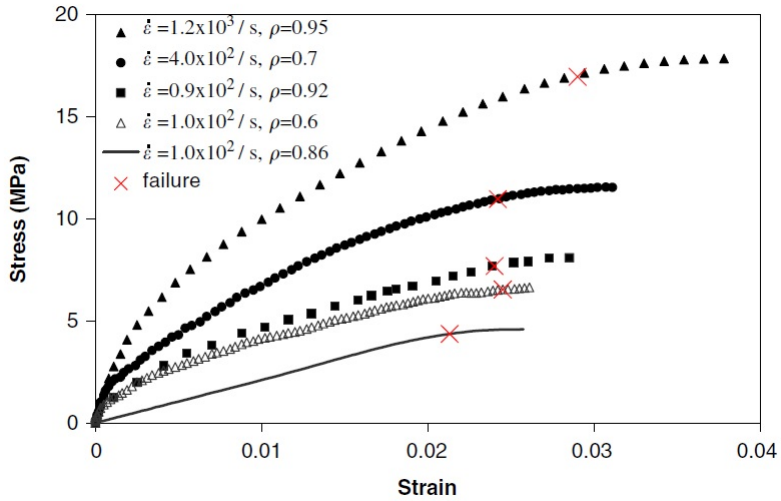

Figure 7.7: High strain rate data as presented by Shim *et.al.* [56]

Bekker [7] and Paul [50] also noted the initial linear behaviour at high strain rates which led to the inclusion of the dashpot within their respective models. As dashpots do not react immediately, the initial displacement is governed by the linear spring due to the dashpot not deforming (which is more easily seen at increased strain rates). As the motion continues, the

dashpot relaxes and additional strain occurs, yielding increased strain for a given stress, or equivalently reduced stress for a given strain. This rate of relaxation of the damper drives the rate dependence. For bone, the assumption is that there must be at least one path where any liquid within can travel from one end to another uninterruptedly. However, this cannot easily be confirmed. Additionally, whether the initial linearity is due to the electric or mechanical feedback of the machinery is unverifiable. The second model counters these assumptions by replacing the damper within the Voigt element by a third Maxwell element. As a Maxwell element primarily governs fluid response, the assumption is that bone will have a base strength or structure, and then be supplemented in strength or stiffness by the fluid trapped within at low, intermediate and high strain rates. This fluid may be governed by a nonlinear viscosity. It has already been shown in chapter 6 that bone may be considered as a highly porous structure with the presence of large and micro vascular channels within and so either of these models is acceptable. The equations and subsequent final integrated forms are demonstrated followed by a visual comparison to the data reported by Paul.

For the purposes of the model presented by Paul, the coefficients are as follows:

Table 7.1: Parameters used in the model presented by Paul [50]

E_o (MPa)	E_m (MPa)	E_n (MPa)	η_p (MPa.s)	η_m (MPa.s)	η_n (MPa.s)	p	m	n
9e03	1.25e03	5.5e03	0.05	75	0.11	0.63	0.63	3

Model one

In order to derive an analytical solution to model one, the integral form is firstly constructed.

$$\sigma(t) = E_o\varepsilon + \mu_p\left(\frac{\dot{\varepsilon}}{\dot{\varepsilon_{op}}}\right)^p + \int_0^t E_n\varepsilon(\dot{\tau})e^{\frac{E_n}{\mu_n}\left(\frac{\varepsilon\dot{o}n}{\dot{\varepsilon}}\right)^{n-1}(\tau-t)}d\tau + \int_0^t E_m\varepsilon(\dot{\tau})e^{\frac{E_m}{\mu_m}\left(\frac{\varepsilon\dot{o}m}{\dot{\varepsilon}}\right)^{m-1}(\tau-t)}d\tau \tag{7.6}$$

Under the assumption of constant strain rate, this can be simplified to:

$$\begin{aligned}\sigma = E_o\varepsilon + \mu_p\left(\frac{\dot{\varepsilon}}{\dot{\varepsilon_{op}}}\right)^p + \mu_n\left(\frac{\dot{\varepsilon}}{\dot{\varepsilon_{on}}}\right)^{n-1}\dot{\varepsilon}\left[1 - e^{-\left(\frac{E_n\varepsilon}{\mu_n\dot{\varepsilon}}\right)\left(\frac{\varepsilon\dot{o}n}{\dot{\varepsilon}}\right)^{n-1}}\right] \\ +\mu_m\left(\frac{\dot{\varepsilon}}{\dot{\varepsilon_{om}}}\right)^{m-1}\dot{\varepsilon}\left[1 - e^{-\left(\frac{E_m\varepsilon}{\mu_m\dot{\varepsilon}}\right)\left(\frac{\varepsilon\dot{o}m}{\dot{\varepsilon}}\right)^{m-1}}\right]\end{aligned} \tag{7.7}$$

Where E is the spring stiffness, μ is the dashpot viscosity constant, the exponents represent the power law parameters, $\dot{\varepsilon_0}$ is the reference strain rate and τ is a variable of integration.

The model by Paul and model one are compared on a plot of stress vs strain rate, at increasing strain intervals in Figure 7.8:

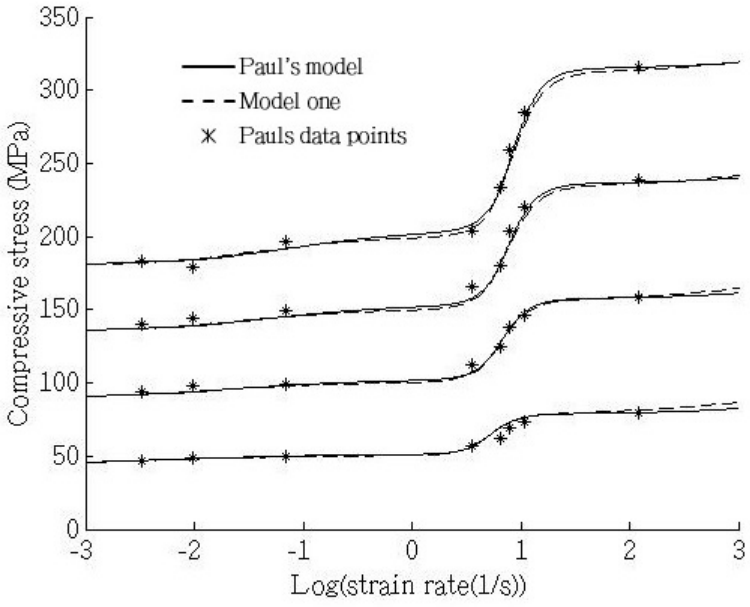

Figure 7.8: Model one (dashed) in comparison to the model reported by Paul [50] (solid) for 0.5, 1, 1.5 and 2 percent strain

Table 7.2: Parameters used for the first model

E_o (MPa)	E_m (MPa)	E_n (MPa)	μ_p (MPa)	μ_m (MPa)	μ_n (MPa)	p	m	n	$\dot{\varepsilon_{op}}$ s^{-1}	$\dot{\varepsilon_{om}}$ s^{-1}	$\dot{\varepsilon_{on}}$ s^{-1}
9e03	5.5e03	1e03	0.6	1	50	0.4	2.9	0.7	1	2.8	16

Model two

In order to derive an analytical solution to model two, the integral form is firstly constructed.

$$\sigma(t) = E_o\varepsilon + \int_0^t E_p\dot{\varepsilon(\tau)}e^{\frac{E_p}{\mu_p}\left(\frac{\varepsilon\dot{o}p}{\dot{\varepsilon}}\right)^{p-1}(\tau-t)}d\tau + \int_0^t E_n\dot{\varepsilon(\tau)}e^{\frac{E_n}{\mu_n}\left(\frac{\varepsilon\dot{o}n}{\dot{\varepsilon}}\right)^{n-1}(\tau-t)}d\tau + \int_0^t E_m\dot{\varepsilon(\tau)}e^{\frac{E_m}{\mu_m}\left(\frac{\varepsilon\dot{o}m}{\dot{\varepsilon}}\right)^{m-1}(\tau-t)}d\tau \quad (7.8)$$

Under the assumption of constant strain rate, this is simplified to:

$$\sigma = E_o\varepsilon + \mu_p\left(\frac{\dot{\varepsilon}}{\dot{\varepsilon_{op}}}\right)^{p-1}\dot{\varepsilon}\left[1 - e^{-\left(\frac{E_p\varepsilon}{\mu_p\dot{\varepsilon}}\right)\left(\frac{\varepsilon\dot{o}p}{\dot{\varepsilon}}\right)^{p-1}}\right] + \mu_n\left(\frac{\dot{\varepsilon}}{\dot{\varepsilon_{on}}}\right)^{n-1}\dot{\varepsilon}\left[1 - e^{-\left(\frac{E_n\varepsilon}{\mu_n\dot{\varepsilon}}\right)\left(\frac{\varepsilon\dot{o}n}{\dot{\varepsilon}}\right)^{n-1}}\right] + \mu_m\left(\frac{\dot{\varepsilon}}{\dot{\varepsilon_{om}}}\right)^{m-1}\dot{\varepsilon}\left[1 - e^{-\left(\frac{E_m\varepsilon}{\mu_m\dot{\varepsilon}}\right)\left(\frac{\varepsilon\dot{o}m}{\dot{\varepsilon}}\right)^{m-1}}\right] \quad (7.9)$$

where the constant definitions within equation (7.9) are identical to those within model one. The model presented by Paul and model two are compared on a plot of stress vs strain rate, at increasing strain intervals in Figure 7.9:

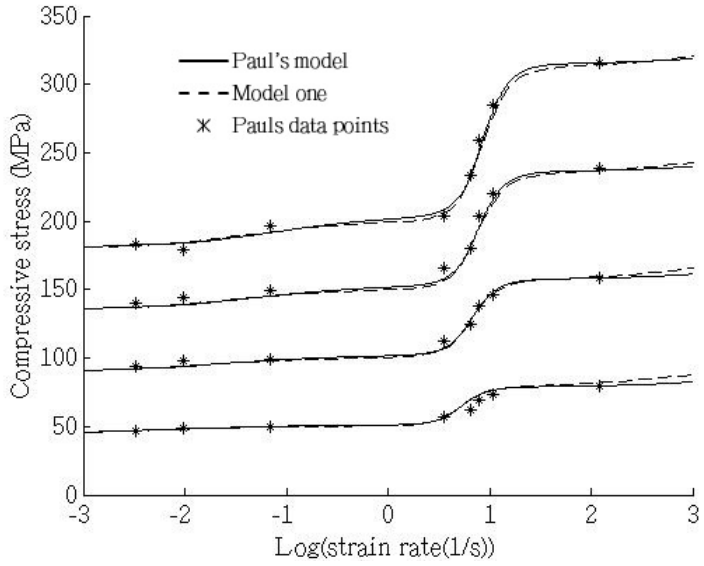

Figure 7.9: Model two (dashed) in comparison to the model reported by Paul [50] (solid) for 0.5, 1, 1.5 and 2 percent strain

Table 7.3: Parameters used for the second model

E_o (MPa)	E_m (MPa)	E_n (MPa)	E_p (MPa)	μ_p (MPa)	μ_m (MPa)	μ_n (MPa)	p	m	n	$\dot{\varepsilon_{op}}$ s^{-1}	$\dot{\varepsilon_{om}}$ s^{-1}	$\dot{\varepsilon_{on}}$ s^{-1}
9e03	5.5e03	1e03	10e03	0.6	1	50	0.4	2.9	0.7	1	2.8	16

The damper(model one) and Maxwell(model two) elements primarily focus upon the high strain rate portion of the data. This results in the low and intermediate portion remaining almost completely unchanged.

7.4 Presented model on current data

As there has been no high strain rate testing performed, the numerical model will not be accurate within this regime. Furthermore, the numerical model will only cover the radial and longitudinal directions as bone orientated in the transverse direction did not have statistically significant strain rate sensitivity. For the following numerical modelling, the apparent modulus has been chosen for analysis as this was more consistent over the previously used compressive stresses.

Radial

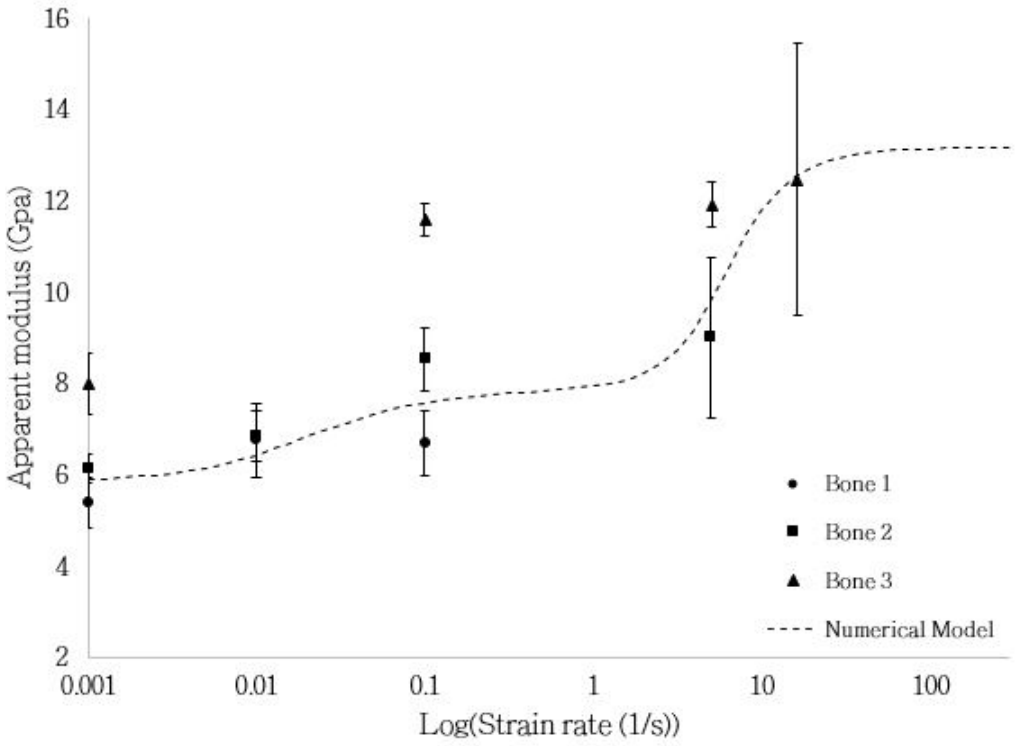

Figure 7.10: Numerical model fitted to experimental radial apparent modulus averages

Table 7.4: Parameters used for the presented radial model

E_o (MPa)	E_m (MPa)	E_n (MPa)	E_p (MPa)	μ_p (MPa)	μ_m (MPa)	μ_n (MPa)	p	m	n	$\dot{\varepsilon_{op}}\ s^{-1}$	$\dot{\varepsilon_{om}}\ s^{-1}$	$\dot{\varepsilon_{on}}\ s^{-1}$
580	520	200	100	0.1	1	60	0.1	2	1	1	12	1

With the residual sum of squares = 3.72 GPa^2 and the mean of the residuals being 0.40 GPa as per the least squares regression performed. Both these numbers are required to be as close to zero as possible and therefore even though visually the fit is good, and for this initial study the fit is good, more data points are required increase the accuracy.

Longitudinal

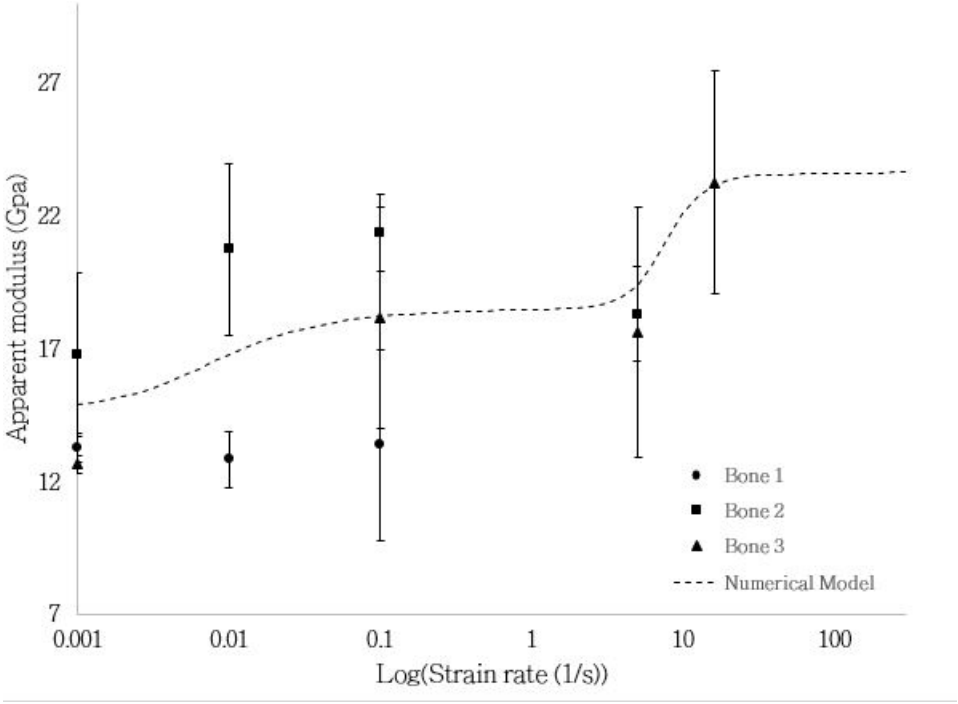

Figure 7.11: Numerical model fitted to experimental longitudinal apparent modulus averages

Table 7.5: Parameters used for the presented longitudinal model

E_o (MPa)	E_m (MPa)	E_n (MPa)	E_p (MPa)	μ_p (MPa)	μ_m (MPa)	μ_n (MPa)	p	m	n	$\dot{\varepsilon_{op}}\ s^{-1}$	$\dot{\varepsilon_{om}}\ s^{-1}$	$\dot{\varepsilon_{on}}\ s^{-1}$
1450	500	380	10	0.2	1	300	0.1	3	1	1	12	1

With the residual sum of squares = 2.26 GPa^2 and the mean of the residuals being -0.28 GPa as per the least squares regression performed. Both these numbers are required to be as close to zero as possible and therefore even though visually the fit is good, and for this initial study the fit is good, more data points are required increase the accuracy.

7.5 Discussion

Previously, the numerical model developed by Paul proved to be incomplete, with inconsistent units throughout the formula. The presented numerical model, whilst still phenomenological, is unit-consistent throughout the integration process and so provides a usable numerical model.

As demonstrated in section 7.4, the numerical model is able to capture the complex strain rate sensitivity in each direction, however, the model is still not able to be represented physically. As the model is built on a collection of conceptual physical elements, the basis upon which this model is built it represented by the physical models one and two, in Figures 7.5 and 7.6.

Within the longitudinal data, the model is adjusted to capture the average behaviour for the data of a given strain rate. However, this model still requires significantly more testing in order to increase the accuracy of this model as demonstrated by the least squares regression analyses performed.

Chapter 8

Conclusions

This chapter summarises the overall findings of this project. These are discussed with regards to the machine design, testing and imaging procedures, and the numerical modelling. Recommendations stemming from these are presented in chapter 9.

8.1 Machine design

Fabricating a more user friendly load cell has increased the compliance substantially. Previously, the load cell and system compliance was not evaluated experimentally and thus an arguable comparison cannot be drawn. What can be concluded, however, is that the compliance does impact the data substantially and must be taken into account in future testing and designs.

8.2 Specimen manufacturing and measurements

During manufacturing of the samples, only circumferential locations were kept for the specimens. After analyzing literature which came available after the manufacturing was complete, it was found that the location along the length of the bone should be noted too. Unfortunately within this study, too few specimens were machined to determine any statistically significant variation in mechanical properties between the circumferential locations.

After calculating the density and analysing the scatter in comparison to literature, it was found that there is significant scatter present within the data. As the average mass of a specimen is 0.10g - 0.12g with a scale resolution of 0.01g, this allows for a 10% variation in measurement which can increase the level of scatter and uncertainty. This is a possible reason for the large scatter displayed within the density measurements recorded.

As the measurements for mass were taken post freezing, there is no way to indicate possible moisture changes internally. A possible manner in which this could be eliminated would be to measure masses of the specimens after machining, prior to storage.

8.3 Quasi static testing

Unlike previously, compliance of the Zwick quasi-static mechanical testing apparatus was taken into account and shown to have a significant impact on the data.

8.4 Intermediate strain rate testing

Compliance of the wedge bar apparatus was measured experimentally and found to have a significant impact on the recorded data.

The wedge bar performed successfully at strain rates of 3/s - 17/s. Higher strain rates yielded a high degree of noise which resulted in unusable data.

The gas gun designed for the wedge bar was able to propel the striker at the correct velocities consistently. A constant repeatable strain rate was accomplished for the duration of the testing period .

8.5 Imaging

Using SEM imaging, the specimens are found to have a high degree of porosity present in the form of both larger and smaller micro-channels. Observing the structure of these channels reveals a complicated and porous wall network.

Freezing of the bone appears to induce micro fractures within the longitudinal and radial directions. Within the transverse direction, the reason for the presence of the parallel fractures is still unknown.

Imaging of the fractured specimens revealed a distinct difference between the quasi-static and intermediate strain rate regimes. It is therefore postulated that during quasi-static testing, there is sufficient time for any internal fluid to escape from the specimen whereas within the intermediate regime, this is not possible. This results in the fracture following no distinct direction in the quasi-static regime and the path of least resistance within the intermediate regime.

8.6 Numerical model

The new model successfully retains all units throughout the integration process. The numerical model successfully demonstrated the ability to be modified and adapted to different sets of data and so its ability to capture complex strain rate sensitive behaviour.

The model is phenomenological, but built on a collection of conceptual physical elements. It may be possible to match each of these to a physiological feature of the bone in future research.

Chapter 9

Recommendations

9.1 Specimen manufacturing and measurement recommendations

- Location of the specimens circumferentially and along the length should be taken note of with a study being performed on location based modulus variation.
- In order to begin to eliminate inaccuracies in measurement, a micrometer and an electron balance scale with a greater order of accuracy must be used.
- To eliminate any form of mass measurement error due to moisture content variation, the mass and dimensions of the specimens must be taken post machining, prior to any form of storage.

9.2 Quasi static testing recommendations

- A rigid anvil should be constructed to fit the Zwick mechanical testing apparatus base plate so as to decrease the amount of allowable movement and hence compliance of the system.
- A method to directly measure the strain of the specimen must be implemented to increase the accuracy of the results. This may be achieved with the use of clip gauges.

9.3 Wedge bar recommendations

- Wedge angles for the wedge bars and accompanying platforms should be wire cut to increase precision of sliding surfaces.
- An investigation into lower and higher strain rate testing, through the use of larger diameter bars, should be performed on the wedge bar apparatus as larger diameter bars may decrease the signal noise.
- A stiffer load cell, possibly designed using Titanium, should be designed and constructed to decrease compliance of the system. This should incorporate both preload nuts.
- Instead of the Picoscope, a high speed data capturing card should be utilised to increase the data density. This will allow analysing methods such as fast fourier transforms to be performed which may help in reducing the noise generated when exceeding strain rates of 17/s.
- Instead of inferring the vertical displacement, alternative direct measurement methods should be investigated with an adequate sampling rate. Such methods include using laser measurement methods to directly measure the movement of the specimen platform.

9.4 Imaging

- Investigate using a variety of different casting solutions instead of resin in order to prevent the solution from penetrating the fractures completely. Alternatively wrapping the specimens in a form of non permeable film could prevent this resin penetration. This would be useful as the fracture surface could then be observed as the resin currently seeps fully into the specimens.
- Perform more imaging on a range of fracture stages to investigate the postulate which suggests that the fracture path is strain rate dependent
- An investigation into fresh versus frozen samples should be performed in order to determine the impact freezing may have on the scatter and strength in samples.

9.5 Numerical Modeling

- An investigation into Ricatti equations should be performed in order to verify and expand on Monsia's work.
- A further investigation should be performed into fractional calculus of nonlinear viscoelastic models due to the versatility these models present.
- Finite element methods may be used in order to numerical model the behaviour of each orientation and the associated fracture behaviour.

The recommendations presented are not feasible for a single masters student due to the amount of work and attention to detail required for the time allocated. However, this work may be achieved if spread over approximately three masters as when working with biological material, new complications and additional work arises when attempting to complete a single project, therefore widening the depth of the initial scope for the project.

References

[1] R. Rajesh A. Mayya, A. Banerjee. Haversian microstructure in bovine femoral cortices: An adaptation for improved compressive strength. *Materials Science and Engineering*, (C 59):454 – 463, October 2015.

[2] R. R. Adharapurapu, F. Jiang, and K. S. Vecchio. Dynamic fracture of bovine bone. *Materials Science and Engineering: C*, 26(8):1325–1332, Sep 2006.

[3] Z. Asgharpour, D. Fressmann, E. Schuller, and S. Peldschus. Implementation of a strain rate dependent human bone model. *Institut fur Rechtsmedizin der Universitat Munchen, Munich, Germany and Dynamore GmbH, Stuttgart, Germany*, 2001.

[4] P. Augat. The role of cortical bone and its microstructure in bone strength. *Age and Ageing*, 35(Supplement 2):p27 – 31, Sep 2006.

[5] D. Walsh P. Hansma B. Kaye, C. Randall. The effect of freezing on the mechanical properties of bone. *The Open Bone Journal*, (4):14–19, 2012.

[6] M. Foster P. Moy B. Sanborn, C. A. Gunnarsson and T. Weerasooriya. Effect of loading rate and orientation on the compressive response of human and cortical bone. *Army Research Laboratory*, 2014.

[7] A. Bekker. *The strain rate dependent mechanical properties and modelling of bovine cortical bone in compression, University of Cape Town.* Phd thesis, 2008.

[8] A. Bekker, T.J. Cloete, A. Chinsamy-Turan, G.N. Nurick, and S. Kok. Constant strain rate compression of bovine cortical bone on the split-hopkinson pressure bar. *Materials Science and Engineering: C*, 46:443–449, Jan 2015.

[9] A. Bekker, S. Kok, T.J. Cloete, and G.N. Nurick. Introducing objective power law rate dependence into a visco-elastic material model of bovine cortical bone. *International Journal of Impact Engineering*, 66:28–36, Apr 2014.

[10] A. L Boskey. Bone composition: relationship to bone fragility and antiosteoporotic drug effects. *BoneKEy Reports*, 2, Dec 2013.

[11] D. Carter and W. Hayes. Bone compressive strength: the influence of density and strain rate. *Science*, 194(4270):1174–1176, Dec 1976.

[12] T. J. Cloete and S. Oxtoby. A new technique for compression tests at intermediate strain rates: Prototype results. *DYMAT 2009 - 9th International Conferences on the Mechanical and Physical Behaviour of Materials under Dynamic Loading*, 2009.

[13] T. J. Cloete, G. Paul, and E. B. Ismail. Hopkinson bar techniques for the intermediate strain rate testing of bovine cortical bone. *Philosophical Transactions of the Royal Society A: Mathematical, Physical and Engineering Sciences*, 372(2015):20130210–20130210, Apr 2014.

[14] T. J. Cloete, A. van der Westhuizen, S. Kok, and G. N. Nurick. A tapered striker pulse shaping technique for uniform strain rate dynamic compression of bovine bone. *DYMAT 2009 - 9th International Conferences on the Mechanical and Physical Behaviour of Materials under Dynamic Loading*, 2009.

[15] M. Conry. 3rd year engineering materials lecture - viscoelasticity, www.acronymchili.com/noteshtml/3rdmaterials/3rdmat06handout.pdf, 2004.

[16] G. Dubois. Personal communication, January 2016.

[17] E. N. Ebbesen, J. S. Thomsen, H. Bech-Nielsen, H. J. Nepper-Rasmussen, and L. Mosekilde. Age and gender related and differences in vertebral and bone and mass and density and strength. *Journal of Bone and Mineral Research*, Volume 14(Number 8), 1999.

[18] R. Magin F.C. Meral, T.J. Royston. Fractional calculus in viscoelasticity: An exerimental study. *Commun Nonlinear Sci Nummer Simulat*, (15):939:945, May 2010.

[19] M. Figueiredo, A. Fernando, G. Martins, J. Freitas, F. Judas, and H. Figueiredo. Effect of calcination temperature on the composition and microstructure of hydroxyapatite derived from human and animal bone. *Ceramics International*, 2015.

[20] U.S. Food and Drug Administration. Bam r63: Physiological saline solution 0.85

[21] Y. H. An; R. J. Friedman. *Animal Model in Orthopaedic Research*. CRC Press, 1999.

[22] Y. Fung. *A First Course in Continuum Mechanics*. Prentice Hall, 1994.

[23] A. Schmidt; L. Gaul. Application of fractional calculus to viscoelastically damped sstructure in the finite element method. *Institut A faur Mechanik, Universitaat Stuttgart Pfaffenwaldring 9, 70550 Stuttgart, Germany.*

[24] A. Halldin, M. Ander, M. Jacobsson, and S. Hansson. On a constitutive material model to capture time dependent behavior of cortical bone. *WJM*, 04(11):348–361, 2014.

[25] P. Zioupos; J. D. Currey; A. J. Hamer. The role of collagen in the declining mechanical properties of aging human cortical bone. *Journal of Biomedical Materials Research*, (45):108–116, 1999.

[26] U. Hansen, P. Zioupos, R. Simpson, J. D. Currey, and D. Hynd. The effect of strain rate on the mechanical properties of human cortical bone. *J. Biomech. Eng.*, 130(1):011011, 2008.

[27] T.M. Wright; W.C. Hayes. Tensile testing of bone over a wide range of strain rates: effects of strain rate, microstructure and density. *Department of Materials Science and Division of Applied Mechanics, Department of Mechanical Engineering, Stanford University, Stanford, Calif, 94305, USA*, 1976.

[28] N. Heymans. Fractional calculus description of non-linear viscoelastic behaviour of polymers. *Nonlinear Dynamics*, Nonlinear Dynamics(38):221:231, 2004.

[29] S. L. Hui, C. W. Slemenda, and C. C. Johnston. Age and bone mass as predictors of fracture in a prospective study. *J. Clin. Invest.*, 81(6):1804–1809, Jun 1988.

[30] E. Tanck; G. Hannink; R. Ruimerman; P. Buma; E. H. Burger; R. Huiskes. Cortical bone development under the growth plate is regulated by mechancial load transfer. *Journal of Anatomy*, (208):73–79, 2006.

[31] P. Zioupos; R. B. Cook; J. R. Hutchinson. Some basic relationships between density values in cancellous and cortical bone. *Journal of Biomechanics*, (41):1961–1968, 2008.

[32] T. Iyo, Y. Maki, N. Sasaki, and M. Nakata. Anisotropic viscoelastic properties of cortical bone. *Journal of Biomechanics*, 37(9):1433–1437, Sep 2004.

[33] McElhaney J. H. Dynamic response of bone and muscle tissue. *Journal of Applied Physiology*, (21):1231–1236, 1966.

[34] S. Ott J. Lian, J. Gorski. Bone structure and function. https://depts.washington.edu/bonebio/ASBMRed/structure.html, January 2004.

[35] A. Wree R. Bader J. Wieding, E. Mick. Influence of three different preservative techniques on the mechanical properties of the ovine cortical bone. *Acta of Bioengineering and Biomechanics*, 17(17), 2014.

[36] T.P.M. Johnson, S. Socrate, and M.C. Boyce. A viscoelastic, viscoplastic model of cortical bone valid at low and high strain rates. *Acta Biomaterialia*, 6(10):4073–4080, Oct 2010.

[37] R. C. Koeller. Applications of fractional calculus to the theory of viscoelasticity. *Journal of Applied Mechanics*, 51(2):299, 1984.

[38] M. Kuninori, H. Kikugawa, T. Asaka, and H. Kasuya. Effect of different preservative methods on fracture behavior of bovine cortical bone. *Material Transactions*, 50(2):305–312, 2009.

[39] R. Lakes. Viscoelasticity notes adapted from viscoelastic materials, http://silver.neep.wisc.edu/ lakes/venotes.html, 2016.

[40] S. Lakshmanan, A. Bodi, and K. Raum. Assessment of anisotropic tissue elasticity of cortical bone from high-resolution, angular acoustic measurements. *IEEE Trans. Ultrason., Ferroelect., Freq. Contr.*, 54(8):1560–1570, Aug 2007.

[41] E. Lefavre, P. Lasaygues, C. Baron, C. Payan, F. Launay, H. Follet, and M. Pithioux. Analyzing the anisotropic hookes law for childrens cortical bone. *Journal of the Mechanical Behavior of Biomedical Materials*, 49, Sep 2015.

[42] P. Lucksanasombool, W.A.J. Higgs, R.J.E.D. Higgs, and M.V. Swain. Fracture toughness of bovine bone: influence of orientation and storage media. *Biomaterials*, (22):3127–3132, 2001.

[43] Z. Manilay, E. Novitskaya, E. Sadovnikov, and J. McKittrick. A comparative study of young and mature bovine cortical bone. *Acta Biomaterialia*, 9(2):5280–5288, Feb 2013.

[44] J. Minster. Modeling of viscoelastic deformation of cortical bone tissue. *Acta of Bioengineering and Biomechanics*, 5(1), 2003.

[45] M. D. Monsia. A simplified nonlinear generalized Maxwell model for predicting the time dependent behavior of viscoelastic materials. *WJM*, 01(03):158–167, 2011.

[46] S. Muller, M. Kastner, J. Brummund, and V. Ulbricht. A nonlinear fractional viscoelastic material model for polymers. *Computational Materials Science*, 50(10):2938–2949, aug 2011.

[47] E. Novitskaya, P. Chen, S. Lee, A. Castro-Ceseña, G. Hirata, V. A. Lubarda, and J. McKittrick. Anisotropy in the compressive mechanical properties of bovine cortical bone and the mineral and protein constituents. *Acta Biomaterialia*, 7(8):3170–3177, Aug 2011.

[48] C. Ohman, C. Baleani, Mand Pani, F. Taddei, M. Alberghini, M. Viceconti, and M. Manfrini. Compressive behaviour of child and adult cortical bone. *Bone*, 49(4):769–776, Oct 2011.

[49] A. A. Espinoza Orias. *The relationship between the mechancial anisotropy of human cortical bone tissue and its microstructure.* PhD thesis, Graduate School of the University of Notre Dame, 2005.

[50] G. Paul. The strain rate dependent properties of bovine cortical bone. Master of science in engineering, Unvierstiy of Cape Town, 2014.

[51] U. E. Pazzaglia, G. Bonaspetti, F. Ranchetti, and P. Bettinsoli. A model of the intracortical vascular system of long bones and of its organization: an experimental study in rabbit femur and tibia. *Journal of Anatomy*, 213(2):183–193, aug 2008.

[52] U. E. Pazzaglia, T. Congiu, M. Raspanti, F. Ranchetti, and D. Quacci. Anatomy of the intracortical canal system: Scanning electron microscopy study in rabbit femur. *Clinical Orthopaedics and Related Research®*, 467(9):2446–2456, mar 2009.

[53] M. Prot and T. J. Cloete. A tandem momentum trap for dynamic specimen recovery during split hopkinson pressure bar testing of cancellous bone. *J. dynamic behavior mater.*, 2(1):50–58, jan 2016.

[54] D. Roylance. Engineering viscoelasticity, http://web.mit.edu/course/3/3.11 /www/modules/visco.pdf, 2001.

[55] R.K. Saxena. Fractional calculus and fractional differential equations with scilab, http://www.scilab.in/files/workshops/23042010nanded/ scilabworkshopppt/ppts/-day2/psvnfcandfdeslides.pdf, 2010.

[56] V.P.W. Shim, L.M. Yang, J.F. Liu, and V.S. Lee. Characterisation of the dynamic compressive mechanical properties of cancellous bone from the human cervical spine. *International Journal of Impact Engineering*, 32(1-4):525–540, Dec 2005.

[57] M. Stander. Development of an intermediate strain rate compression testing machine. Master of science in engineering, Universtiy of Cape Town, 2014.

[58] U. Stefan, B. Michael, and S. Werner. Effects of three different preservation methods on the mechanical properties of human and bovine cortical bone. *Bone*, 47(6):1048–1053, Dec 2010.

[59] M.E. Szaba and P.J. Thurner. Anisotropy of bovine cortical bone tissue damage properties. *Journal of Biomechanics*, 46(1):2–6, Jan 2013.

[60] O. C. Yeh T. M. Keaveny, E. F. Morgan. *Standard Handbook of Biomedical Engineering and Design.* 2004.

[61] E. H. van Haaren, B. C. van der Zwaard, A. J. van der Veen, I. C. Heyligers, P. I. J. M. Wuisman, and T. H. Smit. Effect of long-term preservation on the mechanical properties of cortical bone in goats. *Acta Orthop*, 79(5):708–716, Jan 2008.

[62] T. Weerasooriya, B.t Sanborn, C. A. Gunnarsson, and M. Foster. Orientation dependent compressive response of human femoral cortical bone as a function of strain rate. *Journal of Dynamic Behavior of Materials*, 2(1):74–90, Feb 2016.

[63] W.R. Whittington, A.L. Oppedal, D.K. Francis, and M.F. Horstemeyer. A novel intermediate strain rate testing device: The serpentine transmitted bar. *International Journal of Impact Engineering*, 81:1–7, Jul 2015.

[64] K.P. Wilkie, C.S. Drapaca, and S. Sivaloganathan. A nonlinear viscoelastic fractional derivative model of infant hydrocephalus. *Applied Mathematics and Computation*, 217(21):8693–8704, jul 2011.

[65] J. Yan, K. B. Clifton, J. J. Mecholsky, and L. A. Gower. Effect of temperature on the fracture toughness of compact bone. *Journal of Biomechanics*, 40(7):1641–1645, Jan 2007.

[66] P Zioupos and J.D Currey. Changes in the stiffness, strength, and toughness of human cortical bone with age. *Bone*, 22(1):57–66, Jan 1998.

Appendix A: Intermediate strain rate testing designs

Appendix A-1: Intermediate strain rate testing rig

Working drawings for the intermediate strain rate tester

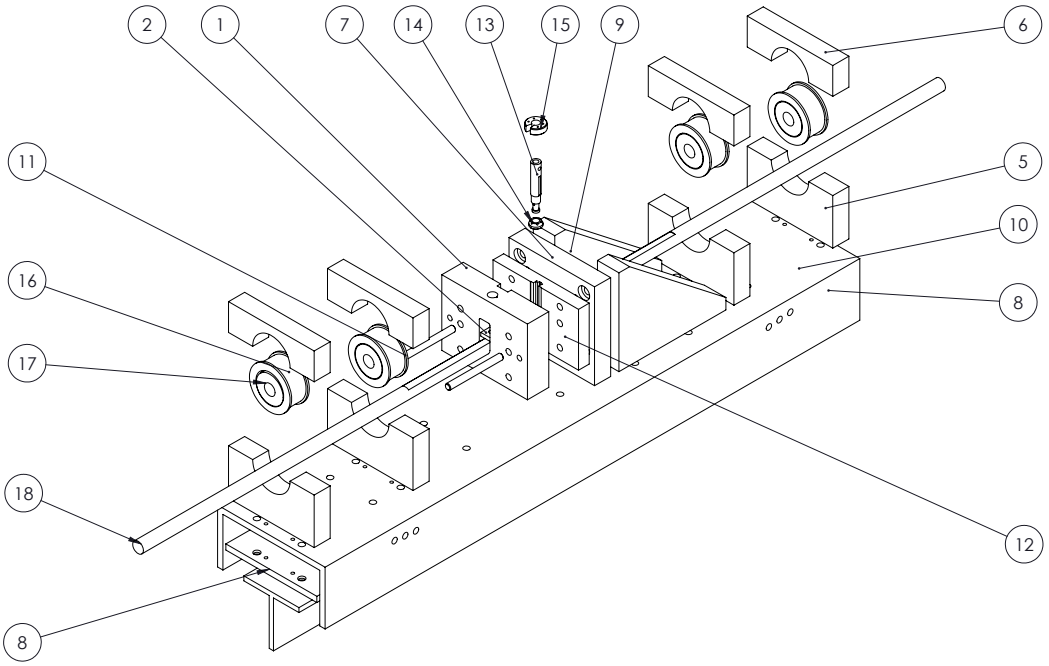

ITEM NO.	PART NUMBER	DESCRIPTION	QTY.
18	500	STAINLESS STEEL	1
17	Teflon Insert	BRASS	4
16	Brass Outer	BRASS	4
15	LOAD CELL TOP NUT	STAINLESS STEEL	1
14	LOAD CELL NUT	STAINLESS STEEL	1
13	LOAD CELL	STAINLESS STEEL	1
12	BACKING PLATE	STAINLESS STEEL	1
11	LOCATING PIN	STAINLESS STEEL	2
10	PLATFORM	PROVIDED	1
9	MLF SUPPORT	MILD STEEL	2
8	PLATFORM BAR	MILD STEEL	1
7	MLF FRAME	STAINLESS STEEL	1
6	MOUNTING PART 2	MILD STEEL	4
5	MOUNTING PART 1	MILD STEEL	4
4	I BEAM	PROVIDED	1
4	BACKING PLATE PART 1	STAINLESS STEEL	1
2	SPECIMEN PLATFORM	Aluminium	1
1	MLF	CAST IRON	1

A3 Landscape	University of Cape Town Department of Mechanical Engineering			
	Title: WEDGE BAR COMPLETED			
Assembly Drawing	Scale: 1:5	Date: 2016/07/06	Sheet1	of 1
	Drawn By: ANDREW ROGINSKY RGNAND001		Drawing Number	

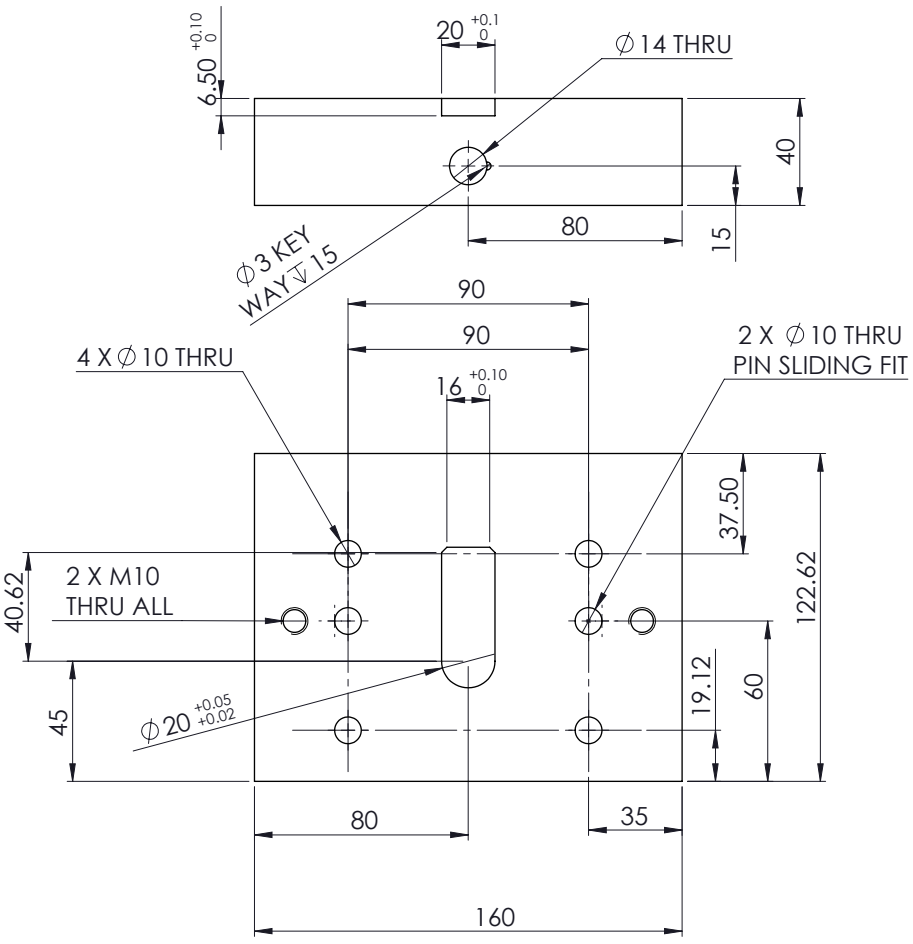

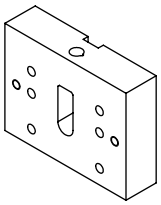

A4 Landscape	University of Cape Town Department of Mechanical Engineering			
	Title: MLF			
Part Finish N/A	Scale: 1:2	Date: 2016/07/06	Sheet1	of 10
Material: CAST IRON	Drawn By: ANDREW ROGINSKY RGNAND001		Drawing Number	

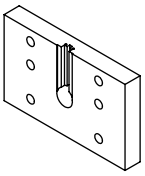

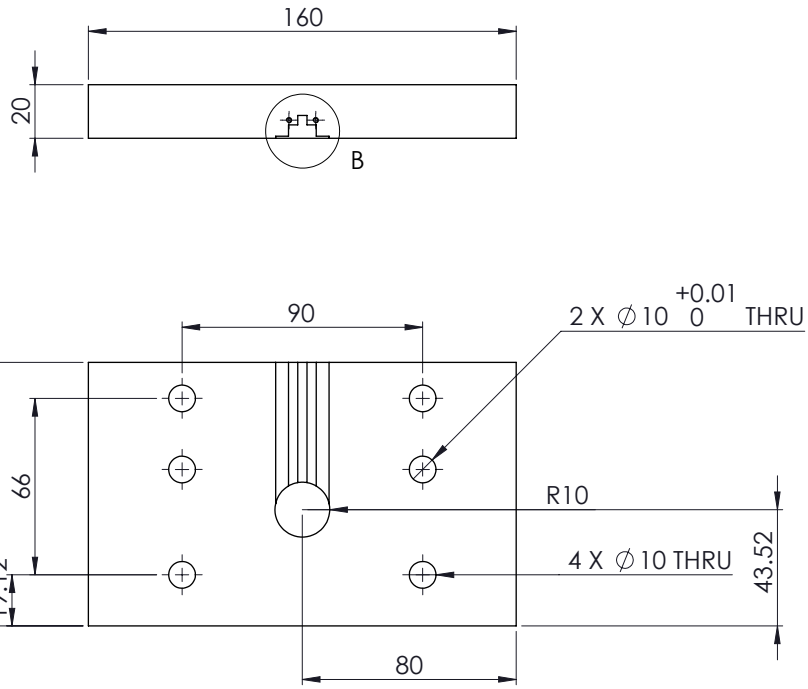

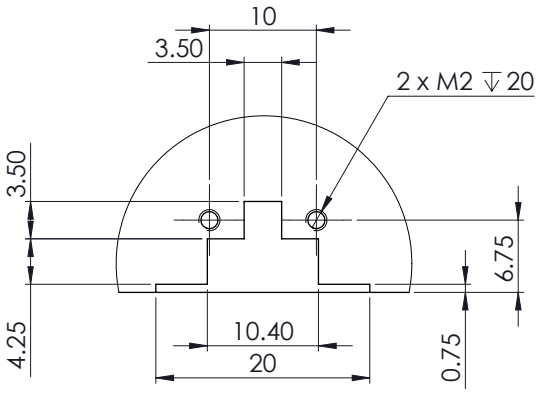

DETAIL B
SCALE 2 : 1

A4 Landscape	University of Cape Town Department of Mechanical Engineering			
	Title: BACKING PLATE			
Part Finish	Scale: 1:2	Date: 2016/07/06	Sheet2	of 10
Material: STAINLESS STEEL	Drawn By: ANDREW ROGINSKY		Drawing Number	

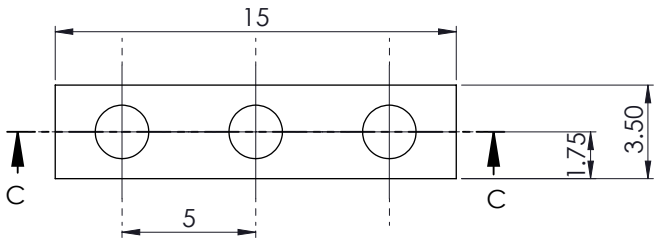

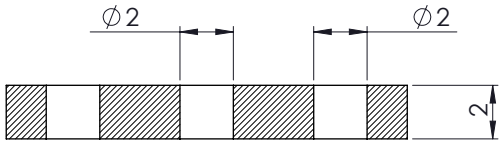

SECTION C-C

A4 Landscape	University of Cape Town Department of Mechanical Engineering			
	Title: BASE			
Part Finish	Scale: 5:1	Date: 2016/07/06	Sheet3	of 10
Material: STAINLESS STEEL	Drawn By: ANDREW ROGINSKY		Drawing Number	

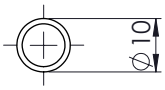

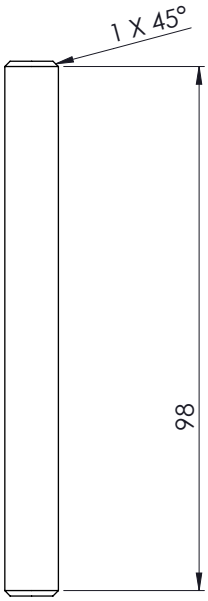

A4 Landscape	University of Cape Town Department of Mechanical Engineering			
	Title: LOCATING PIN			
Part Finish	Scale: 1:1	Date: 2016/07/06	Sheet5	of 10
Material: STAINLESS STEEL	Drawn By: ANDREW ROGINSKY		Drawing Number	

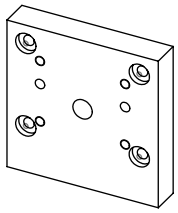

A4 Landscape	University of Cape Town Department of Mechanical Engineering			
	Title: MLF FRAME			
Part Finish	Scale: 1:2	Date: 2016/07/06	Sheet6	of 10
Material: MILD STEEL	Drawn By: ANDREW ROGINSKY		Drawing Number	

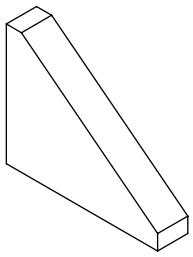

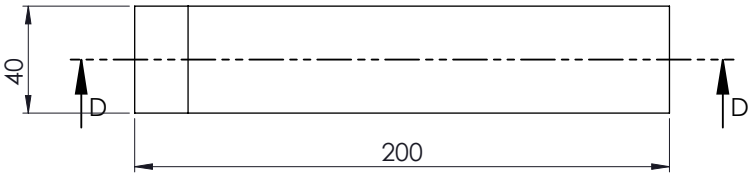

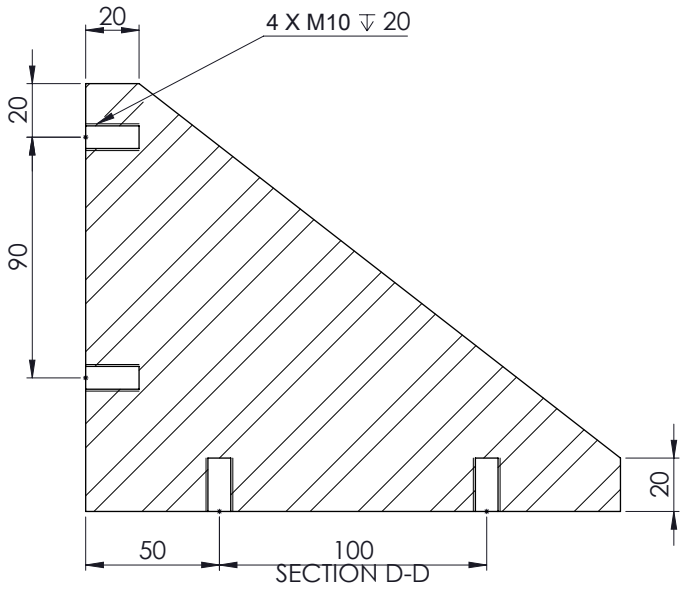

SECTION D-D

A4 Landscape	University of Cape Town Department of Mechanical Engineering			
	Title: MLF SUPPORT			
Part Finish	Scale: 1:2	Date: 2016/07/06	Sheet7	of 10
Material: MILD STEEL	Drawn By: ANDREW ROGINSKY		Drawing Number	

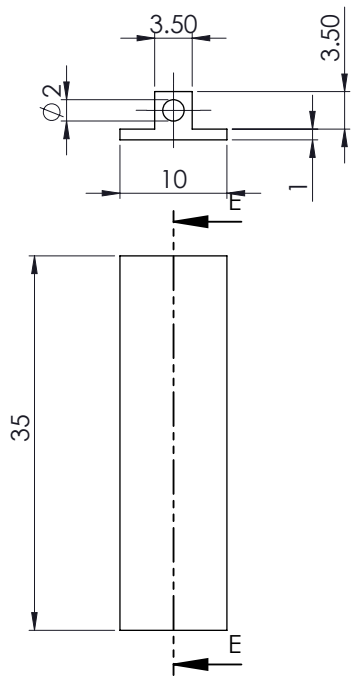

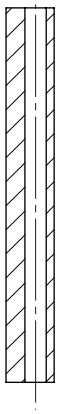

SECTION E-E

NOTE:

To have a sliding fit with the backing plate, sheet 2

A4 Landscape	University of Cape Town Department of Mechanical Engineering			
	Title: PCB SLIDER			
Part Finish	Scale: 2:1	Date: 2016/07/06	Sheet8	of 10
Material: STAINLESS STEEL	Drawn By: ANDREW ROGINSKY		Drawing Number	

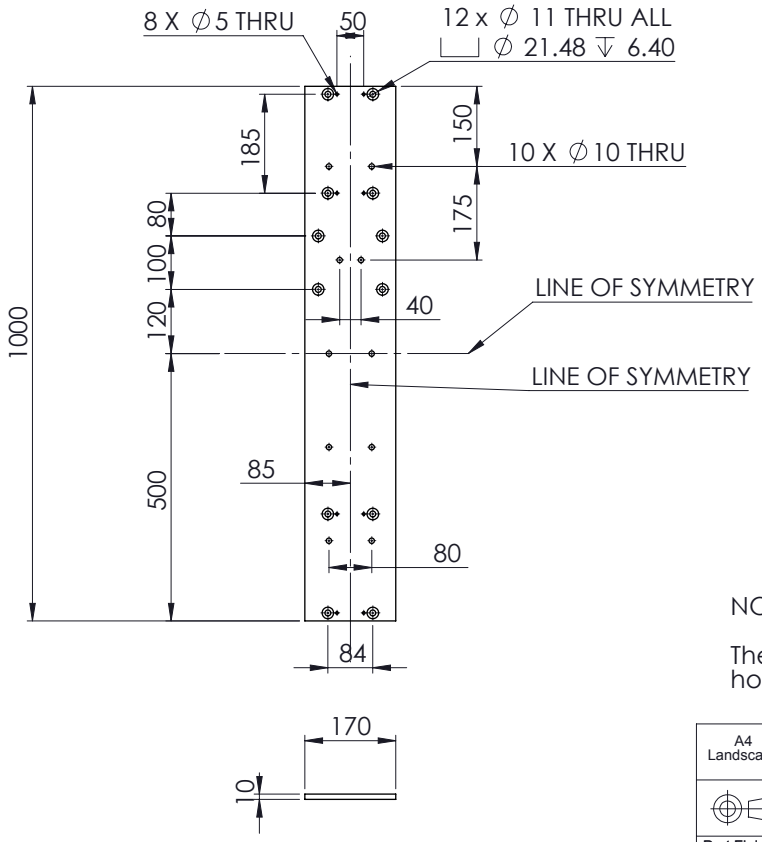

NOTE:

The above is symetric about the horizontal and vertical centerline

A4 Landscape	University of Cape Town Department of Mechanical Engineering			
	Title: PLATFORM BAR			
Part Finish	Scale: 1:10	Date: 2016/07/06	Sheet9	of 10
Material: MILD STEEL	Drawn By: ANDREW ROGINSKY		Drawing Number	

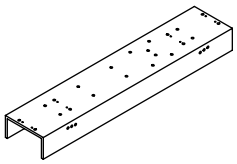

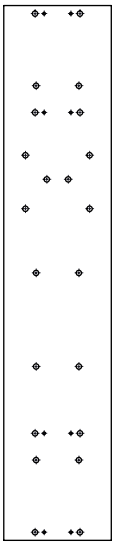

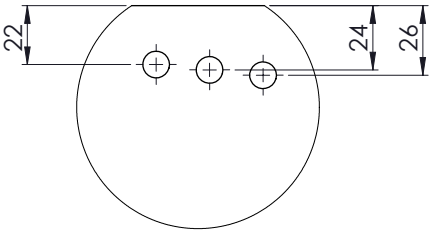

DETAIL F
SCALE 1 : 2

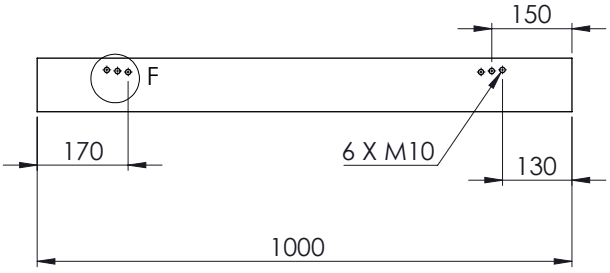

NOTE:

Identical dimensions and specification to be used as for the platform bar, sheet 9 in order to fit sheet 9 & 10 components flush together. This corresponds to the Top View

A4 Landscape	University of Cape Town Department of Mechanical Engineering			
	Title: PLATFORM			
Part Finish	Scale: 1:10	Date: 2016/07/06	Sheet10	of 10
Material: PROVIDED	Drawn By: ANDREW ROGINSKY		Drawing Number	

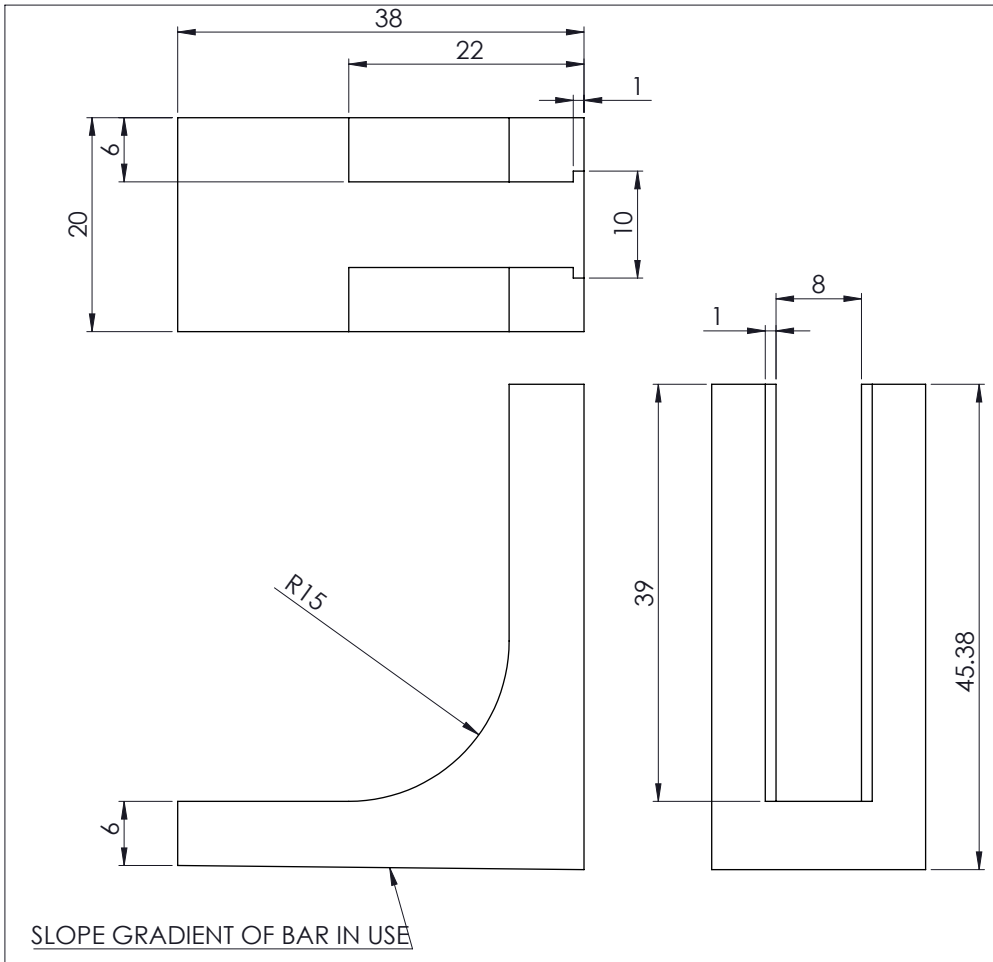

A4 Landscape	University of Cape Town Department of Mechanical Engineering			
	Title: SPECIMEN PLATFORM			
Part Finish	Scale: 2:1	Date: 2016/07/06	Sheet11	of 10
Material: ALUMINIUM	Drawn By: ANDREW ROGINSKY		Drawing Number	

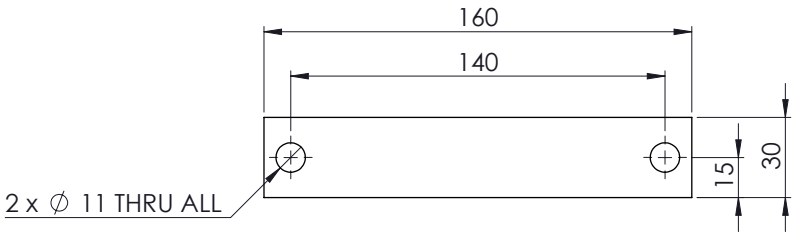

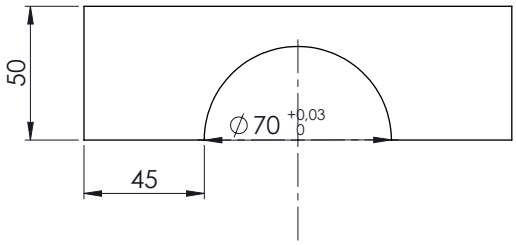

TO BE MATCHED WITH MOUNTING PART 1

A4 Landscape	University of Cape Town Department of Mechanical Engineering			
	Title: MOUNTING PART 2			
Part Finish	Scale: 1:2	Date: 2016/11/16	Sheet1	of 2
Material: Stainless Steel	Drawn By: Andrew Roginsky		Drawing Number	

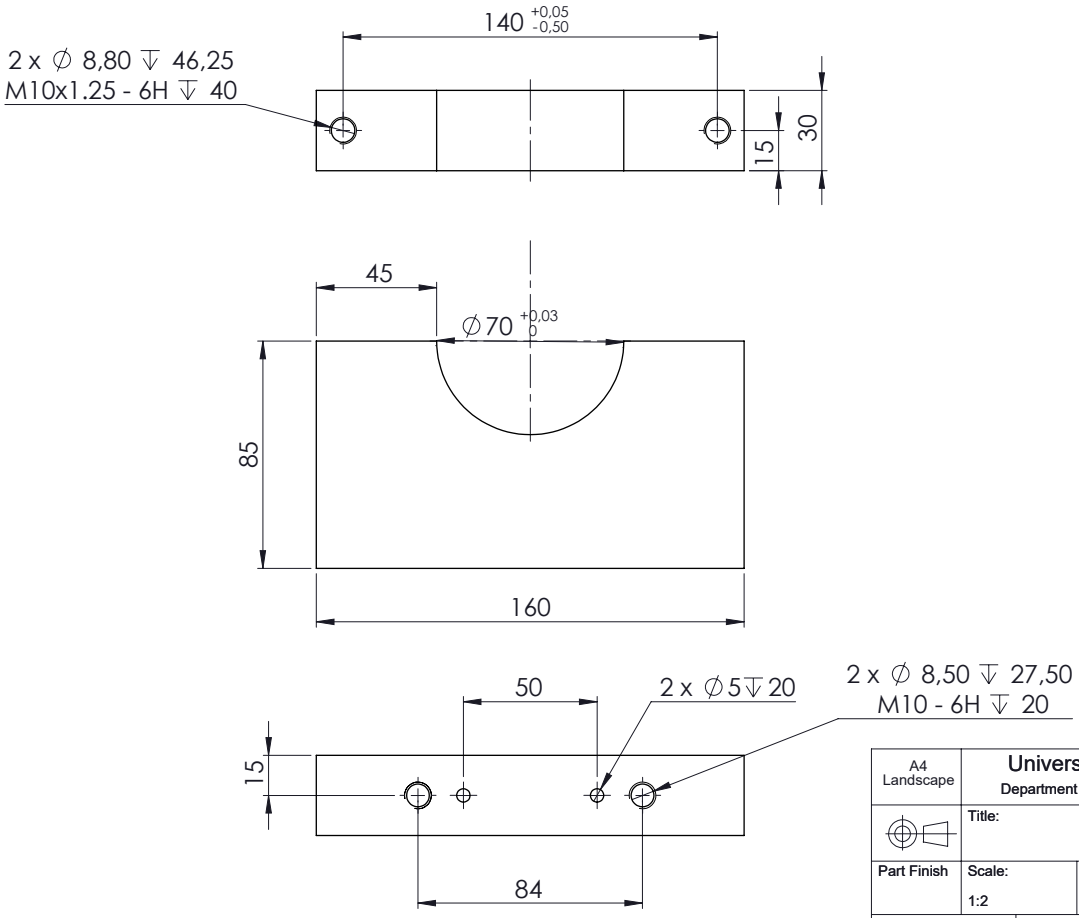

TO BE MATCHED WITH MOUNTING PART 2

A4 Landscape	University of Cape Town Department of Mechanical Engineering			
	Title: MOUNTING PART 1			
Part Finish	Scale: 1:2	Date: 2016/11/16	Sheet2	of 2
Material: Stainless Steel	Drawn By: Andrew Roginsky		Drawing Number	

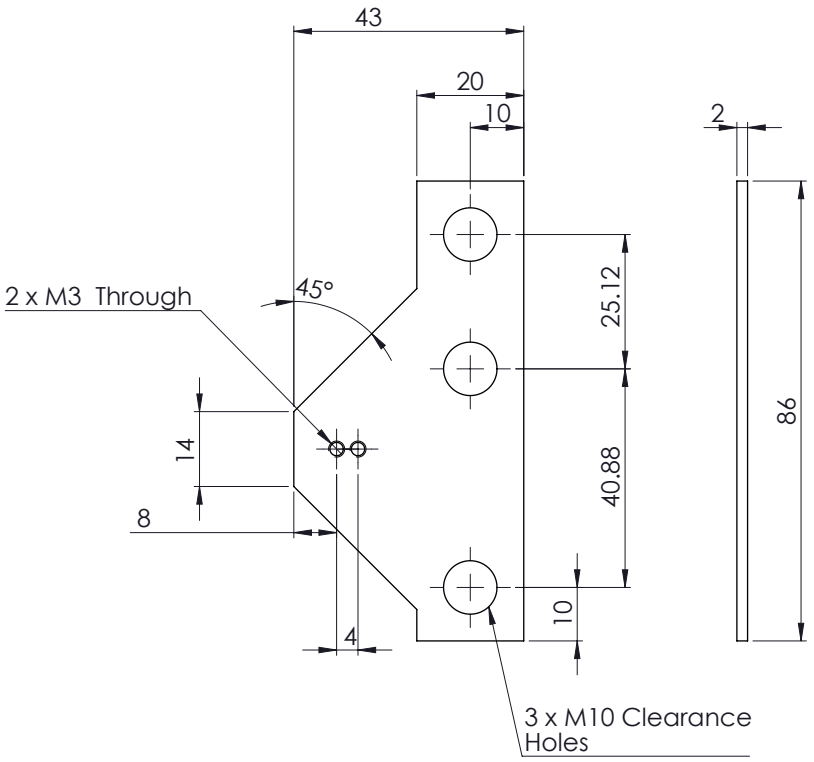

A4 Landscape	University of Cape Town Department of Mechanical Engineering			
	Title: ROS Mounting			
Part Finish	Scale: 1:1	Date: 2015/11/30	Sheet1	of 1
Material: Stainless Steel	Drawn By: Andrew Roginsky		Drawing Number	

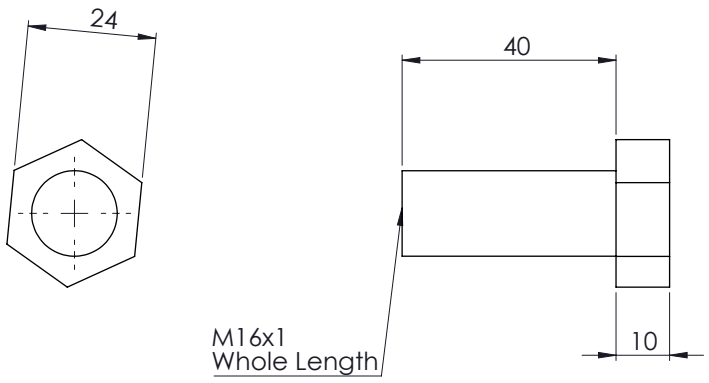

Quantity of 4

A4 Landscape	University of Cape Town Department of Mechanical Engineering			
	Title: Fine Thread Bolt			
Part Finish	Scale: 1:1	Date: 2015/11/25	Sheet1	of 1
Material: Stainless Steel	Drawn By: Andrew Roginsky		Drawing Number	

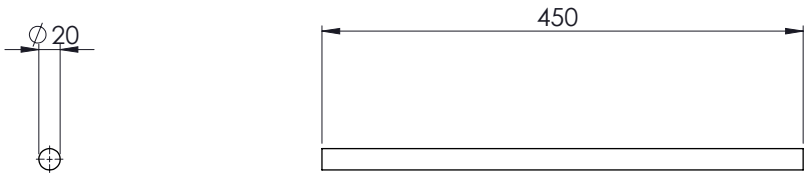

A4 Landscape	University of Cape Town Department of Mechanical Engineering			
	Title: Transfer			
Part Finish	Scale: 1:5	Date: 2016/02/24	Sheet1	of 1
Material: Provided Round Bar	Drawn By: Andrew Roginsky		Drawing Number	

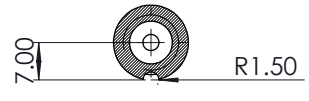

SECTION C-C

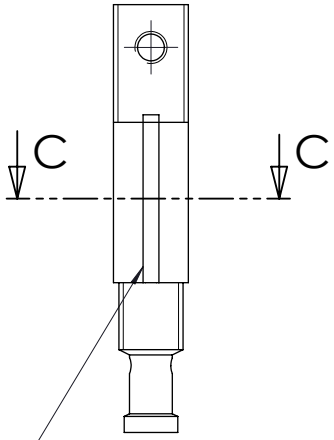

3mm ball nose key way
for 3mm diameter key

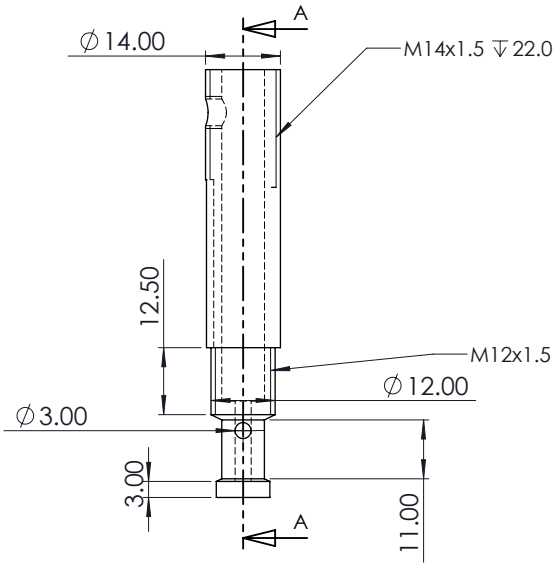

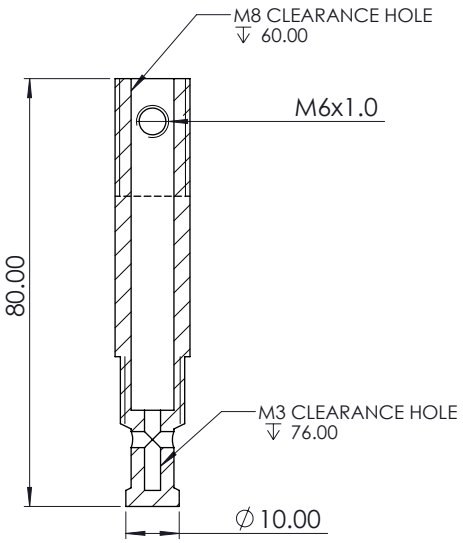

SECTION A-A

SolidWorks Student Edition.
For Academic Use Only.

A4 Landscape	University of Cape Town Department of Mechanical Engineering			
	Title: LOAD CELL			
Part Finish	Scale: 1:1	Date: 2016/06/27	Sheet1	of 1
Material: Stainless Steel	Drawn By: Kelsey Hilton & Andrew Roginsky		Drawing Number 1	

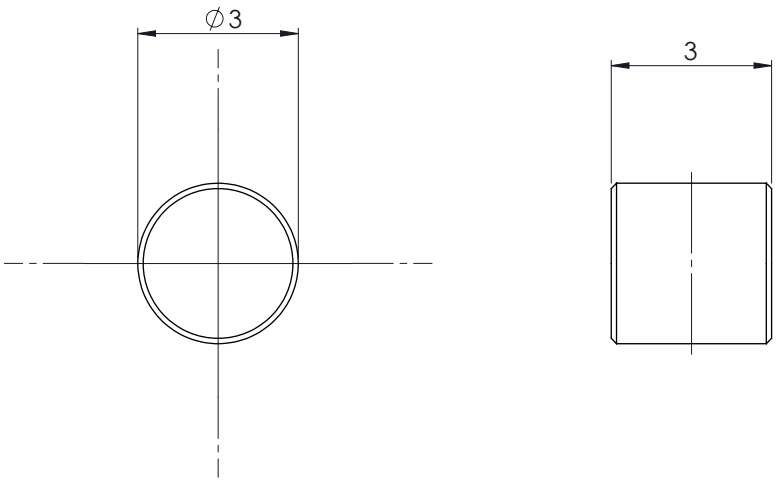

A4 Landscape	University of Cape Town Department of Mechanical Engineering			
	Title: KEY			
Part Finish	Scale: 10:1	Date: 2016/11/16	Sheet1	of 1
Material: Stainless Steel	Drawn By: Andrew Roginsky		Drawing Number	

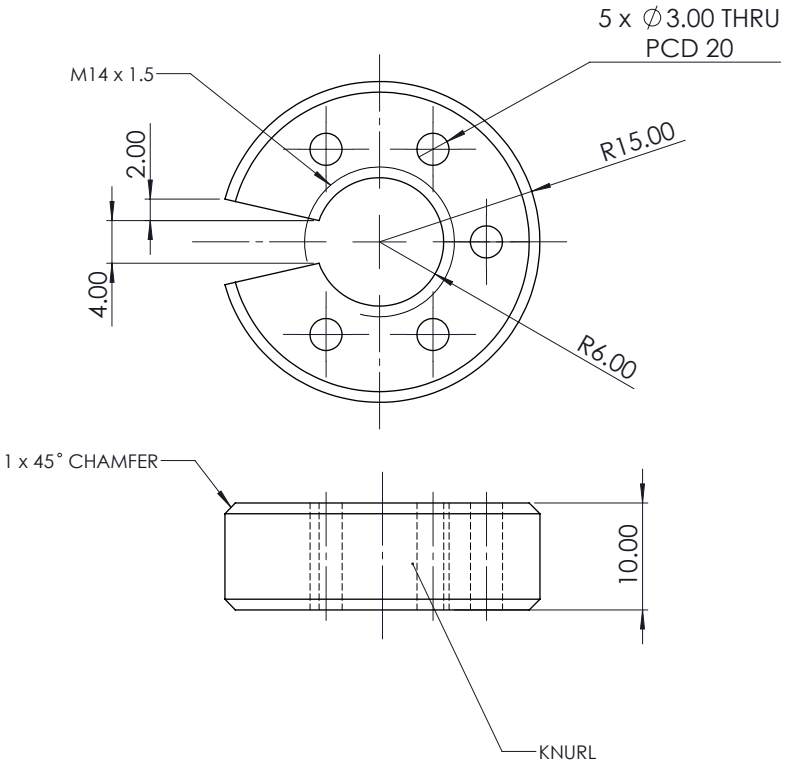

SolidWorks Student Edition.
For Academic Use Only.

A4 Landscape	University of Cape Town Department of Mechanical Engineering			
	Title: LOAD CELL TOP NUT			
Part Finish	Scale: 2:1	Date: 2016/06/30	Sheet1	of 1
Material: Stainless Steel	Drawn By: Kelsey Hilton & Andrew Roginsky		Drawing Number 3	

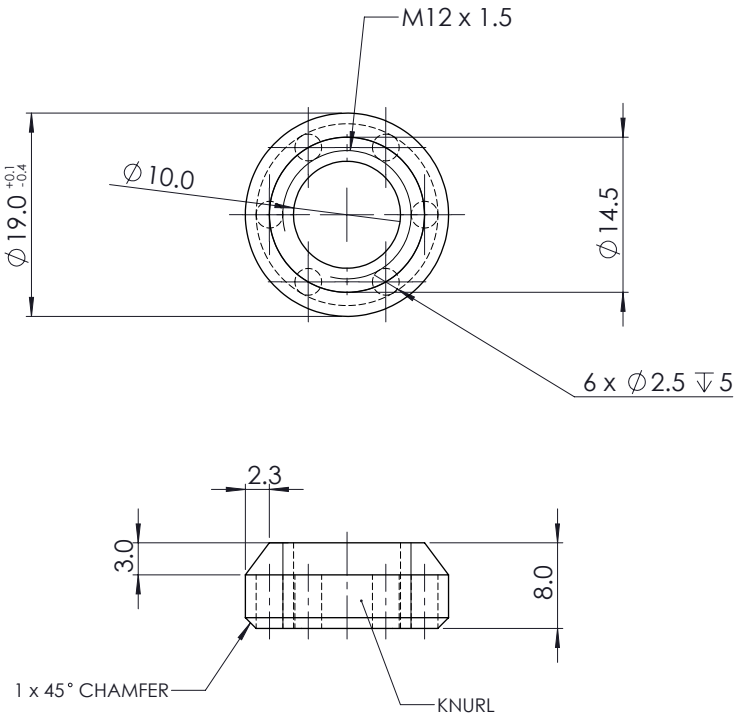

SolidWorks Student Edition.
For Academic Use Only.

A4 Landscape	University of Cape Town Department of Mechanical Engineering			
	Title: LOAD CELL NUT			
Part Finish	Scale: 2:1	Date: 2016/06/30	Sheet1	of 1
Material: Stainless Steel	Drawn By: Kelsey Hilton & Andrew Roginsky		Drawing Number 2	

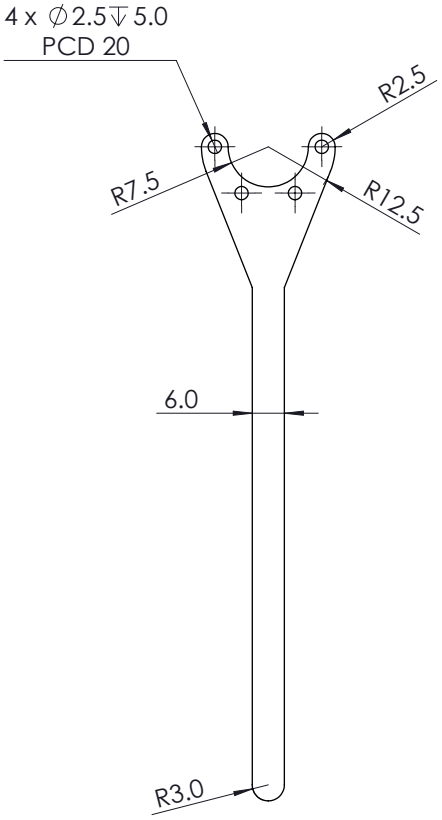

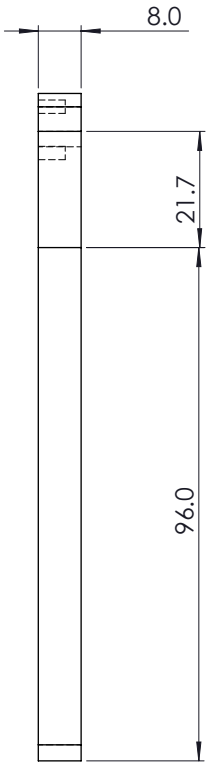

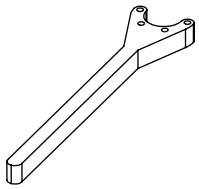

SCALE 1:2

SolidWorks Student Edition.
For Academic Use Only.

A4 Landscape	University of Cape Town Department of Mechanical Engineering			
	Title: LOADCELL TOOL TOP			
Part Finish	Scale: 1:1	Date: 2016/06/30	Sheet1	of 1
Material: TOOL STEEL	Drawn By: Kelsey Hilton & Andrew Roginsky		Drawing Number 1	

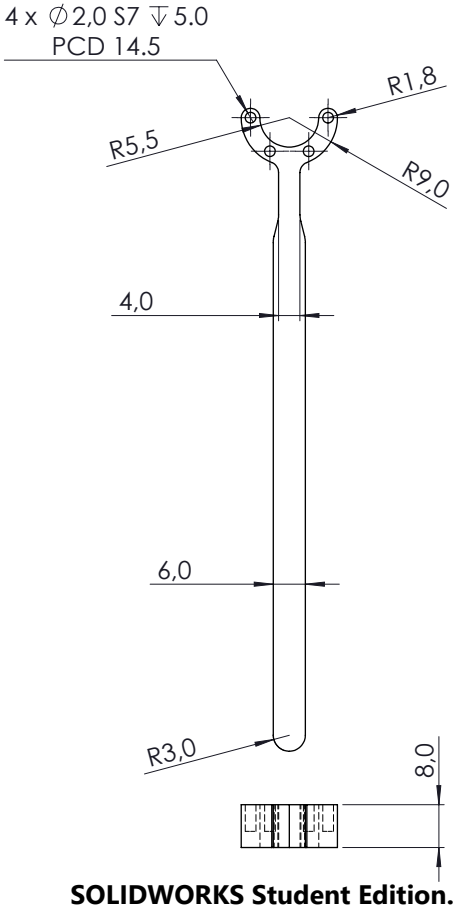

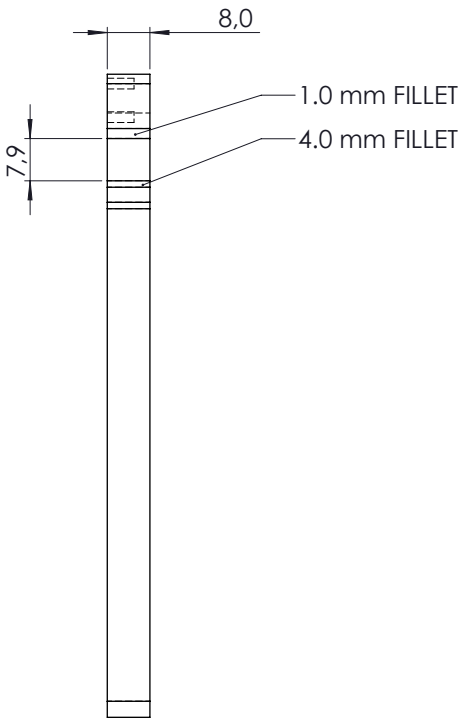

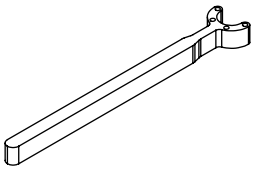

SCALE 1:2

NOTE: HOLES MUST HAVE S7/h6 INTERFERENCE FIT TOLERANCE WITH 1.5 x 8 PINS

SOLIDWORKS Student Edition.
For Academic Use Only.

A4 Landscape	University of Cape Town Department of Mechanical Engineering			
	Title: LOADCELL TOOL			
Part Finish	Scale: 1:1	Date: 2016/11/16	Sheet 2	of 2
Material: TOOL STEEL	Drawn By: Kelsey Hilton & Andrew Roginsky		Drawing Number 2	

Wedge bars

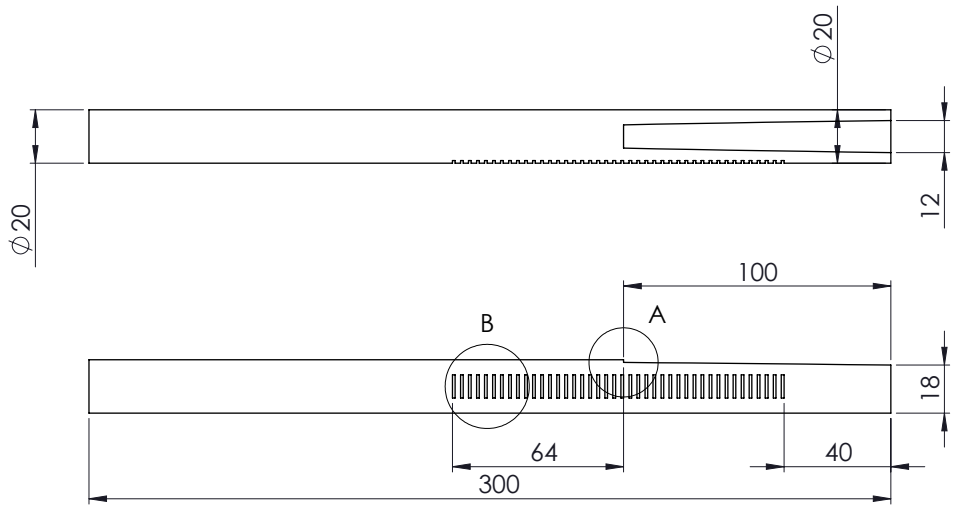

NOTE: DEPTH OF CUT IS NOT CRITICAL BUT MUST BE ROUGHLY 1mm

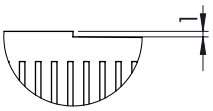

DETAIL A
SCALE 1 : 1

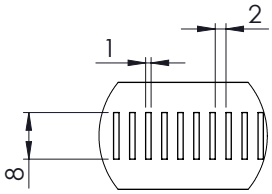

DETAIL B
SCALE 1 : 1

SLOPE GRADIENT 1:100

A4 Landscape	University of Cape Town Department of Mechanical Engineering			
	Title: 100			
Part Finish	Scale: 1:2	Date: 2016/11/16	Sheet 4	of 4
Material: PROVIDED	Drawn By: Andrew Roginsky & Kelsey Hilton		Drawing Number 4	

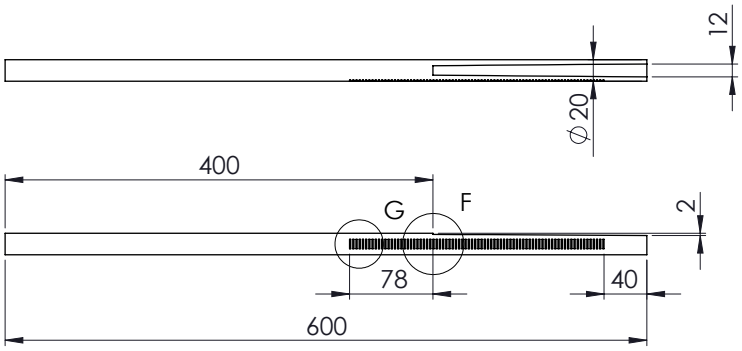

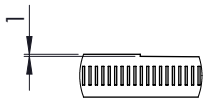

DETAIL F
SCALE 2 : 5

NOTE: DEPTH OF CUT IS NOT CRITICAL BUT MUST BE ROUGHLY 1mm

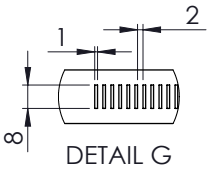

DETAIL G
SCALE 1 : 2

SLOPE GRADIENT 1:200

A4 Landscape	University of Cape Town Department of Mechanical Engineering			
	Title: 200			
Part Finish	Scale: 1:5	Date: 2016/11/16	Sheet 3	of 4
Material: PROVIDED	Drawn By: Andrew Roginsky & Kelsey Hilton		Drawing Number 3	

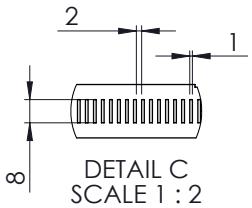

DETAIL C
SCALE 1 : 2

NOTE: DEPTH OF CUT
IS NOT CRITICAL BUT
MUST BE ROUGHLY 1mm

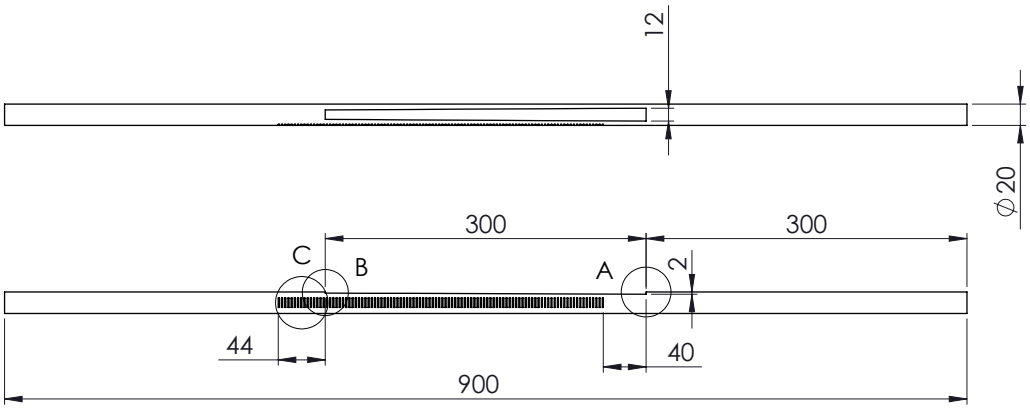

SLOPE GRADIENT 1:300

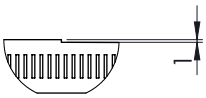

DETAIL B
SCALE 1 : 2

DETAIL A
SCALE 1 : 2

A4 Landscape	University of Cape Town Department of Mechanical Engineering			
	Title: 300			
Part Finish	Scale: 1:5	Date: 2016/11/16	Sheet 2	of 4
Material: PROVIDED	Drawn By: Andrew Roginsky & Kelsey Hilton		Drawing Number 2	

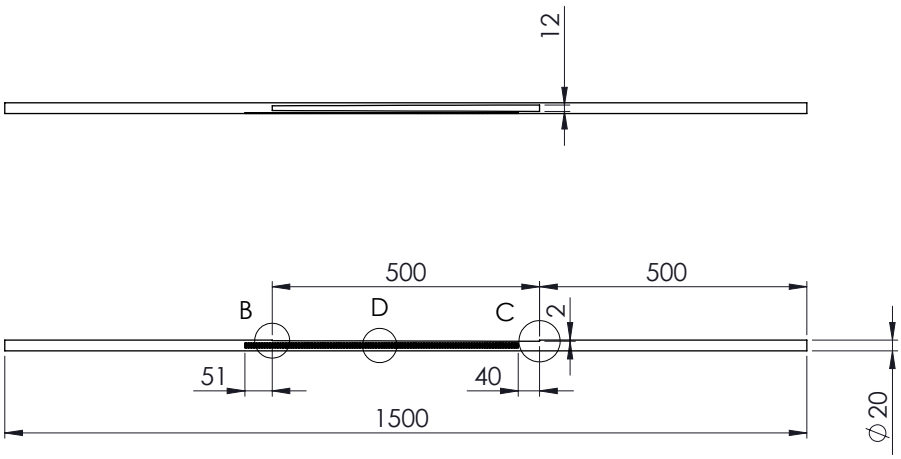

NOTE: DEPTH OF CUT
IS NOT CRITICAL BUT
MUST BE ROUGHLY 1mm

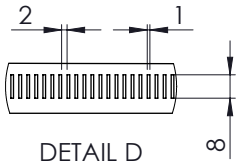

DETAIL D
SCALE 1 : 2

SLOPE GRADIENT 1:500

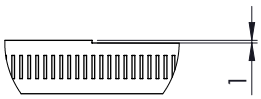

DETAIL B
SCALE 1 : 2

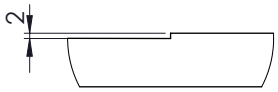

DETAIL C
SCALE 1 : 2

A4 Landscape	University of Cape Town Department of Mechanical Engineering			
	Title: 500			
Part Finish	Scale: 1:10	Date: 2016/11/16	Sheet1	of 4
Material: PROVIDED	Drawn By: Andrew Roginsky & Kelsey Hilton		Drawing Number 1	

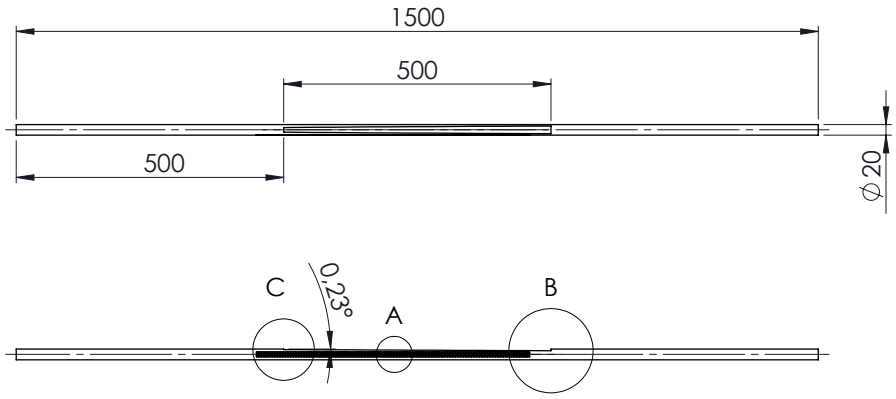

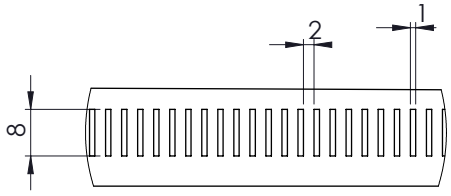

DETAIL A
SCALE 1 : 1

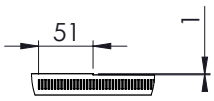

DETAIL C
SCALE 1 : 5

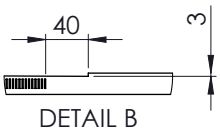

DETAIL B
SCALE 1 : 5

NOTE:
GRADIENT OF SLOPE 1: 250

NOTE: DEPTH OF CUT
IS NOT CRITICAL BUT
MUST BE ROUGHLY 1mm

A4 Landscape	University of Cape Town Department of Mechanical Engineering			
	Title: 2500			
Part Finish	Scale: 1:10	Date: 2016/11/16	Sheet1	of 1
Material: PROVIDED	Drawn By: Andrew Roginsky & Kelsey Hilton		Drawing Number	

Sliding platforms

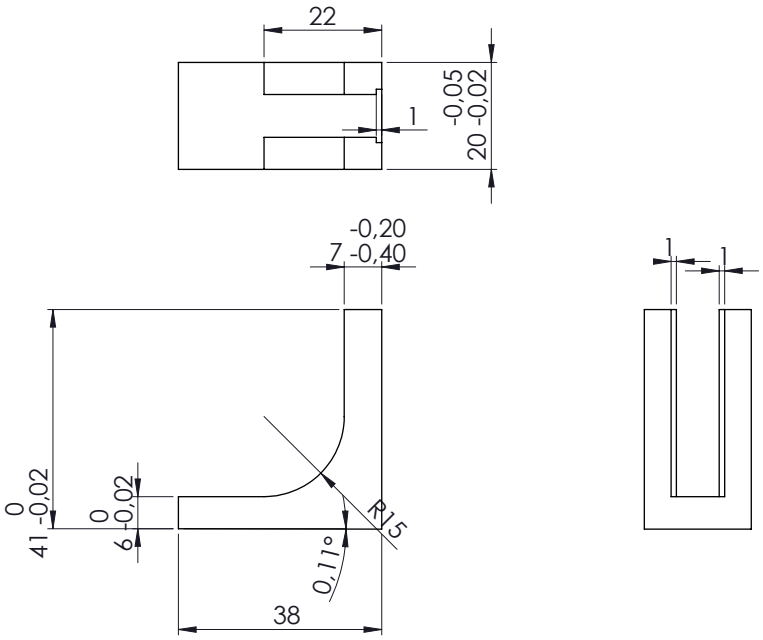

SLOPE GRADIENT
1:500

A4 Landscape	University of Cape Town Department of Mechanical Engineering			
	Title: SPECIMEN PLATFORM-500			
Part Finish	Scale: 1:1	Date: 2016/11/16	Sheet1	of 4
Material: ALUMINIUM	Drawn By: Andrew Roginsky		Drawing Number	

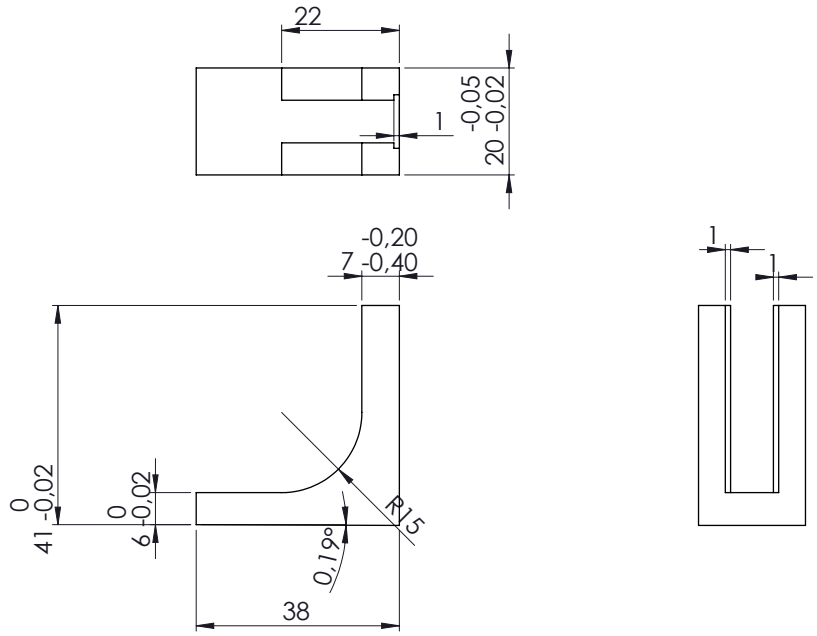

SLOPE GRADIENT
1:300

A4 Landscape	University of Cape Town Department of Mechanical Engineering			
	Title: SPECIMEN PLATFORM-300			
Part Finish	Scale: 1:1	Date: 2016/11/16	Sheet2	of 4
Material: ALUMINIUM	Drawn By: Andrew Roginsky		Drawing Number	

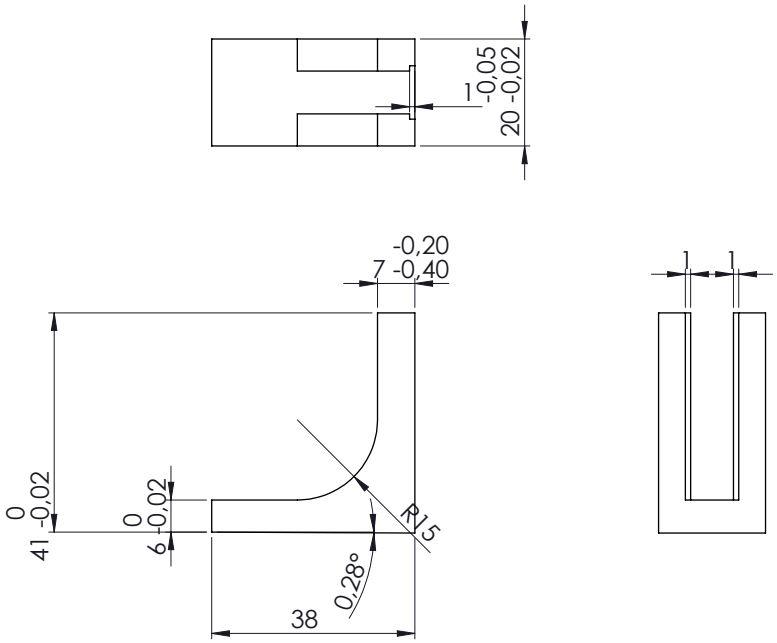

SLOPE GRADIENT
1:200

A4 Landscape	University of Cape Town Department of Mechanical Engineering			
	Title: SPECIMEN PLATFORM-200			
Part Finish	Scale: 1:1	Date: 2016/11/16	Sheet3	of 4
Material: ALUMINIUM	Drawn By: Andrew Roginsky		Drawing Number	

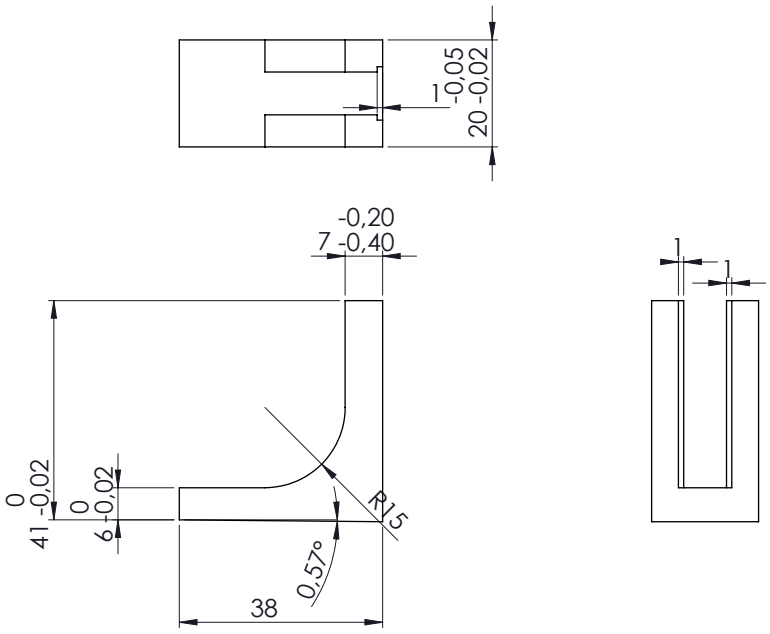

SLOPE GRADIENT
1:100

A4 Landscape	University of Cape Town Department of Mechanical Engineering			
	Title: SPECIMEN PLATFORM-100			
Part Finish	Scale: 1:1	Date: 2016/11/16	Sheet4	of 4
Material: ALUMINU	Drawn By: Andrew Roginsky		Drawing Number	

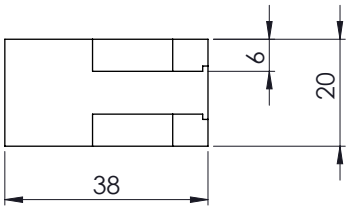

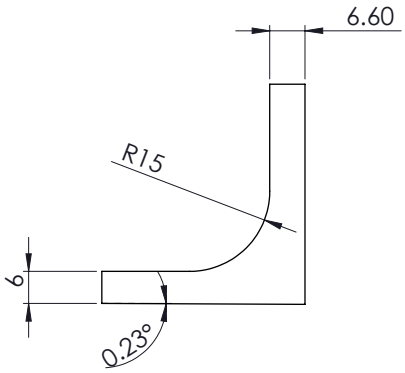

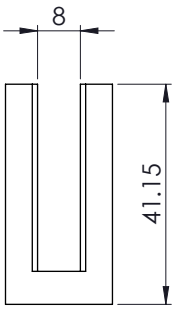

A4 Landscape	University of Cape Town Department of Mechanical Engineering			
	Title: SPECIMEN PLATFORM-2500			
Part Finish	Scale: 1:1	Date: 2016/02/24	Sheet1	of 1
Material: Aluminium	Drawn By: ANDREW ROGINSKY		Drawing Number	

Appendix A-2: Gas gun

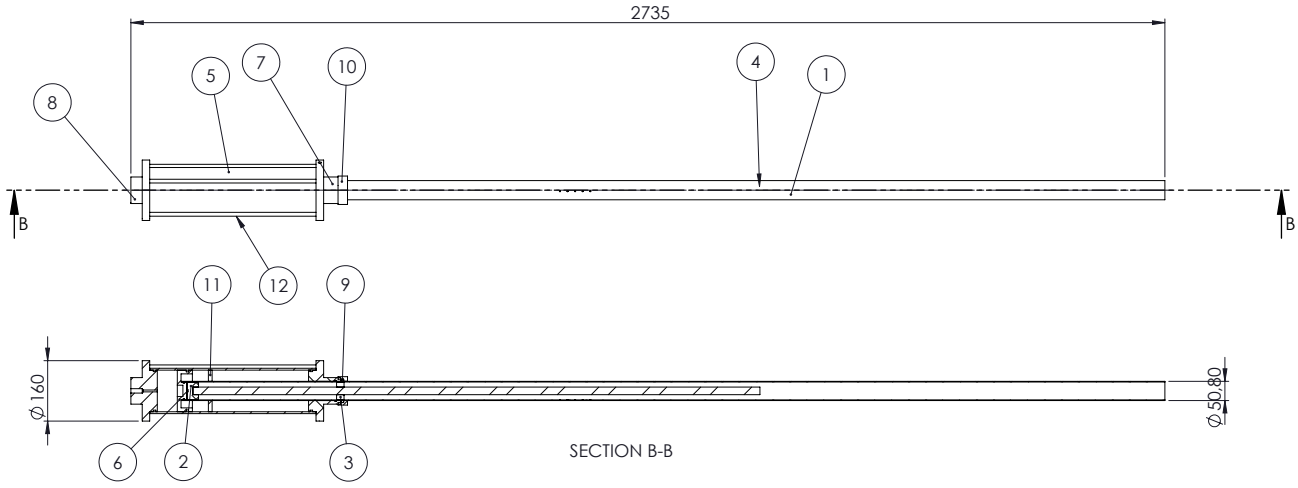

SECTION B-B

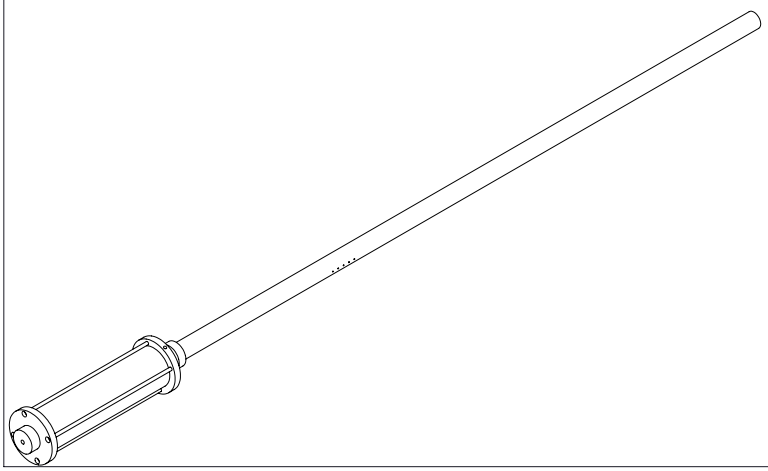

ITEM NO.	PART NUMBER	DESCRIPTION	QTY.
12	Tie Rod	Stainless Steel	4
11	Support	Aluminium	1
10	Fastener	Aluminium	1
9	Stopper	Aluminium	1
8	Rear Seal	Aluminium	1
7	Front Seal	Aluminium	1
6	Piston	Aluminium	1
5	Outer Shell	Aluminium	1
4	Striker	Stainless Steel (provided)	1
3	Collar	Nylon	1
2	Barrel End	Nylon	1
1	Barrel	Aluminium	1

A3 Landscape	University of Cape Town Department of Mechanical Engineering			
	Title: Gas Gun			
Assembly Drawing	Scale: 1:10	Date: 2016/11/16	Sheet1	of 1
	Drawn By: Andrew Roginsky		Drawing Number	

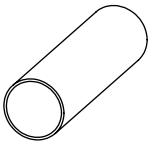

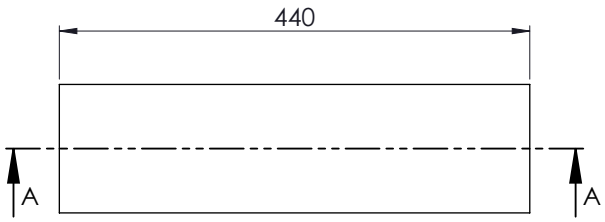

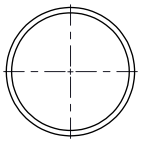

SECTION A-A

A4 Landscape	University of Cape Town Department of Mechanical Engineering			
	Title: Outer Shell			
Part Finish	Scale: 1:5	Date: 2016/05/06	OUTER SHELL	of 12
Material: ALUMINIUM	Drawn By: ANDREW ROGINSKY		Drawing Number	

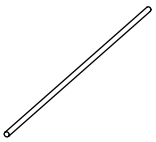

A4 Landscape	University of Cape Town Department of Mechanical Engineering			
	Title: Striker			
Part Finish	Scale: 1:10	Date: 2016/05/06	STRIKER	of 12
Material: STAINLESS STEEL PROVIDED	Drawn By: ANDREW ROGINSKY		Drawing Number	

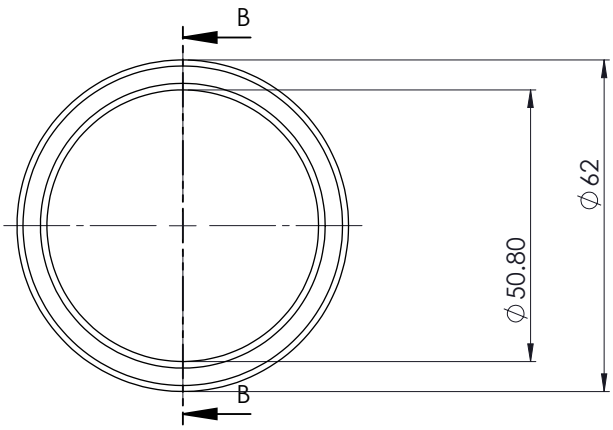

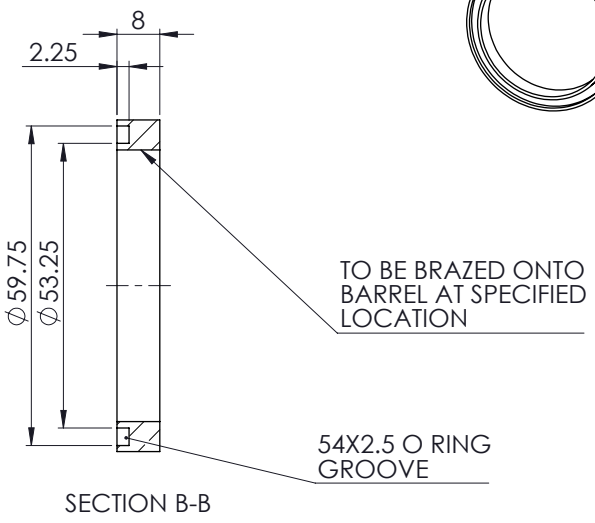

SECTION B-B

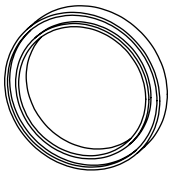

A4 Landscape	University of Cape Town Department of Mechanical Engineering			
	Title: Stopper			
Part Finish	Scale: 1:1	Date: 2016/05/06	STOPPER	of 12
Material: ALUMINIUM	Drawn By: ANDREW ROGINSKY		Drawing Number	

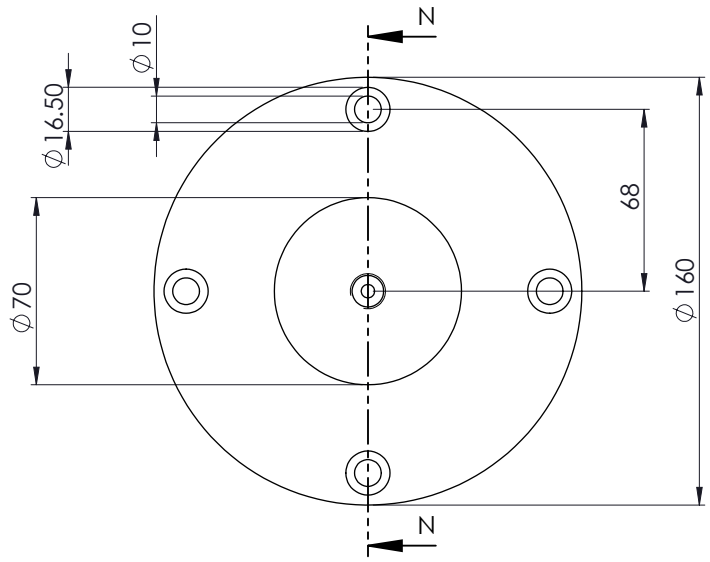

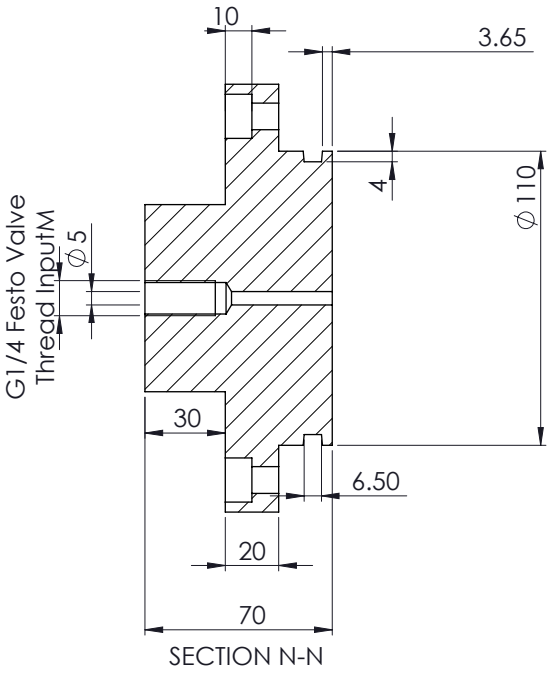

SECTION N-N

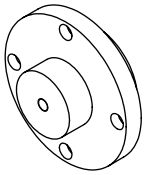

A4 Landscape	University of Cape Town Department of Mechanical Engineering			
	Title: Rear Seal			
Part Finish	Scale: 1:2	Date: 2016/05/06		of REAR SEAL 12
Material: ALUMINIUM	Drawn By: ANDREW ROGINSKY		Drawing Number	

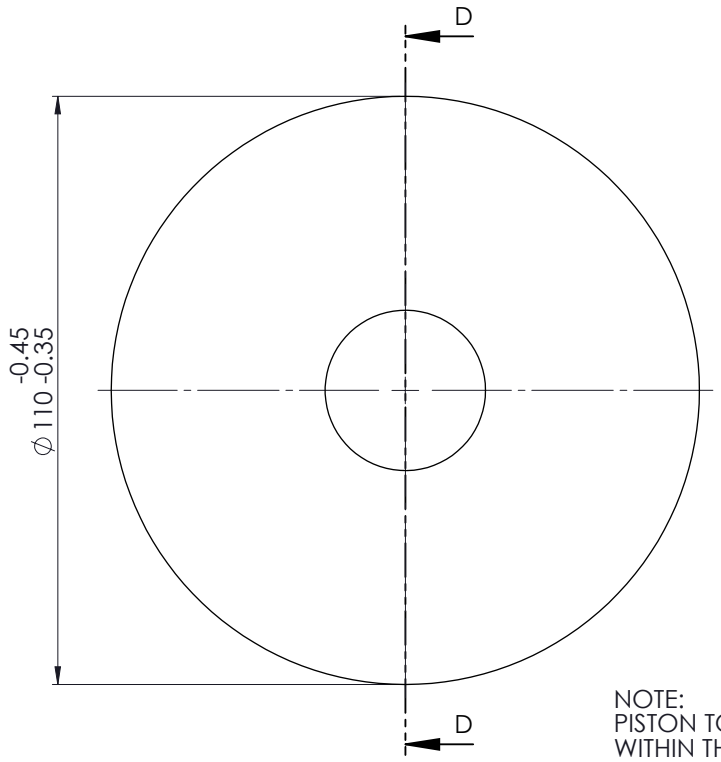

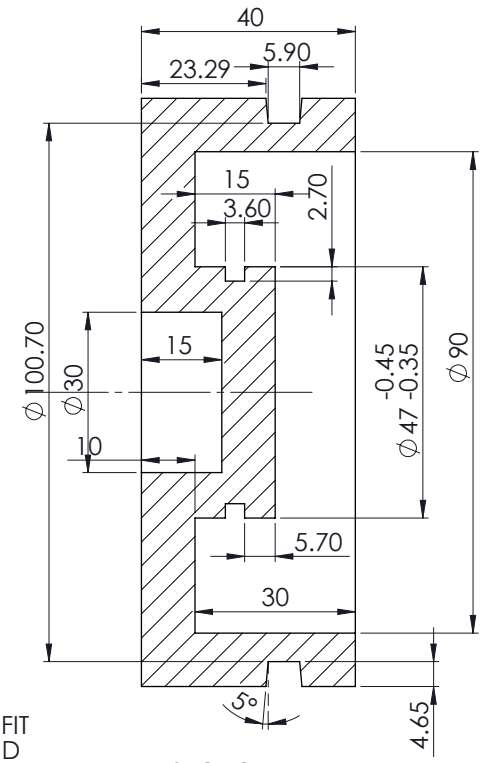

SECTION D-D

NOTE:
PISTON TO HAVE A SLIDING FIT WITHIN THE OUTER SHELL AND BARREL PRIOR TO O RING PLACEMENT

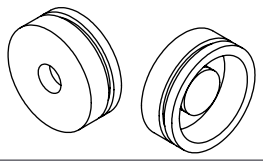

A4 Landscape	University of Cape Town Department of Mechanical Engineering			
	Title: Piston			
Part Finish	Scale: 1:1	Date: 2016/05/06	PISTON	of 12
Material: ALUMINIUM	Drawn By: ANDREW ROGINSKY		Drawing Number	

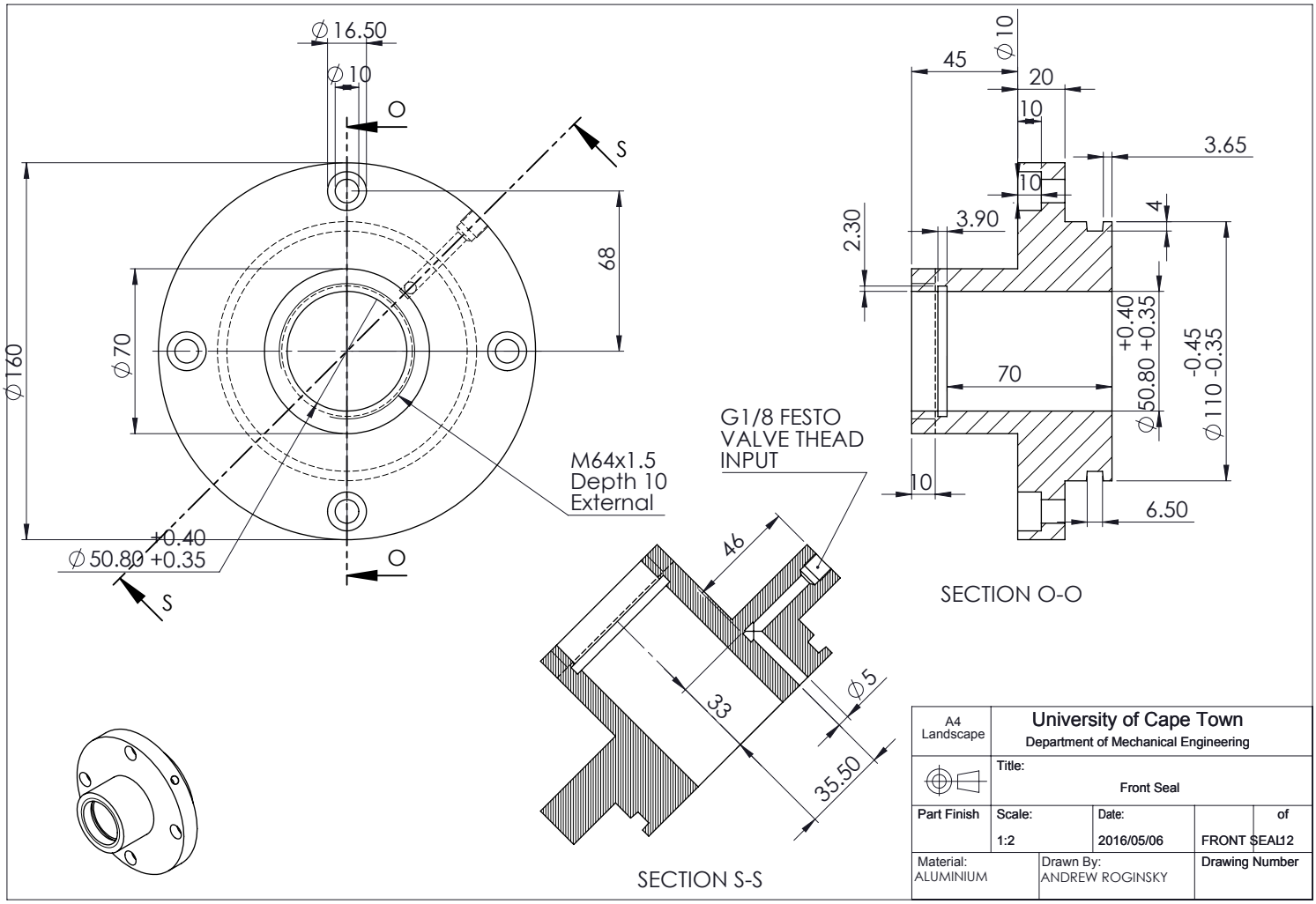

A4 Landscape	University of Cape Town Department of Mechanical Engineering			
	Title: Front Seal			
Part Finish	Scale: 1:2	Date: 2016/05/06		of FRONT SEAL12
Material: ALUMINIUM	Drawn By: ANDREW ROGINSKY		Drawing Number	

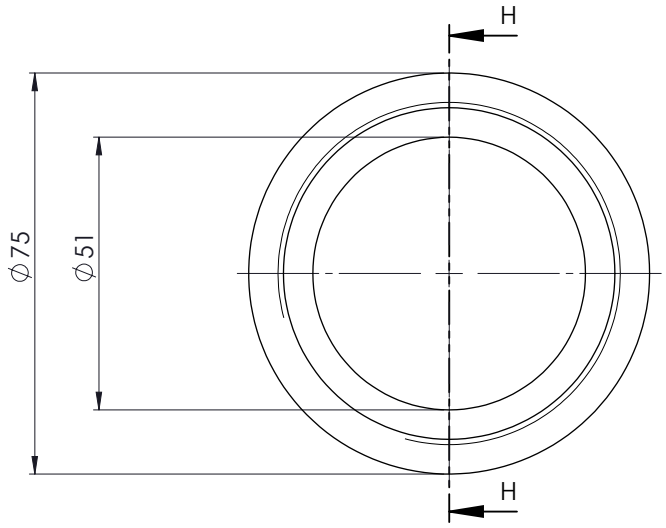

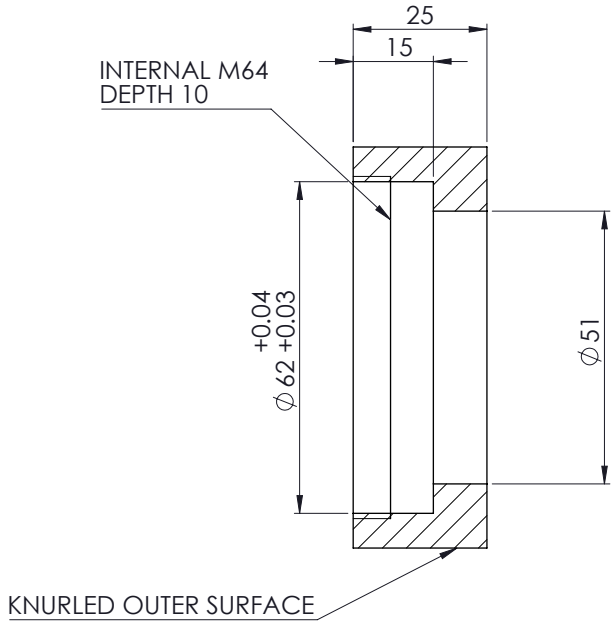

SECTION H-H

A4 Landscape	University of Cape Town Department of Mechanical Engineering			
	Title: Fastener			
Part Finish	Scale: 1:1	Date: 2016/05/06		of FASTENER 12
Material: ALUMINIUM	Drawn By: ANDREW ROGINSKY		Drawing Number	

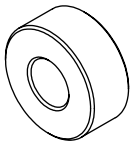

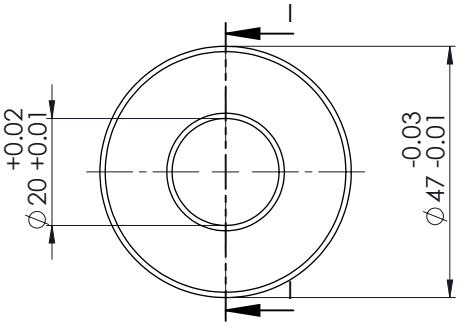

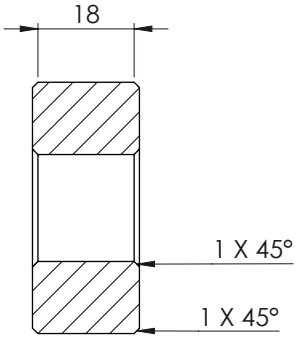

SECTION I-I

NOTE:
TO HAVE A SLIDING FIT WITH THE INNER OF THE BARREL

A4 Landscape	University of Cape Town Department of Mechanical Engineering			
	Title: Collar			
Part Finish	Scale: 1:1	Date: 2016/05/06	COLLAR	of 12
Material: NYLON	Drawn By: ANDREW ROGINSKY		Drawing Number	

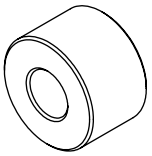

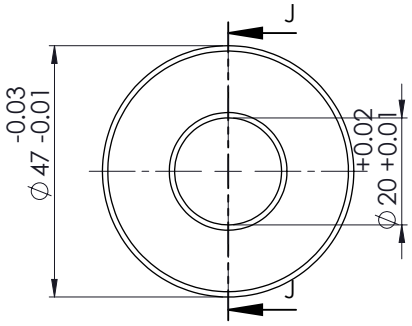

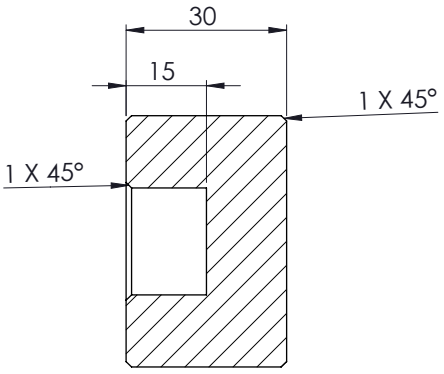

SECTION J-J

NOTE:
TO HAVE A SLIDING FIT
WITH THE INNER OF THE
BARREL

A4 Landscape	University of Cape Town Department of Mechanical Engineering			
	Title: Barrel End			
Part Finish	Scale: 1:1	Date: 2016/05/06	BARREL END	of 2
Material: NYLON	Drawn By: ANDREW ROGINSKY		Drawing Number	

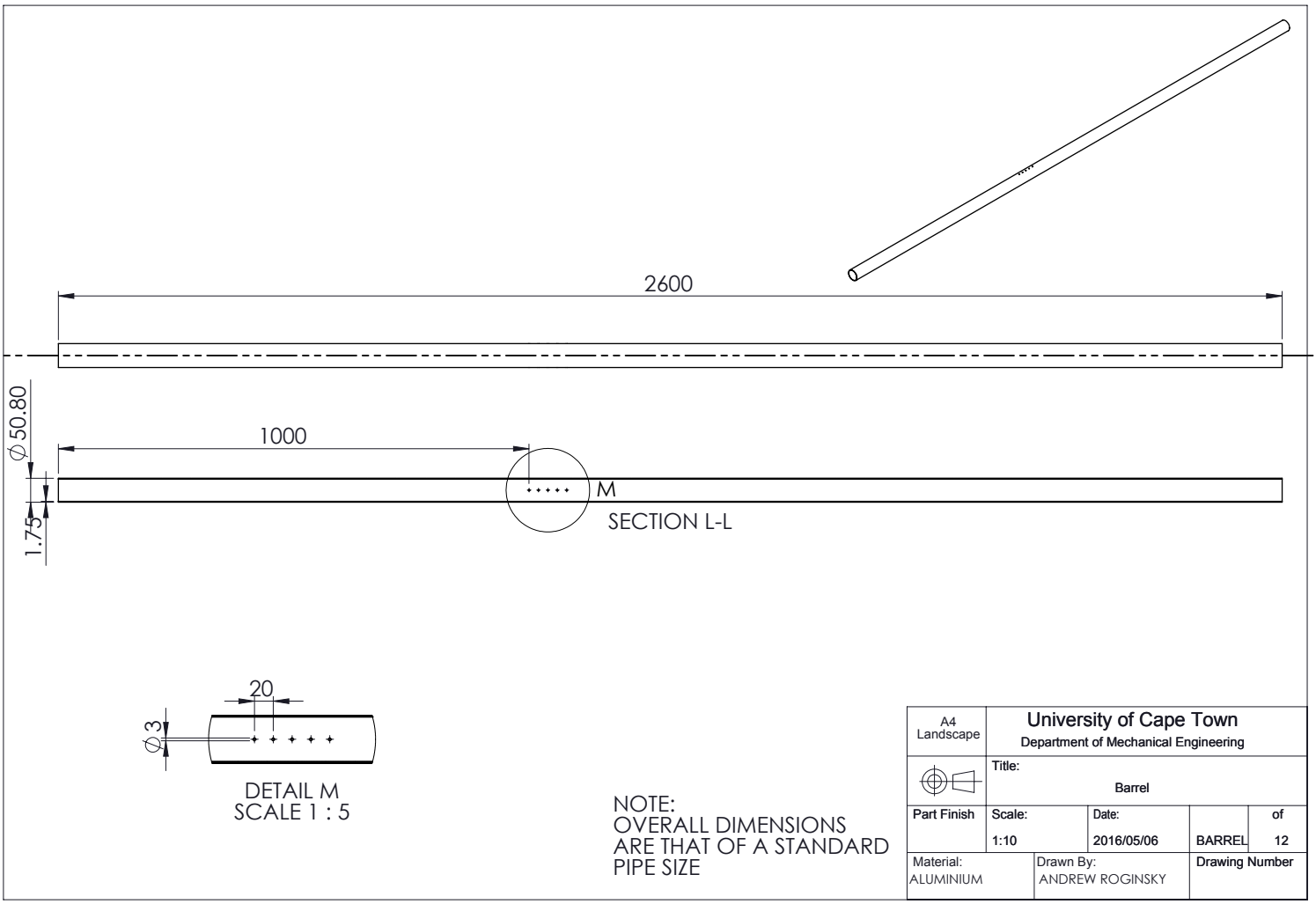

DETAIL M
SCALE 1 : 5

NOTE:
OVERALL DIMENSIONS
ARE THAT OF A STANDARD
PIPE SIZE

A4 Landscape	University of Cape Town Department of Mechanical Engineering			
	Title: Barrel			
Part Finish	Scale: 1:10	Date: 2016/05/06	BARREL	of 12
Material: ALUMINIUM	Drawn By: ANDREW ROGINSKY		Drawing Number	

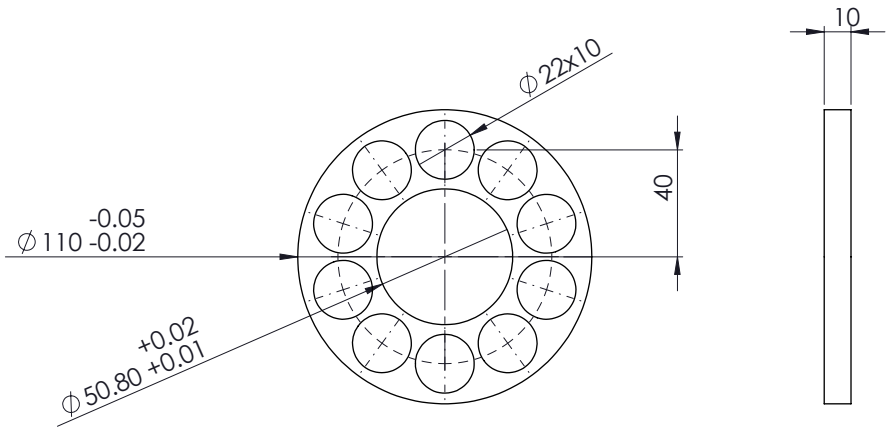

NOTE:
TO HAVE A SLIDING FIT
WITH THE INNER OF THE
CYLINDER SHELL

A4 Landscape	University of Cape Town Department of Mechanical Engineering			
	Title: Support			
Part Finish	Scale: 1:2	Date: 2016/05/06	SUPPORT	of 12
Material: ALUMINIUM	Drawn By: ANDREW ROGINSKY		Drawing Number	

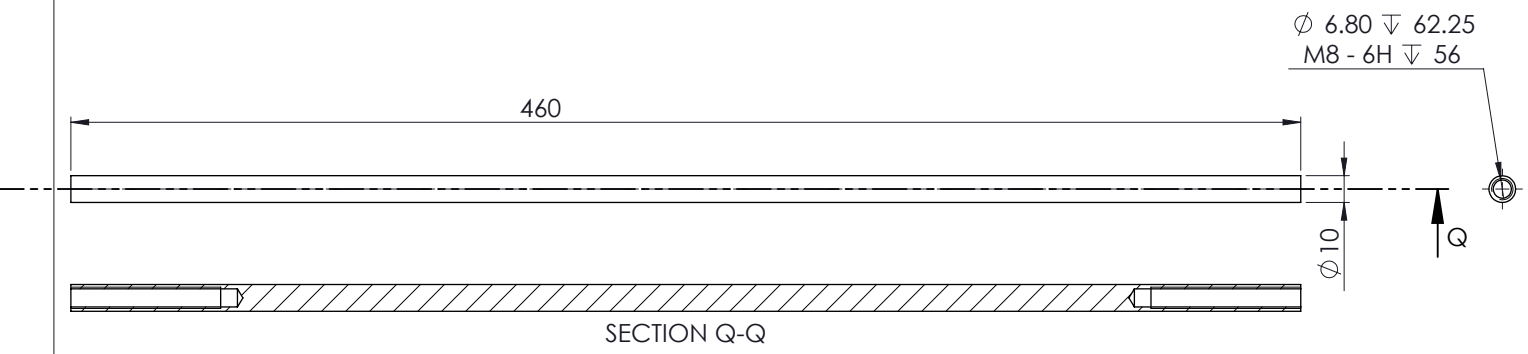

SECTION Q-Q

A4 Landscape	University of Cape Town Department of Mechanical Engineering			
	Title: Tie Rod			
Part Finish	Scale: 1:2	Date: 2016/05/06	TIE ROD	of 12
Material: STAINLESS STEEL	Drawn By: ANDREW ROGINSKY		Drawing Number	

Appendix B: Assessment of Ethics in Research Projects

EBE Faculty: Assessment of Ethics in Research Projects

Any person planning to undertake research in the Faculty of Engineering and the Built Environment at the University of Cape Town is required to complete this form before collecting or analysing data. When completed it should be submitted to the supervisor (where applicable) and from there to the Head of Department. If any of the questions below have been answered YES, and the applicant is NOT a fourth year student, the Head should forward this form for approval by the Faculty EIR committee: submit to Ms Zulpha Geyer (Zulpha.Geyer@uct.ac.za; Chem Eng Building, Ph 021 650 4791). Students must include a copy of the completed form with the thesis when it is submitted for examination.

Name of Principal Researcher/Student: Andrew Roginsky

Department: Mech Eng

If a Student: Degree:

Supervisor: Mr Trevor Cloete

If a Research Contract indicate source of funding/sponsorship:

Research Project Title: Fracture & deformation of Bone

Overview of ethics issues in your research project:

Question 1: Is there a possibility that your research could cause harm to a third party (i.e. a person not involved in your project)?	YES	(NO)
Question 2: Is your research making use of human subjects as sources of data? If your answer is YES, please complete Addendum 2.	YES	(NO)
Question 3: Does your research involve the participation of or provision of services to communities? If your answer is YES, please complete Addendum 3.	YES	(NO)
Question 4: If your research is sponsored, is there any potential for conflicts of interest? If your answer is YES, please complete Addendum 4.	YES	(NO)

If you have answered YES to any of the above questions, please append a copy of your research proposal, as well as any interview schedules or questionnaires (Addendum 1) and please complete further addenda as appropriate.

I hereby undertake to carry out my research in such a way that

- there is no apparent legal objection to the nature or the method of research; and
- the research will not compromise staff or students or the other responsibilities of the University;
- the stated objective will be achieved, and the findings will have a high degree of validity;
- limitations and alternative interpretations will be considered;
- the findings could be subject to peer review and publicly available; and
- I will comply with the conventions of copyright and avoid any practice that would constitute plagiarism.

Signed by:

	Full name and signature	Date
Principal Researcher/Student:		21/01/2015

This application is approved by:

Supervisor (if applicable):		03/02/2015
HOD (or delegated nominee): Final authority for all assessments with NO to all questions and for all undergraduate research.		06/02/2015
Chair : Faculty EIR Committee For applicants other than undergraduate students who have answered YES to any of the above questions.		

ADDENDUM 1:
Please append a copy of the research proposal here, as well as any interview schedules or questionnaires:

ADDENDUM 2: To be completed if you answered YES to Question 2:

It is assumed that you have read the UCT Code for Research involving Human Subjects (available at http://web.uct.ac.za/depts/educate/download/uctcodeforresearchinvolvinghumansubjects.pdf) in order to be able to answer the questions in this addendum.

2.1 Does the research discriminate against participation by individuals, or differentiate between participants, on the grounds of gender, race or ethnic group, age range, religion, income, handicap, illness or any similar classification?	YES	NO
2.2 Does the research require the participation of socially or physically vulnerable people (children, aged, disabled, etc) or legally restricted groups?	YES	NO
2.3 Will you not be able to secure the informed consent of all participants in the research? (In the case of children, will you not be able to obtain the consent of their guardians or parents?)	YES	NO
2.4 Will any confidential data be collected or will identifiable records of individuals be kept?	YES	NO
2.5 In reporting on this research is there any possibility that you will not be able to keep the identities of the individuals involved anonymous?	YES	NO
2.6 Are there any foreseeable risks of physical, psychological or social harm to participants that might occur in the course of the research?	YES	NO
2.7 Does the research include making payments or giving gifts to any participants?	YES	NO

If you have answered YES to any of these questions, please describe how you plan to address these issues (append to form):

ADDENDUM 3: To be completed if you answered YES to Question 3:

3.1 Is the community expected to make decisions for, during or based on the research?	YES	NO
3.2 At the end of the research will any economic or social process be terminated or left unsupported, or equipment or facilities used in the research be recovered from the participants or community?	YES	NO
3.3 Will any service be provided at a level below the generally accepted standards?	YES	NO

If you have answered YES to any of these questions, please describe how you plan to address these issues (append to form)

ADDENDUM 4: To be completed if you answered YES to Question 4

4.1 Is there any existing or potential conflict of interest between a research sponsor, academic supervisor, other researchers or participants?	YES	NO
4.2 Will information that reveals the identity of participants be supplied to a research sponsor, other than with the permission of the individuals?	YES	NO
4.3 Does the proposed research potentially conflict with the research of any other individual or group within the University?	YES	NO

If you have answered YES to any of these questions, please describe how you plan to address these issues(append to form)